

## Chapter 4

# Stratospheric aerosols

### 4.1 Formation, Physical, Chemical, Radiative and Optical effects

Research on stratosphere grew into a separate discipline and developed a great deal after 1970s, which till then was an unexplored region in space. The concern in 1970 [Crutzen, 1970] that supersonic transports which produce water vapour and oxides of nitrogen and the discovery of Molina and Rowland [1974] in 1974 that chlorine compounds produced by the chemical industry, commonly known as CFCs or Freons could disturb the protective ozone layer brought a large number of scientists from the adjacent fields to this sphere. But not until recently that the role stratosphere plays in global climate and in global change was recognised adequately. Stratosphere suffers from a variety of issues, some of them being the ozone depletion, changes in thermal structure and how effective are the stratospheric aerosols in wrecking the ozone abundances, especially after a major volcanic eruption when the depletion gets more deeper due to the availability of abundantly large number of aerosols and how these aerosols play a role in the radiative and climatic impacts.

Stratospheric aerosols exist in a stratified layer beginning near the tropopause and extending up to 30 km. The height and thickness of the layer exhibit temporal and latitudinal variations and exhibits an apparent correlation with tropopause height [Rosen *et al.*, 1975]. The background stratospheric aerosol layer has a mode radius of about 0.05-0.1  $\mu\text{m}$  and has a number density of about 1-10 particles  $\text{cm}^{-3}$ . But immediately after volcanic eruptions the mode radius can increase to 1.0  $\mu\text{m}$  in the stratosphere and

the number density can go up by more than an order of magnitude, when compared to the background conditions.

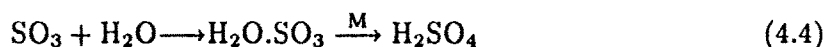
Stratospheric aerosols are formed after major volcanic eruptions and diffusion of natural gases such as  $\text{H}_2\text{S}$ ,  $\text{COS}$ ,  $\text{CS}_2$ ,  $\text{SO}_2$ , etc. from troposphere. Most of the sulphur present in the Earth's atmosphere ends up as sulphate, as it is the thermodynamically stable form of sulphur in the presence of oxygen. Sulphur bearing gases are generated both naturally and anthropogenically. *Charlson et al.* [1987] estimate that marine flora and terrestrial biota account for 50% of the total natural flux of the sulphur present in the atmosphere. The only significant nonbiological natural flux is the emission of  $\text{SO}_2$  and  $\text{H}_2\text{S}$  by volcanoes and fumaroles, which account for 10-20% of the total natural flux of gaseous sulphur in the atmosphere. The anthropogenic counterpart arises from combustion processes such as coal burning, oil burning, smelting and petroleum refining and traffic and their relative contributions are 70%, 8.4%, 21% and 0.6% respectively [*d'Almeida et al.*, 1991].

The marine emissions are almost exclusively in the form of dimethyl sulphide (DMS), the chemical formula being  $\text{CH}_3\text{SCH}_3$ . The highest production of DMS occurs in the warmest, most saline and most intensely illuminated regions of the ocean i.e. the tropical regions [*Charlson et al.*, 1987]. The terrestrial emissions occur from a variety of species, including  $\text{H}_2\text{S}$ , DMS,  $\text{CS}_2$ ,  $\text{COS}$  among others.  $\text{SO}_2$  is mainly produced by fossil fuel combustion, biomass burning and volcanic eruptions. While the  $\text{SO}_2$  emitted from fossil fuel combustion and biomass burning are the major sources of sulphate aerosols in the troposphere,  $\text{SO}_2$  from volcanic eruptions and other sources of  $\text{SO}_2$  from troposphere by diffusion accounts for sulphate aerosols in the stratosphere.

Stratospheric aerosols are mostly sulphate particles (70-75%  $\text{H}_2\text{SO}_4$  and 30-25%  $\text{H}_2\text{O}$  with some traces of other sulphates, nitrates etc.). They are formed due to conversion from gaseous sulphur dioxide. The key process is the reaction with OH which initiates the oxidation.



The sulphur trioxide so produced gets converted into sulphuric acid particles, through condensation and coagulation.



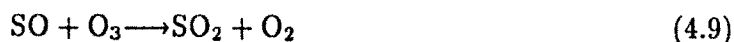
The sulphuric acid particles finally get converted into sulphate aerosols. The detailed mechanism has several uncertainties but the presence of clouds and other chemicals like  $\text{NH}_3$  seem to help. Typical life times for conversion of  $\text{SO}_2$  to  $\text{H}_2\text{SO}_4$  is estimated to be 24 days [McPeters., 1993]. Volcanic eruptions pump in large quantities of  $\text{SO}_2$  into the atmosphere. But the reaction scheme from (4.1) to (4.3) which converts  $\text{SO}_2$  to  $\text{H}_2\text{SO}_4$  and sulphate aerosols is valid even in the background (nonvolcanic) conditions. In the background case  $\text{SO}_2$  comes from oxidation of carbonyl sulphide ( $\text{COS}$ ) and carbon disulphide ( $\text{CS}_2$ ) which are of biospheric origin. The oxidation is either through  $\text{O}^1\text{D}$  or through photodissociation.



Further oxidation gives rise to  $\text{SO}_2$ .



More important at the tropospheric altitudes are the following reactions.



Crutzen [1976] has estimated that the above scheme can give rise to  $\text{SO}_2$  in the range of  $10^6 - 10^7$  molecules  $\text{cm}^{-2} \text{sec}^{-1}$  in the free troposphere.

Volcanic aerosols can cause warmings (of about  $3-4^\circ\text{C}$ ) in the stratosphere primarily by the absorption of upwelling terrestrial radiation and by reducing the amount of total solar radiation reaching the troposphere, can cause cooling (of about  $0.5^\circ\text{C}$ ) globally [Ackerman, 1988] and also these aerosols by backscattering (as these aerosols are efficient scatterers

but only weak absorbers at visible wavelengths) more amount of solar radiation into space, increase the planetary albedo. For example, following El Chichon the transmission of direct solar radiation was found reduced by about 15% and did not recover for about 3 years [Hofmann, 1988] and after the more recent Mt. Pinatubo, the transmission was found decreased by about 25-30%, resulting in a cooling of the troposphere by 0.5°C, globally [Dutton and Christy, 1992]. The major development during the recent years has been the recognition that heterogeneous chemistry, in which aerosols play a key role, is the dominant process responsible not only for the polar spring time ozone depletion (Antarctic and Arctic ozone holes) but also for global ozone depletion [Hofmann and Solomon, 1989], the only difference being the medium on which the depletion occurs i.e. the polar stratospheric clouds in the former, which is replaced by the increased number of large size aerosols offering large surface area formed after the volcanic eruption, in the latter. Aerosols added to the stratosphere can affect ozone concentrations in other ways, such as by absorbing the sunlight can heat the stratosphere and alter its usual circulation patterns [Kinne *et al.*, 1992]. In the atmosphere the aerosol characteristics are altitude dependent [Subbaraya and Jayaraman, 1982] and the stratospheric aerosols are quite different from the lower tropospheric aerosols. Unlike tropospheric aerosols, which are shortlived due to gravitational settling and rainwash and produce only local and seasonal effects, stratospheric aerosols on the other hand are long lived [Prospero *et al.*, 1983] and can produce long term global effects.

The location, time of the year, injection altitude and the amount of SO<sub>2</sub> injected by the eruption are important not only in determining the global impact, but also in determining the eventual stratospheric aerosol particle size [Hofmann, 1987]. In general, low latitude eruption can have a larger impact because of the global coverage it can provide. However, generalisation and extrapolation of the effects, from one eruption to the other, is not possible. Even though qualitatively the effects have been known for a long time, it is the recent volcanic eruptions after Mt. St. Helens (1980), especially the El Chichon (1982) and now the Mt. Pinatubo (1991) that have given opportunities to determine the detailed physical characteristics of volcanic aerosols and enable a study of their impact in the middle atmosphere.

The size distribution of volcanic aerosols typically shows a trimodal structure that

varies with time. The principal size modes are: the nucleation mode, which is most prominent within one month after the eruption having particles of size around  $0.01 \mu\text{m}$ ; the sulphate accumulation mode, which evolves initially from the nucleation mode (by condensation and coagulation) and increases in size to about  $0.3 \mu\text{m}$  after about an year; the large particle 'ash' mode (of silicate mineral and possibly salt particles) of micron size that settles out of the layer within the first month of an eruption [Turco *et al.*, 1993]. Figure 4.1 schematically illustrates the time evolution of the stratospheric aerosol size distribution, after a major volcanic eruption. The evolution process involves a variety of physico-chemical interactions such as  $\text{H}_2\text{SO}_4$  vapour nucleation, condensational growth and evaporation, coagulation, gravitational sedimentation and dynamical process such as diffusion (Figure 4.2). While the dust or silicate particulate matter settles out rapidly and does not play an important role after a few months, the sulphurous gases which are injected get converted into sulphuric acid droplets (as explained above) while other gases may affect the ozone layer. The 'optically effective' aerosols are in the size range from  $0.05 \mu\text{m}$  to  $10 \mu\text{m}$  which can alter the Earth's radiation budget by scattering away the incoming solar radiation and to some extent by absorbing the outgoing Earth's longwave radiation. The possible consequences are heating of the stratosphere and a cooling effect at the Earth's surface. Ice core data show a clear record of the sulphur emissions from major historical eruptions [Delmas, 1992]. The sulphur dioxide after conversion to sulphate is transported to high latitudes in the stratosphere, from where it is deposited on glacial ice sheets over a period of several years. Ice core data provides the much needed information on the time and magnitude of major eruptions that have disturbed the stratosphere [Legrand and Delmas, 1984; Kirchner and Delmas, 1988] and gives an opportunity for gaining a more profound understanding of the relation between volcanic eruptions and climate change.

## 4.2 Volcanic aerosols: An assessment of the effects

Our awareness on the effects of volcanic eruptions on the stratosphere appreciably improved after the eruption of Mt. St. Helens in 1980. This is mainly due to the availability of techniques for measuring these effects by both direct and remote sensing, at our disposal. It was also clear that the large quantities of  $\text{SO}_2$  injected into the stratosphere,

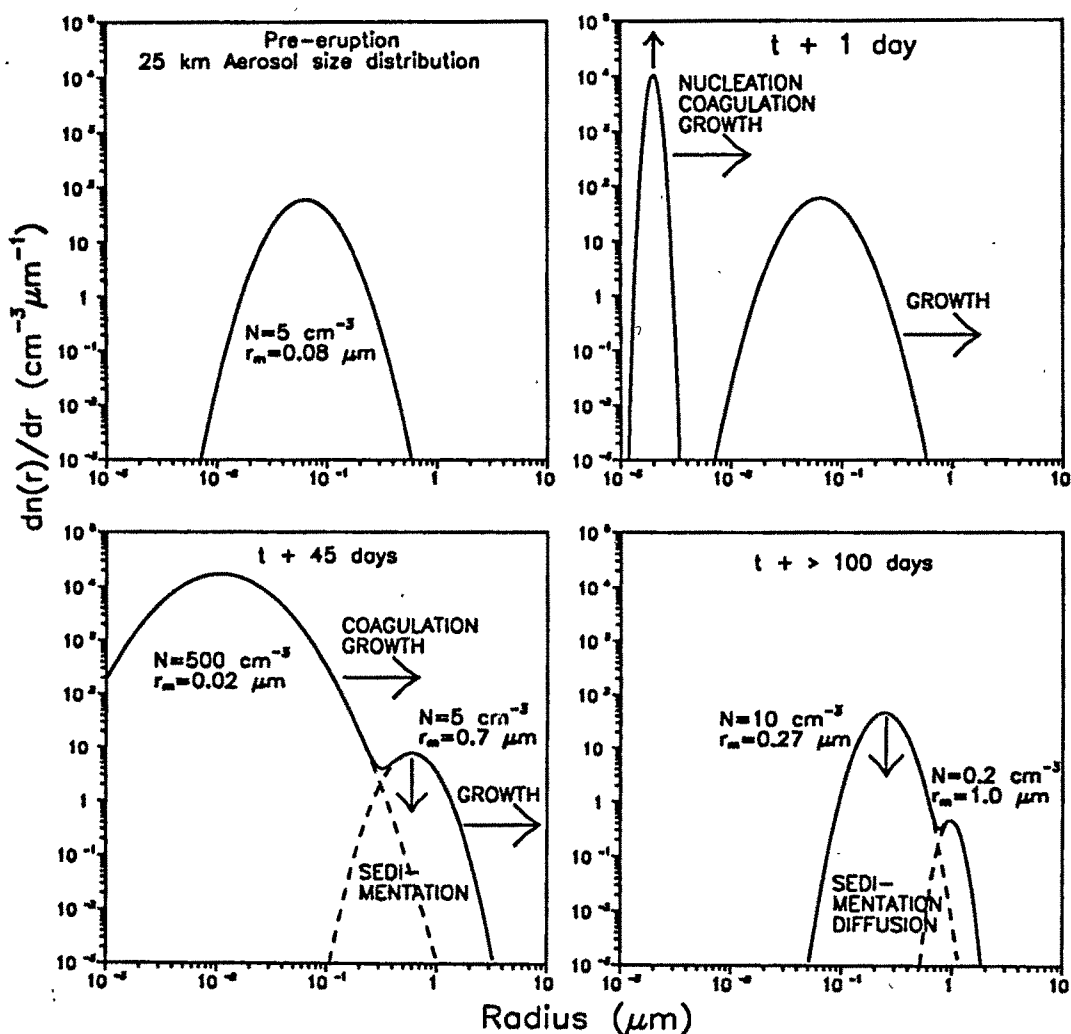


Figure 4.1: Schematic illustration of the time evolution of the stratospheric aerosol size distribution after a major volcanic eruption, due to various physico-chemical and dynamical processes in the atmosphere (adopted from Hofmann, 1988).

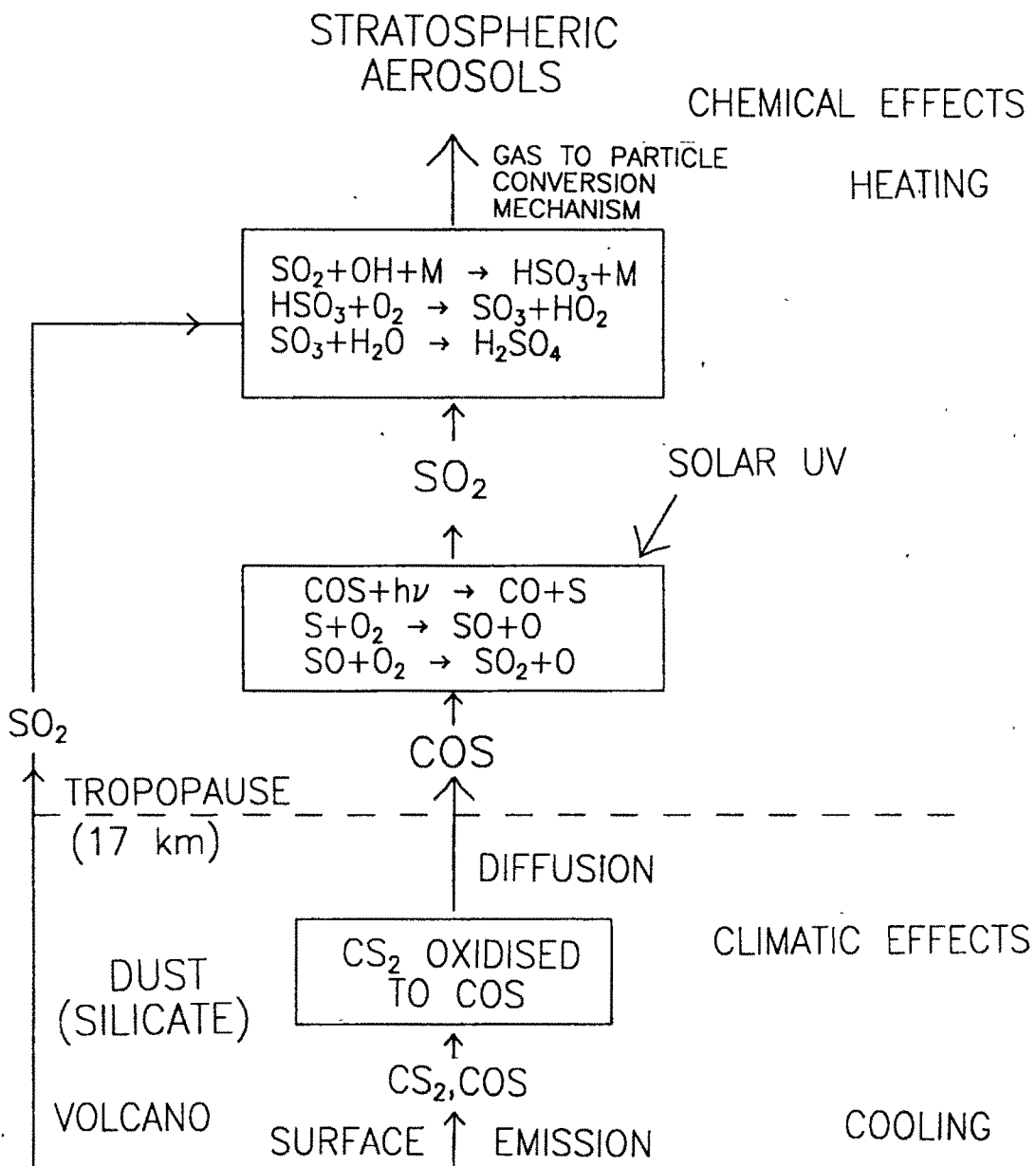


Figure 4.2: Schematic representation of the formation, importance and effects of stratospheric aerosols (adopted from Hofmann, 1987; Jayaraman, 1993).

after conversion to sulphate aerosols can have a chemical, physical, radiative and climatic influence on a global scale, due to the prevailing atmospheric circulation.

Mt. St. Helens volcano (46.2°N, 122.2°W) erupted on 18 May 1980 injecting about 0.6 megatons (Mt) of SO<sub>2</sub> into the atmosphere, with the debris reaching up to 24 km in the atmosphere [Turco *et al.*, 1983]. The average optical depth at 1.0 μm over the midlatitudes was about 0.006 following the eruption [Kent and McCormick, 1984] as compared to a prevolcanic, background value of 0.001. The condensation nuclei concentration had increased by more than one order of magnitude and the mode radius was found to be around 0.1 μm between 10 and 25 km, few months after the eruption [Hofmann and Rosen, 1982]. The aerosol mixing ratios (particles per milligram ambient air) in the two size ranges ( $r \geq 0.15 \mu\text{m}$ ,  $r \geq 0.25 \mu\text{m}$ ) over Laramie, Wyoming (41°N), increased by about more than one order of magnitude, as compared to the background conditions [Hofmann, 1987]. As the St. Helens eruption was from midlatitude and also as the amount of SO<sub>2</sub> injected was comparatively less, the global effects were small and had little influence on climate and can not be classified as a major eruption in terms of stratospheric aerosol effects.

This century witnessed two of the strongest volcanic eruptions ever recorded namely El Chichon in April 1982 and Mount Pinatubo in June 1991. El Chichon (17.3°N, 93.2°W) in Mexico erupted on 4 April 1982 injecting about 10 megatons of SO<sub>2</sub> which penetrated altitudes in excess of 25 km [Hofmann, 1987]. The 500 nm aerosol optical depth measured at Mauna Loa (19.53°N) in Hawaii increased from a preeruption value of 0.02 to about 0.3 by the middle of 1982, indicating the magnitude of the eruption. The aerosol cloud was found confined over the tropics in the early months after the eruption. Lidar results on scattering ratio obtained immediately after the eruption showed an increase of about 2 orders of magnitude in the scattering ratios. Hofmann and Rosen [1983] have shown using balloonborne optical particle counters at Laramie, Wyoming (41°N), that the aerosol ( $r \geq 0.15 \mu\text{m}$ ) concentration at the stratosphere has increased by about an order, from about a few particles (during background, volcanically quiescent periods) to a few tens of particles in May 1982, 45 days after the eruption. The mean radius of aerosols in the 17-25 km altitude region was found to be around 0.2 to 0.3 μm even after an year of eruption, whereas the background mean radii are around 0.1 μm. Also for the first time a

correlation between the increased aerosol loading and ozone depletion at the stratospheric altitudes over midlatitudes was found [Hofmann, 1987]. But the role of aerosols in altering the ozone abundances through heterogeneous chemistry, was demonstrated later, in 1989 [Hofmann and Solomon, 1989]. While a stratospheric heating of around 3-4°C has been observed after the El Chichon eruption, a surface cooling was not very apparent.

On 15 June 1991 Mt. Pinatubo (15.14°N, 120.35°E) in the Philippines, after being dormant for about 635 years, erupted producing the largest impact at the stratospheric altitudes [McCormick and Veiga, 1992; Bluth et al., 1992]. This colossal eruption gave an opportunity to study the various physico-chemical processes involved in the formation of stratospheric aerosol layer and its decay and predict the impending climatic effects. Stratospheric Aerosol and Gas Experiment (SAGE) II extinction measurements of the Pinatubo aerosols in the stratosphere during June, July and early August 1991 show that aerosols in the tropics reached altitudes as high as 29 km. At altitudes above 20 km, the aerosol cloud moved rapidly to the west with the leading edge circling the globe in about 3 weeks [McCormick and Veiga, 1992]. Figure 4.3 shows the 6.5 year record of SAGE II optical depth at 1020 nm over the altitude range from 3 km above the tropopause to 40 km. The time series shows aerosol perturbations caused by the eruptions of Nevado del Ruiz (November, 1985), Kelut (February, 1990) and the first indication of Pinatubo (June, 1991). The stratospheric optical depth following Pinatubo has increased by about 2 orders of magnitude.

A number of investigations have been carried out by several groups on the globally dispersed aerosol due to the Pinatubo eruption using airborne lidar [Winker and Osborn, 1992], particle counters [Deshler et al., 1992, 1993], ship-borne and stationary lidars in the northern hemisphere [Avdyushin et al., 1993; Nardi et al., 1993]. Thomason and Osborn [1992] have reported on the vertical profiles of aerosol extinction using SAGE II data. All these results in general show that the eruption has put as much as 2 to 3 times more material (about 15 to 30 megatons of SO<sub>2</sub> [McPeters, 1993; Bluth et al., 1992]) into the stratosphere compared to the El Chichon eruption in Mexico in 1982, which resulted in a global stratospheric aerosol mass load of about 20-30 Mt [McCormick and Veiga, 1992]. Also for the first few months after the eruption the bulk of the material was confined over the tropics [Stowe et al., 1992; Trepte et al., 1993] from the tropopause

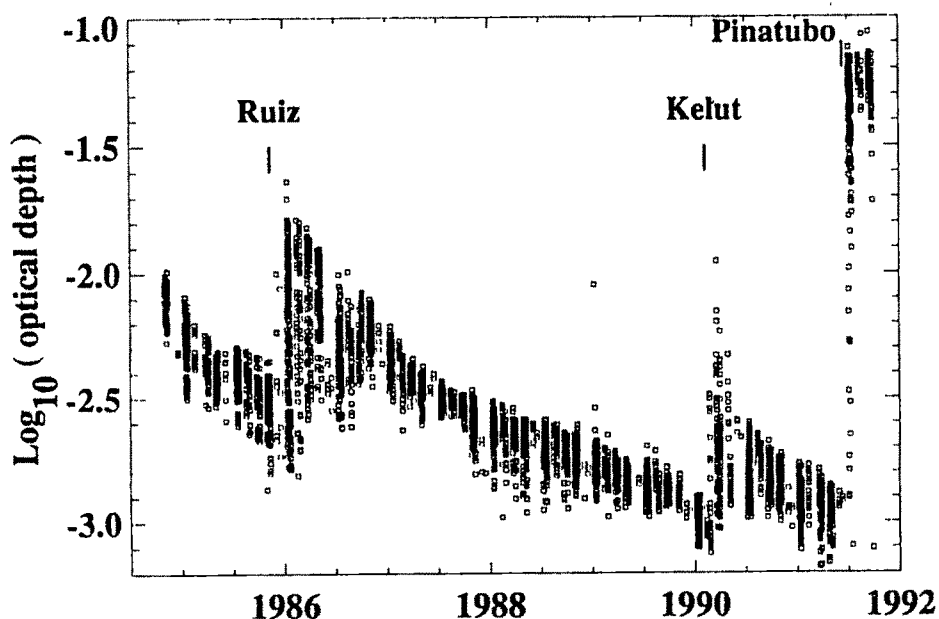


Figure 4.3: *SAGE II aerosol optical depths computed from integration of the 1020 nm extinction profiles over the altitude range from 3 km above the tropopause to 40 km (from McCormick and Veiga, 1992).*

level to about 28 km [DeFoor *et al.*, 1992]. Labitzke and McCormick [1992] using analyses of rawinsonde-derived temperature profile data have shown that warming occurred at 30 mb and 50 mb (approximately 24 and 20 km, respectively) at latitudes over the tropics and the warming at the equator in September 1991 was as high as 4°C. Stowe *et al.* [1992] state that the globally averaged net radiation may be reduced by about  $2.5 \text{ Wm}^{-2}$  (equivalent to a cooling effect of at least 0.5°C) at the surface once the aerosol is distributed globally over the next 2 to 4 years. Minnis *et al.* [1993] determined from the radiative flux anomalies derived from the Earth Radiation Budget Experiment measurements that the radiative cooling caused due to Mt. Pinatubo eruption during August-September 1991 was  $2.7 \pm 1.0 \text{ Wm}^{-2}$ . After a volcanic eruption, the large ash particles settle out during the first few months and the sulphuric acid droplets and sulphate aerosols become important in determining the radiative forcing. Pollack *et al.* [1981] have demonstrated that the radiative forcing varied as a function of aerosol composition, size and altitude. For example, the size distributions of stratospheric aerosols measured after El Chichon eruption showed that the particle size decreased from an effective radius of about  $1.4 \mu\text{m}$  after 1.5 months after the eruption to about  $0.5 \mu\text{m}$  after 6.5 months [Hofmann and Rosen, 1983], hence such a drastic change in the size of the aerosol particle will have a considerable

effect on the volcanic aerosol forcing. Recently *Lacis et al.* [1992] showed that though the climate forcing is a function of the aerosol size distribution, the size dependence can well be described by a single parameter namely effective radius  $r_{\text{eff}}$ . When the effective radius  $r_{\text{eff}}$ , defined as the mean radius of the size distribution weighed by the cross sectional area, becomes greater than  $2 \mu\text{m}$  the global average of the greenhouse effect of the aerosols is found to exceed the albedo effect, causing a surface heating [*Lacis et al.*, 1992].

*Krueger et al.* [1992] using TOMS data have found that the 1991 Antarctic springtime ozone decline was the maximum, when the columnar ozone concentration values were 8 DU less than 1987 and 1990 springtime declines, earlier deep ozone hole years. Recent report [*Ozone Trends Panel*, 1994] shows that both the 1992 and 1993 springtime ozone values are still lower than that of the 1991 values. This has been attributed to the presence of Pinatubo aerosols. The fact that the 1994 ozone loss is not as severe compared to the previous years further substantiates this view. Using electrochemical concentration cell sondes, airborne UV differential absorption lidar system and SAGE II measurements, *Grant et al.* [1994] have found ozone decreases of up to 33%, over the tropics, in the 16 and 28 km altitude region, which coincided with enhanced aerosol loading due to Pinatubo eruption. *Hofmann et al.* [1994] using the aerosol backscatter lidar data at 532 nm, the aerosol concentrations using particle counters and the ozone vertical profiles, have found ozone deficits as large as 30% between 14 and 20 km over Laramie, Wyoming ( $41^\circ\text{N}$ ) (Figure 4.4). This figure also shows the close correspondence between the region of maximum ozone deficit and the location of Pinatubo aerosol layer. The large ozone depletion in the Antarctic as well as in the tropics is attributed to the presence of large amount of Pinatubo aerosols, which aided the heterogeneous chemistry to take place much faster. Using differential absorption lidar measurements *D'Altorio et al.* [1993] have found that the aerosol surface area densities have increased by about 20 times over midlatitudes, between 17 and 22 km. At Laramie, Wyoming ( $41^\circ\text{N}$ ) the surface areas have increased by a factor of 10 to 20 in the stratosphere, below 25 km, during the June 1991 - January 1993 period [*Deshler et al.*, 1993].

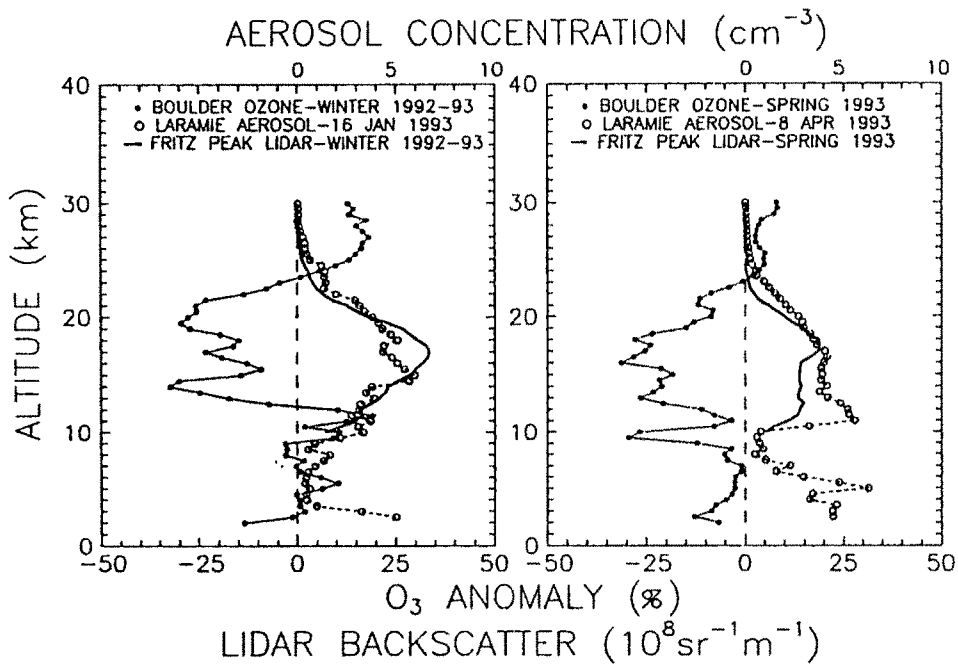


Figure 4.4: Profiles of ozone anomaly (as compared to 1985-1988 average), lidar backscatter and aerosol concentration as measured during the winter (December, January and February) and spring (March, April and May) of 1992-93 at Boulder, Fritz Peak and Laramie respectively, indicating a close relation with the enhanced aerosol loading which through heterogeneous phase chemistry has led to ozone depletion (from Hofmann *et al.*, 1994).

### 4.3 Measurement techniques

Much of what we know today about stratospheric aerosols, started with the pioneering work of Junge [Junge *et al.*, 1961] about 4 decades ago, who by *in situ* measurements collected aerosol samples using balloonborne cascade impactors and discovered the existence of the stratospheric aerosol layer, which is also referred to as 'Junge' layer. Soon after, the availability of high-altitude research aircraft made more spatial and altitude coverage possible [Junge and Manson, 1961]. The measurement of stratospheric aerosols by collecting samples improved with the development of new techniques such as palladium wire impactors [Bigg, 1976; Farlow *et al.*, 1979], cascade impactors [Sheridan *et al.*, 1992] and jet impactors [Goodman *et al.*, 1994]. A different application of the impactor technique was evolved, in which each impaction plate is a tuned piezoelectric quartz crystal oscillator and the change in frequency determines the mass accumulated on each impactor stage [Chuan, 1976].

In all the above methods, the samples collected have to be analysed in the laboratory to determine the physical and chemical characteristics of aerosols, for example the concentration, size distribution and composition which in turn gives the refractive index. These techniques suffer from the drawbacks of contamination or evaporation of samples collected before the laboratory analysis. Also, the microscopic examination of the impaction samples is tedious and time consuming and the accuracy and efficiency of the measurement, are questionable [Bigg, 1976].

Rosen [1964] developed an *in situ* optical particle counter having a light source, a photomultiplier tube and a pulse height analyser. As the particles enter the system, the scattered radiation is converted to electrical pulses and are counted for the number density and analysed for the particle sizes. This system was simple, reliable and could be easily mounted on a balloon gondola and the estimation of the particle density and size distribution could be obtained, altitude wise [Hofmann and Rosen, 1983; Deshler et al., 1993].

Attempts were made in the late 1970s to determine the stratospheric aerosol characteristics by using polar nephelometer [Grams, 1981] and retrieve the aerosol phase functions.

Remote optical sensing of aerosols has the advantage of not disturbing the medium of investigation. Several ground based, balloon and satellite based techniques have been developed and are being used extensively. One of the first techniques was the use of intensity-modulated search lights [Elterman, 1966], in which the search light was pointed vertically upwards or at different elevations and the characteristics of aerosols could be obtained up to about 35 km. This principle could be more effectively used with the availability of lasers to study the vertical profiles of aerosols on a continuous basis and now are being extensively used worldwide [Fiocco and Grams, 1964; Thomas et al., 1981; Parameswaran et al., 1991; Jäger and Hofmann, 1991; Jayaraman et al., 1995a] to determine the aerosol characteristics. In backscatter lidar systems, the transmitter and the receiver are collocated and the backscattering coefficient of aerosols is measured.

Measurements of the direct solar radiation and the scattered radiation intensities is another modest and a refined way of obtaining the aerosol characteristics, such as the aerosol optical depth. The wavelength dependence of the optical depth can be used to infer the size distribution function [Ångström, 1961; Rangarajan, 1972; Michalsky et al.,

1990]. However, in this technique knowledge about the total content of the absorbing gases such as ozone and water vapour are essential. Measurements of twilight radiations [Volz and Goody, 1962; Ashok *et al.*, 1982] and on the intensity distribution around solar aureole [Deepak and Adams, 1983] have been made to determine the aerosol characteristics. Scattering measurements have been done using balloons, aircrafts and rockets [Newkirk and Eddy, 1964; de Bary and Rossler, 1966; Subbaraya and Jayaraman, 1982]. These *in situ* measurements have been successfully used to determine the altitude variation of aerosol characteristics such as, extinction coefficient, mode radius, concentration and size distribution.

Though large information about aerosols can be obtained from ground based and *in situ* measurements, they are usually restricted both in time and space. Also, the balloon-borne measurements are quite costly. For an extensive period of observation and for global coverage, satellites are best suited. The SAM II (Stratospheric Aerosol Measurement II) experiment onboard NASA's NIMBUS 7 satellite launched in October 1978 and the SAGE (Stratospheric Aerosol and Gas Experiment) onboard NASA AEM-2 satellite launched in February 1979 and later SAGE II launched in October 1984, have provided an excellent source of data of aerosol characteristics, for about 2 decades [McCormick *et al.*, 1979; Kent and McCormick, 1984; Lenoble and Brogniez, 1985; McCormick and Veiga, 1992; Trepte *et al.*, 1994]. The SAM II and SAGE satellite sensors consist of Sun photometers designed to measure atmospheric extinction in certain wavelength bands during satellite sunrise and sunset [McCormick *et al.*, 1979]. While SAM II is a one channel instrument providing aerosol extinction profiles at  $1.0 \mu\text{m}$ , SAGE has four wavelength bands centered at  $0.385 \mu\text{m}$ ,  $0.45 \mu\text{m}$ ,  $0.6 \mu\text{m}$  and  $1.0 \mu\text{m}$ , to measure aerosol extinction profiles as well as ozone and nitrogen dioxide profiles. SAGE II launched in October 1984 aboard the Earth Radiation Budget Satellite has been continuously measuring gas and aerosol extinction profiles at the Earth's limb during each solar occultation experienced by the satellite, by Sun photometers at the seven wavelength bands centered at  $0.385 \mu\text{m}$ ,  $0.448 \mu\text{m}$ ,  $0.453 \mu\text{m}$ ,  $0.525 \mu\text{m}$ ,  $0.6 \mu\text{m}$ ,  $0.94 \mu\text{m}$  and  $1.02 \mu\text{m}$ , since its launch [McCormick and Veiga, 1992]. All the above data put together have become an exhaustive and an important data set for the study of both nonvolcanic, background and volcanically perturbed conditions and the decay of stratospheric aerosols, connected throughout in time and space, on a global scale.

More recently, the Improved Stratospheric and Mesospheric Sounder (ISAMS) onboard the Upper Atmospheric Research Satellite (UARS), launched in September 1991, was used to study the spatial and temporal evolution of the volcanic stratospheric aerosol from Mt. Pinatubo [Lambert *et al.*, 1993].

#### 4.4 Balloon-borne optical studies of Pinatubo aerosols over tropical India

*In situ* measurements have the distinct advantage of giving a detailed insight into the various physical processes involved in the formation of sulphate aerosols and their evolution at stratospheric altitudes, especially after large volcanic eruptions as compared to satellite measurements. Though satellite measurements can give a global view of the volcanic impact and have the advantage of not disturbing the medium of investigation, the solar intensity passing through the volcanic aerosol layer will not be often high enough to obtain a transmission measurement reliably and so the measurements are to be truncated at certain altitudes. Especially when the opacity of the atmosphere is large, as when occurred during the Pinatubo time frame, extinction measurements at lower altitudes (near and below the peak of the extinction profile) were not possible.

With this in view two balloon experiments were conducted from the National Balloon Facility at Hyderabad (17.5°N, 78.6°E), one in October 1991 and the other in April 1992, 4 and 10 months respectively after the eruption, to study the impact of the Pinatubo eruption over a tropical site as well as its time evolution.

The two balloons carried identical payloads of multiwavelength filter photometers to obtain the vertical profiles of aerosol extinction as well as the aerosol number density and size distribution parameter from the direct and the scattered radiation intensity measurements. The balloons carried a Sun-scanning and a Sun-tracking photometer systems. While the Sun-scanning photometer system is used to obtain the direct as well as the scattered radiation intensities, the direct solar radiation intensities are also measured using the Sun-tracking photometer system uninterruptedly. While the measurement of extinction coefficients gives details about the scattering and absorption properties, thus their effect on the radiative budget, the study on the size distribution parameter and

the number density of aerosols gives details about the formation, evolution and decay of stratospheric aerosols. As the balloon programme for atmospheric aerosol studies under Indian Middle Atmosphere Programme was in the formative stage and also as the instrument was under fabrication during 1982, the opportunity given by the El Chichon eruption to study the characteristics of volcanic aerosols could not be utilised, though two balloon experiments in the decaying phase of the El Chichon volcanic aerosol layer could be conducted. Hence, these two balloon experiments conducted in 1991 and 1992, have yielded for the first time, the almost complete set of volcanic aerosol parameters needed to study quantitatively their impact on atmospheric radiation balance. Moreover these are the only *in situ* optical measurements made in India and to the best of knowledge anywhere in the tropics around the globe and most of the other measurements of Pinatubo aerosols have been from high latitudes.

While the balloon-borne measurements are the best suited to study the role of various physical processes going on at the stratospheric altitudes which control the aerosol size distribution and the number density, Lidar technique is useful in monitoring the decay of the aerosols, as conducting balloon experiments often, proves costly. Also, as the vertical profiles of aerosol extinction are obtained, a detailed study on the vertical dispersion and sedimentation of aerosols is possible, using the lidar data.

#### 4.4.1 Instrumentation

The Sun-scanning multichannel photometer system, developed [Acharya *et al.*, 1985] to measure the direct as well as the angular distribution of the scattered radiation intensities during balloon ascent, has been in use since 1983 and results on the stratospheric aerosols obtained before the Mt. Pinatubo eruption have been previously reported [Jayaraman *et al.*, 1987]. Previous results show that large variations are found in the aerosol concentrations obtained over Thumba and Hyderabad at all altitude levels, with few hundreds of particles at 10 km and decreasing to a few particles at the stratospheric altitudes. Also, the derived aerosol size distribution parameter (the slope of the Junge power law size distribution) was found to be in the range of 2.8 to 3.4 in the 18 to 30 km altitude region [Jayaraman and Subbaraya, 1988; Jayaraman, 1991].

Figure 4.5 shows the functional block diagram and photograph of the Sun-scanning

multichannel filter photometer system. The instrument consists of a sensor assembly containing six filter photometers, a Sun-tracking mechanism and a motor assembly for scanning the sky along the solar almucantar,  $\pm 90^\circ$  with respect to the Sun for scattered sky radiation measurements. The photometer is a combination of a photodiode/phototube and an interference filter. Baffles are used to restrict the total field of view of photometers to about  $9^\circ$ . The central wavelengths of the photometers used in the Sun-scanning system are 276, 310, 494, 744, 845 and 952 nm having bandwidths (Full Width at Half Maxima) of 10, 9, 10, 14, 20 and 20 nm, respectively. However, in figures and further discussions these photometers are designated to the round off wavelengths as 280, 310, 500, 750, 850 and 950 nm. As the same photometers are used to measure both direct and scattered radiation intensities, the detector and the amplifier should have low noise level and large dynamic range. Hamamatsu R 765 phototube which has a spectral response between 160 and 320 nm is used for 280 and 310 nm and UV-100 (EG & G) photodiodes are used for other wavelengths. The photodiodes are so chosen to have dark currents in the picoampere range which is 2 orders of magnitude less than the minimum expected signal. Current generated by these photodetectors are fed to six temperature compensated logarithmic current to voltage amplifiers which have a dynamic range of six orders of magnitude from 1 nA to 1 mA. During each rotation of the platform, the tracking mechanism is switched on for  $\pm 30^\circ$  near the vicinity of the Sun using a double slit sensor, consisting of two photodiodes and slits separated by an angle of  $60^\circ$ . The scanning is achieved in 18 seconds corresponding to an altitude ascent of about 90 metres by the balloon, which sets the lower limit of the altitude resolution of the various quantities, the aerosol extinction, number density and size distribution parameter, that are measured.

In addition to the Sun-scanning photometer system an automatic two-axis stabilised continuous Sun-tracking photometer system (described in detail in Chapter 3) was also employed in order to get the altitude profiles of the direct solar radiation intensities uninterruptedly. The central wavelengths of the photometers used in the Sun-tracking system are 310, 440, 494, 848, 952 and 1051 nm having bandwidths of 9, 10, 12, 14, 20 and 25 nm, respectively. In figures and further discussions these photometers are referred to as 310, 440, 500, 850, 950 and 1050 nm. Four of the wavelengths are similar to the Sun-scanning system in order to cross validate the data. The two other spectral bands (440

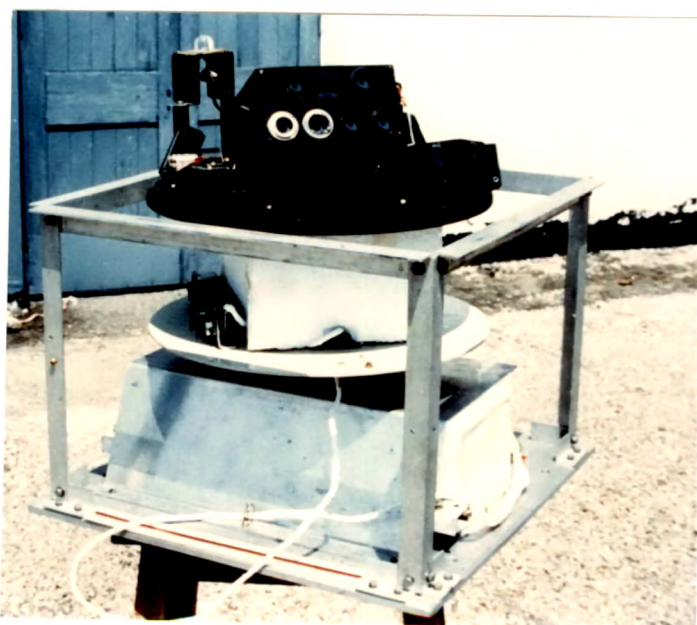
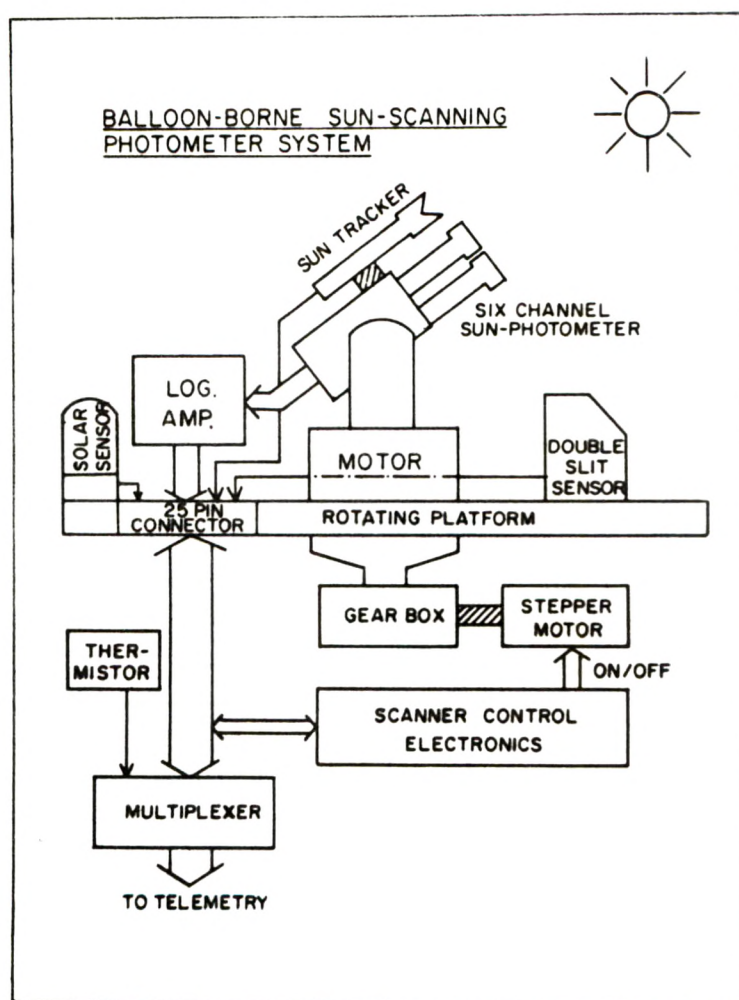


Figure 4.5: Functional block diagram and photograph of the Sun-scanning photometer assembly used onboard balloons for the measurement of the angular distribution of the scattered solar radiation intensities.

and 1050 nm) are used in the Sun-tracking system to increase the spectral resolution and extent of the measurements. Linear amplifiers are used in the Sun-tracking photometer for the direct solar radiation intensity measurements.

The tracking of the Sun in elevation is achieved using two photodiodes mounted perpendicular to each other in the vertical plane. The difference signal is amplified and fed to a servo motor which orients the sensor assembly towards the Sun. The vertical tracking mechanism corrects for the change in the solar elevation during the balloon flight. In Sun-scanning photometer assembly a solar sensor has been used to activate the system only in the presence of the Sun. The solar sensor switches on the power to stepper motor, which is used for azimuthal scanning. A thermistor is used to monitor the temperature inside the detector assembly. The outputs are multiplexed with a 5V and 0V square wave marker to indicate the scanning direction of the photometer. While the data corresponding to 280 nm and 950 nm are aimed at retrieving the vertical profiles of ozone and water vapour number densities, data from the other channels are used for aerosol studies, the results of which are presented here.

#### 4.4.2 Experiment

The hydrogen inflated zero pressure balloons are designed to reach a ceiling altitude exceeding 30 km. Figure 4.6 shows the loadline of the balloon experiment, consisting of the payload, radiosonde, radar reflector, apex valve, parachute etc. The length of the loadline is adjusted such that the balloon shadow does not fall on the instrument at higher solar elevation. The balloon has a volume of about 54,000 m<sup>3</sup> and is made from 'stratofilm' having a thickness of about 20 μm. The balloon is filled with the lifting gas hydrogen to about 1% of its volume, just before the launch. The preflight activity involves among other things, studying the prevailing winds at ceiling altitude by conducting wind sounding flights and logistics associated with launching of a balloon including liaison with local Civil Aviation authorities [Joshi, 1991]. The balloon along with the instruments is launched by dynamic launch method [Damle *et al.*, 1983]. Till 1976, onboard recording of the scientific data was in practice in most of the experiments. But at present a 25 kbit/sec standard PCM telemetry encoder is in use. The telemetry flight data are recorded on high speed tape recorders. The outputs of the photometers are digitised at a rate of 25 samples/sec

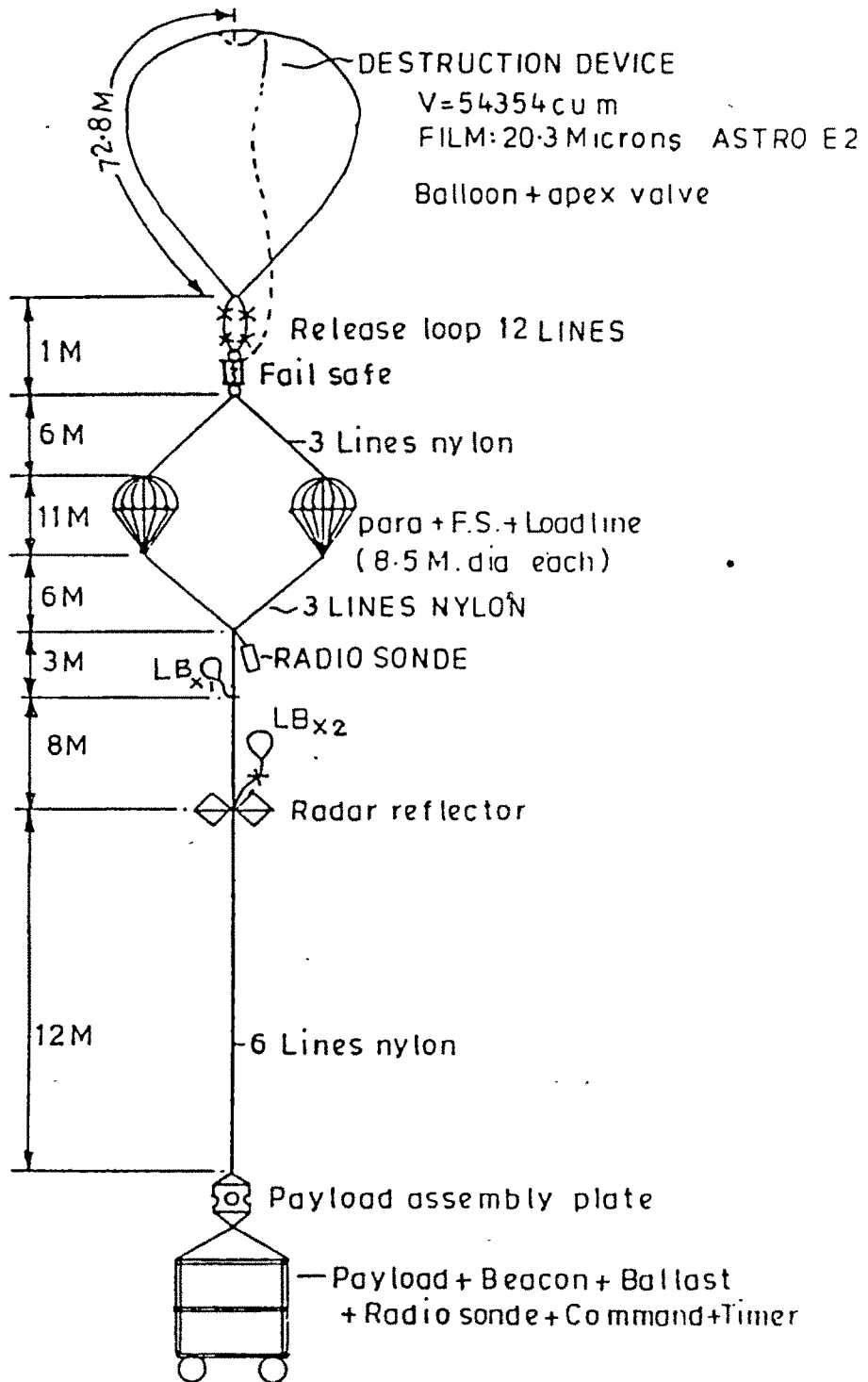


Figure 4.6: Loadline of the 26 October 1991 balloon flight (not to scale).



Figure 4.7: *Picture showing the payload assembly on the launch truck, alongwith the radar target, radiosonde etc. and the launch balloon, minutes before the launch.*

using onboard A/D convertor. Also in these experiments the data are recorded on paper charts for quick look analysis. A PDM/FM/AM telecommand system is used both for inflight control of the scientific experiments and balloon flight control/operation, such as ballast dropping, apex valve control and flight termination. There are three main aspects of the balloon flight control, namely, the balloon tracking, ballast release system and a flight termination device. Additionally, in some flights, balloon apex valve control for slow controlled balloon descent from the ceiling altitude down to about 20 km which enables to get additional data for the important altitude region at which the volcanic aerosol layer resides is also involved. During the balloon flight the temperatures can go as low as  $-20^{\circ}\text{C}$  inside the gondola, especially near the tropopause and hence the instrument and the associated electronics setup are given thermal protection. Figure 4.7 shows the picture of the payload assembly on the launch truck, launch balloons for the radar target, radiosonde and the balloon at the far end of the photograph, minutes before the launch. The first balloon was launched on 26 October 1991 (henceforth referred to as the October flight) at 0608 hrs (local time), close to the local sunrise time. Figure 4.8 shows the balloon ascent a few minutes after take off. The balloon reached the expected ceiling altitude of about 34 km at about 0810 hrs with an average ascent rate of about  $280 \text{ m minute}^{-1}$ . A ground based radar of the India Meteorological Department (IMD), Hyderabad was used for balloon tracking. This provided continuous information on balloon position (latitude,

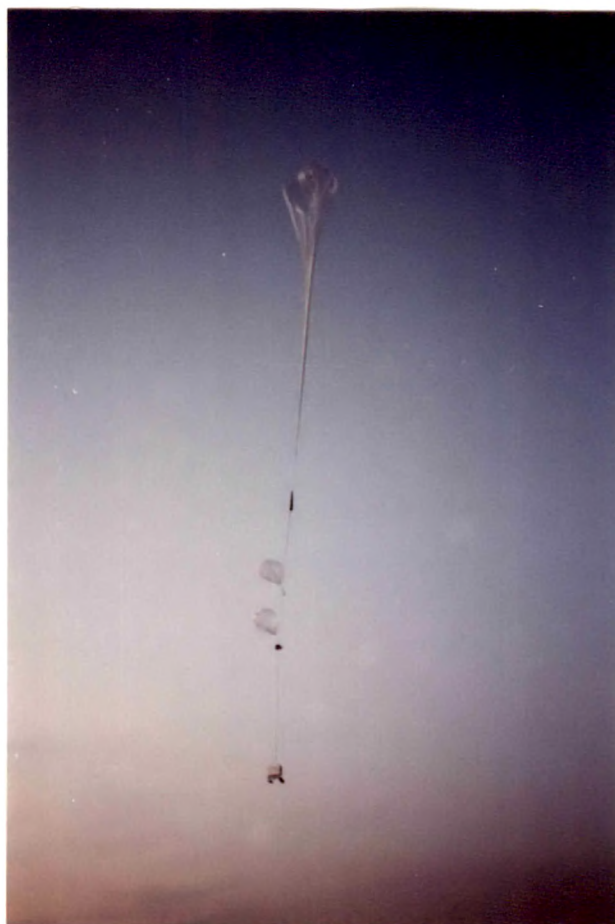


Figure 4.8: *Balloon carrying the gondola, a few minutes after take off.*

longitude of the balloon) and its height in kilometres above the mean sea level during all important phases of the flight. A steerable 2.5 m dish antenna and also a 'radio theodolite' unit that receives 375 MHz balloon telemetry signal provided rough balloon position and the radiosonde gave information on the balloon altitude. A special airborne pressure-altitude (baratron) sensor was also included to determine the balloon altitude more accurately. After about two hours of float duration, the balloon could be brought down to about 26 km by releasing the gas through an apex valve incorporated in the balloon, in about two hours. A ballast release system operating through telecommand was used, when required, to accelerate the balloon during the ascent phase and also to maintain the ceiling altitude by a controlled release of magnetic ballast, which was carried as an additional but controllable load. The flight was terminated at 1300 hrs and the instruments were released on a parachute and recovered. An anti-air collision radio beacon is used which forewarns an approaching aircraft of the descending payload train in

space, by transmitting an electrical signal. A specially developed fail-safe device, which is a spring-loaded switch on the balloon loadline, was incorporated in the flight train. It operates instantaneously in case of an accidental balloon burst in flight and separates the parachute-payload system from the balloon [Damle, 1991]. The entire sequence of the balloon flight operation conducted on 26 October 1991 is shown in Figure 4.9a. The same instruments were flown again on 20 April 1992 (henceforth referred to as the April flight) with an advanced launch time of 0558 hrs to accommodate the earlier sunrise in April (Figure 4.9b). Also the balloon was made to float only an hour at the ceiling level of 33.5 km which helped to get additional descent data for the stratospheric region. The results presented are the average of the ascent and descent data wherever applicable. In both the experiments all the scientific as well as technical instruments such as barotrons for pressure monitoring, radiosonde and telecommands worked satisfactorily. Data corresponding to the altitude region of 10 to 34 km in the case of the October 1991 flight and from 5 to 34 km in the case of the April 1992 flight are presented. The low-altitude data correspond to high solar zenith angles and hence are affected by the curvature of the Earth and multiple scattering through the long optical paths. In the case of the October flight, low-altitude clouds are also found to contaminate the data below 10 km.

## 4.5 Results and Discussion

### 4.5.1 Aerosol extinction coefficients

The data analysis essentially involves the estimation of the attenuation of the incoming solar radiation at each altitude. If  $I$  is the intensity of the solar radiation at altitude  $z$ , then the total atmospheric extinction coefficient  $\beta$  ( $\text{km}^{-1}$ ) at  $z$  could be written using Beer-Lambert's law as,

$$\beta(z) = \frac{dI}{I(z) dz \sec \chi} \quad (4.11)$$

where  $\chi$  is the solar zenith angle at the time of observation and  $\sec \chi$  gives the atmospheric airmass. Vertical profile of the direct solar radiation intensity obtained on 26 October 1991 at 500 nm is given in Figure 4.10, as an example.

The total atmospheric extinction coefficient  $\beta$  is made up of

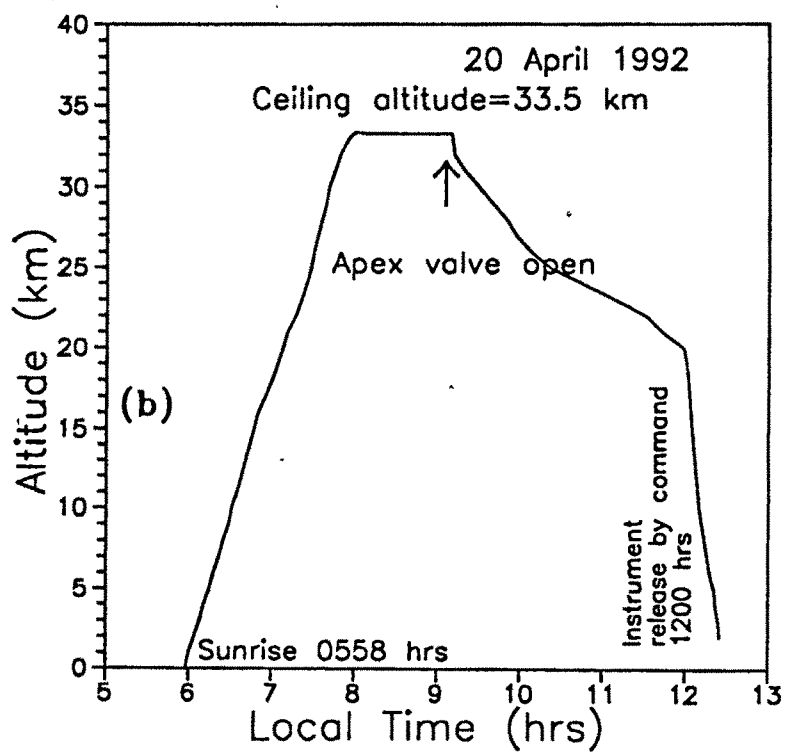
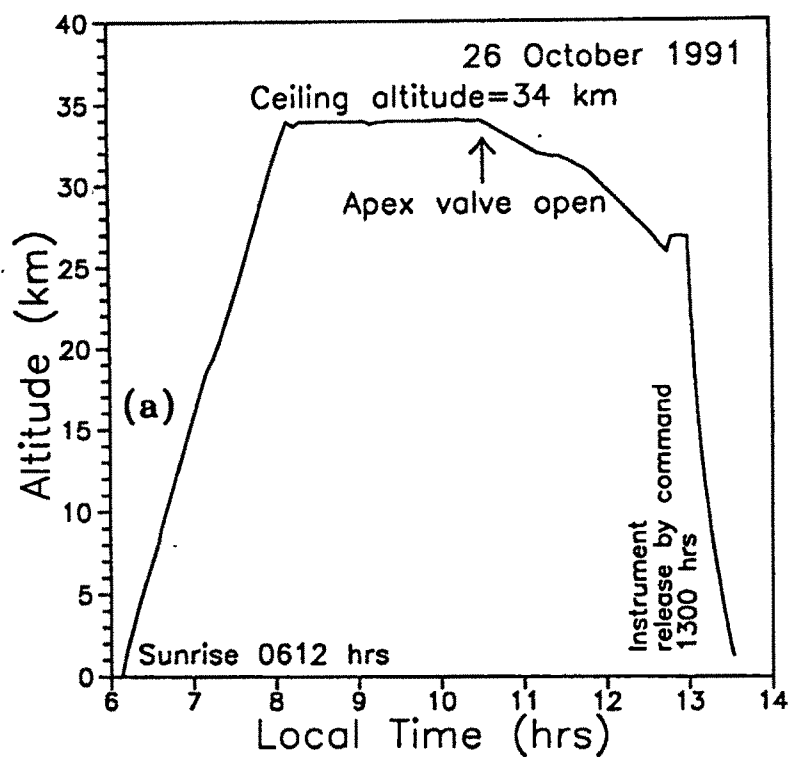


Figure 4.9: History of the (a) 26 October 1991 and (b) 20 April 1992 balloon flights.

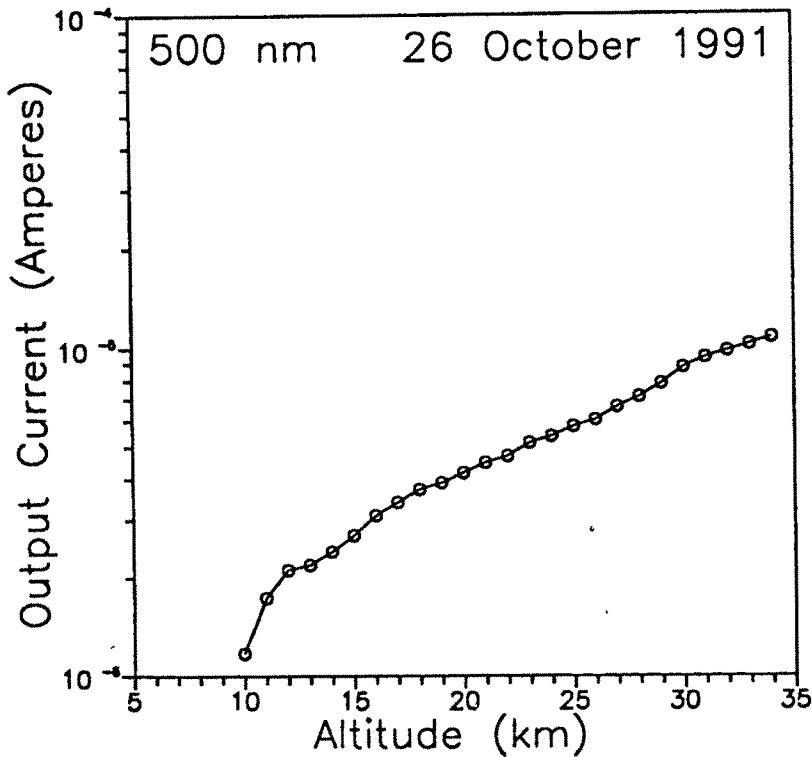


Figure 4.10: Vertical profile of the direct solar radiation intensity obtained on 26 October 1991 at 500 nm.

$$\beta = \beta_{\text{ma}} + \beta_{\text{rs}} + \beta_{\text{aerosol}} \quad (4.12)$$

where  $\beta_{\text{ma}}$  is the absorption coefficient due to molecular gases such as ozone, nitrogen dioxide, water vapour etc.,  $\beta_{\text{rs}}$  is the Rayleigh scattering coefficient (scattering due to air molecules) and  $\beta_{\text{aerosol}}$  is the aerosol extinction coefficient. The air density profile (Figures 4.11a and 4.11b) constructed from the temperature and pressure data obtained from the meteorological balloon soundings on the flight days and the mean ozone density profile available for Hyderabad [Lal *et al.*, 1989] are further used to correct extinction coefficient profiles for Rayleigh scattering and ozone absorption. Absorptions due to nitrogen dioxide in the 400 to 450 nm region, as well as by water vapour at 800 nm, are less than 1% of the total extinction coefficient in the wavelength bands used [Jayaraman and Subbaraya, 1993a]. For the altitudes where measured air density values are not available, *U.S. Standard Atmosphere* [1966] for 15°N is used. Further, the aerosol extinction profiles

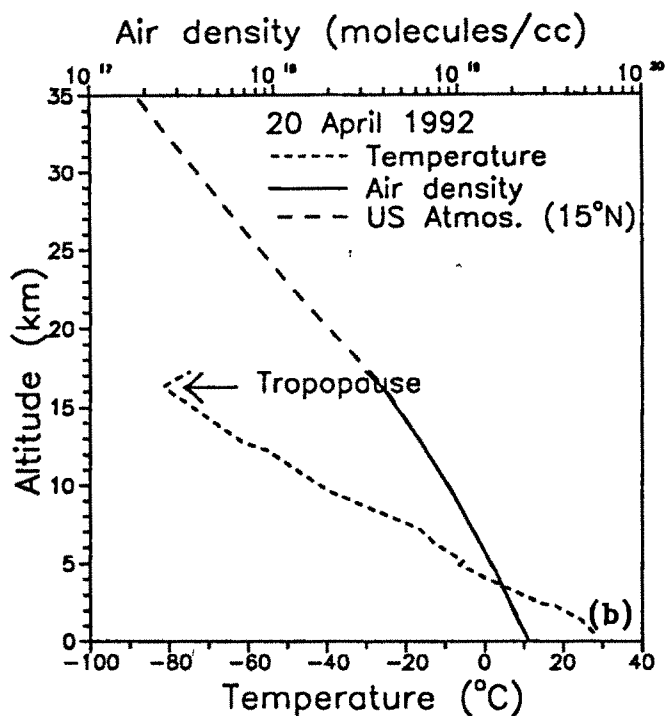
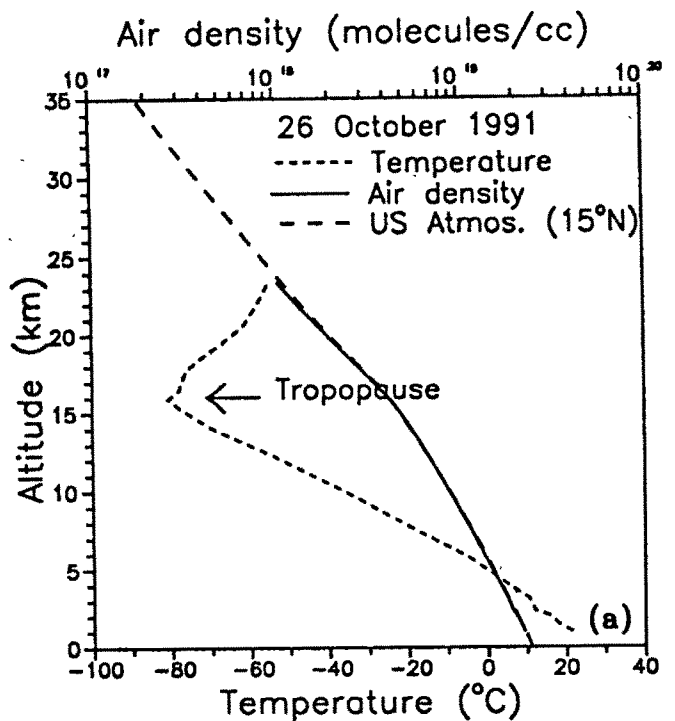


Figure 4.11: The meteorological parameters obtained two hours prior to the aerosol experiments over Hyderabad. The U.S. Standard Atmosphere for 15°N is used in the analysis at altitudes where data are not available.

could be obtained from the direct solar radiation up to about 30 km. Above 30 km, as the altitude increment of the intensities is small, the extinction profiles are calculated from the aerosol number density and  $\nu$ , derived from the scattered sky radiation measurements.

Using Sun-tracking mechanism the solar radiation intensities,  $I(\lambda)$  are measured with an accuracy better than 1%. The analog  $I$  values are digitised and recorded on magnetic tapes for detailed analysis. However, as the aerosol extinction coefficients are derived from the total extinction coefficients after correcting for the contribution due to scattering and absorption by the molecular species, the accuracy of the final results depends on the accuracy of the input parameters. In the absence of meteorological radiosonde data on the air density profile, model values [*U.S. Standard Atmosphere*, 1966] are used. In general, the derived aerosol extinction coefficient profiles have a maximum uncertainty of 10% in the lower altitudes which increases to about 30% at the stratospheric altitude levels.

Figures 4.12a-d show the aerosol extinction coefficient profiles after correcting for molecular scattering and absorption at 310, 440, 500, 750, 850 and 1050 nm for the October and April flights. The Pinatubo aerosol layer is seen as an increase in the extinction values above the tropopause between 16 and 30 km altitude region. The peak of the aerosol layer is seen at 23 km in October 1991 with an aerosol extinction coefficient of about  $10^{-2} \text{ km}^{-1}$ . Typically an order of magnitude increase in the extinction is seen between the tropopause and the aerosol peak layer altitudes. Above about 30 km the aerosol extinction gradually decreases to about  $10^{-3}$  around 33 km. In general, the features observed are the same at all wavelengths. In the April 1992 measurement the extinction profiles are characterised by two layers, one between 16 and 24 km and the other between 25 and 30 km. While the features observed are similar at all the wavelengths, the 310 nm aerosol extinction profile shows a predominant hump structure at the 25 to 30 km region in both the measurements. The 310 nm profiles are corrected for the ozone absorption using the mean ozone profile constructed from several individual ozone measurements made over Hyderabad [*Lal et al.*, 1989]. Interestingly, if the Pinatubo aerosols had an effect on ozone it could have been a decrease in the ambient ozone concentration by about 5% at these altitudes as shown by *Grant et al.* [1992] and hence the use of a mean ozone profile is expected to overestimate the ozone correction and as a consequence a decreased aerosol extinction. In general, the extinction coefficients at all wavelengths are about 2 orders

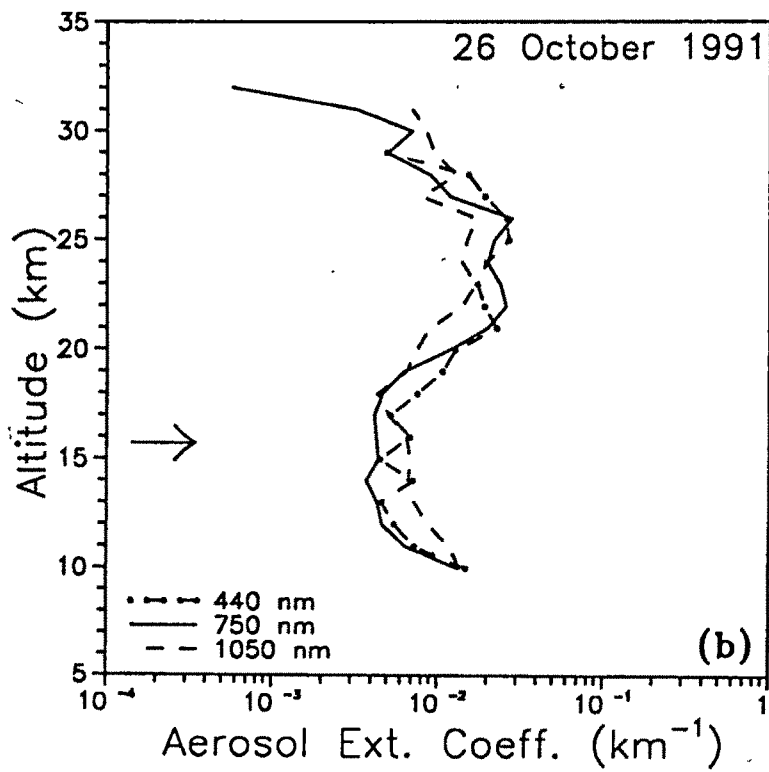
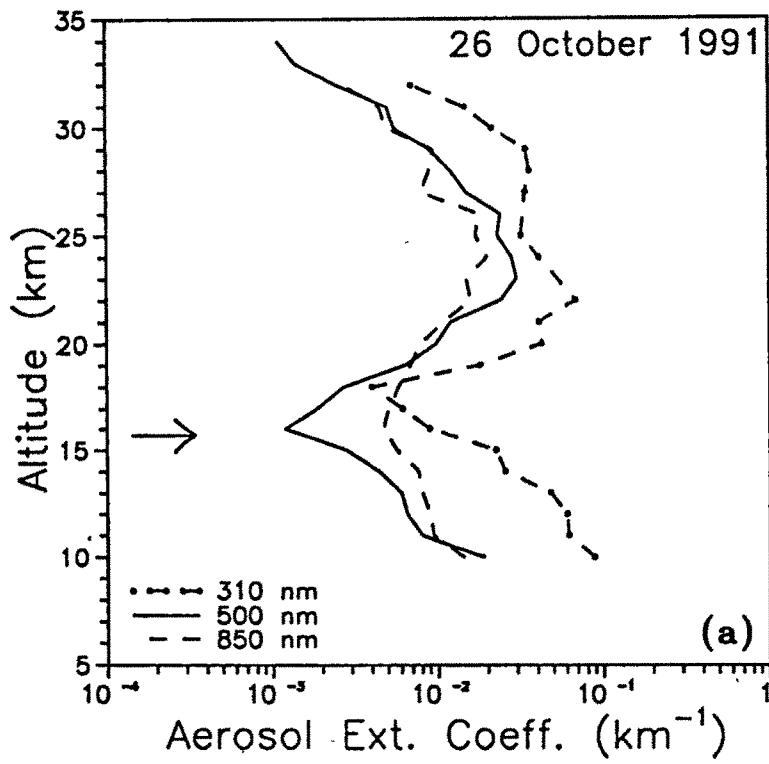
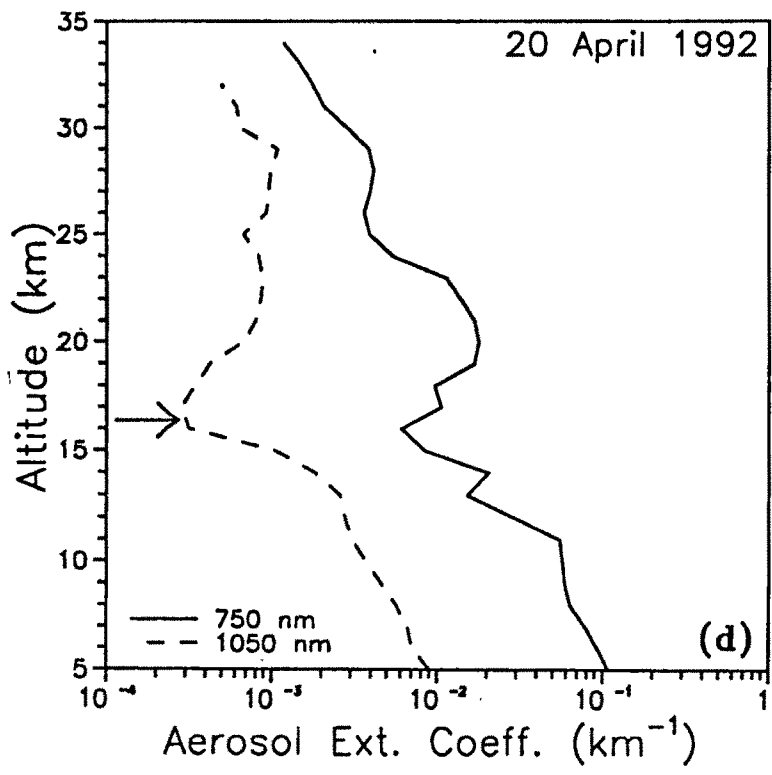
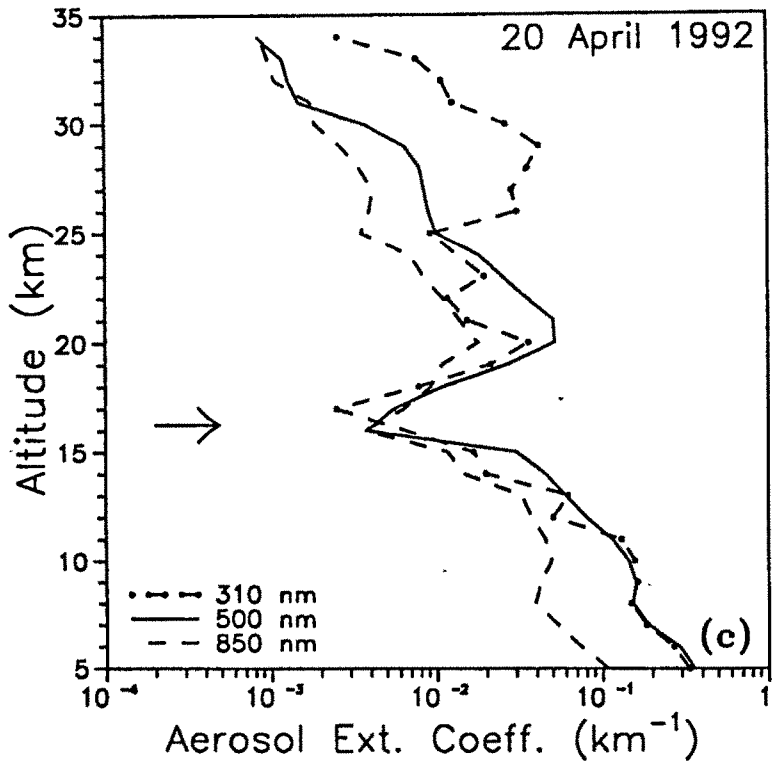


Figure 4.12: Profiles of aerosol extinction coefficients obtained over Hyderabad ( $17.5^\circ\text{N}$ ) during October 1991 and April 1992 balloon experiments. The arrows indicate tropopause level.



higher in magnitude at the peak altitude when compared with that of the 1985 values measured over Hyderabad [Ramachandran *et al.*, 1994b]. The 1985 aerosol extinction coefficient values are the lowest values ever obtained at stratospheric altitudes during a decade of stratospheric aerosol observations over Hyderabad. The 1985 measurement was made 3.5 years after the El Chichon eruption but before the Nevado del Ruiz eruption in November 1985 and therefore can be considered relatively a volcanically quiescent period. The recent results showing the highest values ever obtained over the same site indicate the magnitude of Pinatubo eruption which is estimated to be the strongest in this century [Bluth *et al.*, 1992].

#### 4.5.2 Aerosol number density and size distribution parameter

The aerosol size parameter  $\nu$ , defined as the slope of the power law size distribution is determined by comparing the experimentally observed aerosol scattering phase function with the results of the Mie scattering computation for various  $\nu$  values. The scattering angle  $\theta$  at which the radiation reaches the photometer can be expressed as,

$$\cos \theta = \cos \chi_0 \cos \chi + \sin \chi_0 \sin \chi \cos \phi \quad (4.13)$$

where  $\chi_0$  is the solar zenith angle,  $\chi$  is the zenith angle of the optical axis of the photometer measured from the vertical and  $\phi$  is the azimuthal rotation of the photometer from the Sun. Measurements are performed for the solar almucantar i.e.  $\chi = \chi_0$ . In Figure 4.13 the typical angular distribution of the scattered radiation intensities measured at 5, 10, 20 and 30 km on 20 April 1992 at 500 nm are given, which are further used in determining the aerosol scattering phase functions.

Though the use of a lognormal size distribution may best describe the stratospheric aerosol size distribution, for optically effective particles, in the size range from 0.05 to 10  $\mu\text{m}$ , power law can be taken as a good representation [Volz and Sheehan, 1971; Bigg, 1976]. Though, the power law has a tendency to overestimate the number density of smaller particles, their Mie scattering contribution to the total integrated intensity is however marginal [Jayaraman, 1991]. From the ratio ( $\phi$ ) between the measured aerosol scattering function and the computed Rayleigh scattering function the aerosol number density  $N_z$  can be derived as,

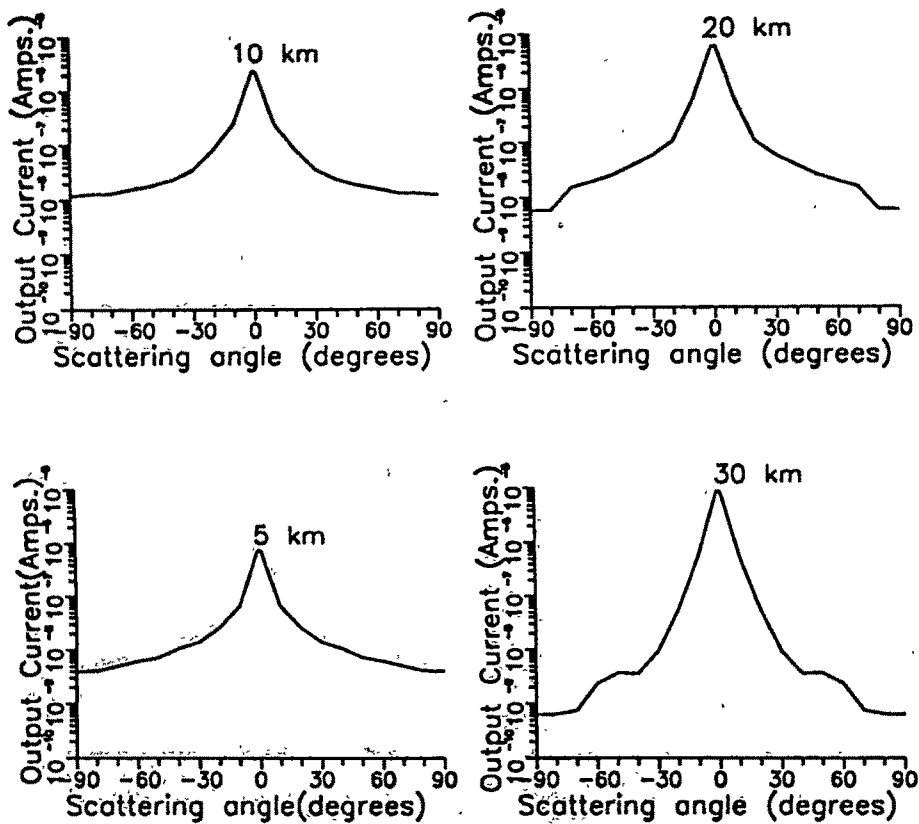


Figure 4.13: Scattered radiation intensities measured at 5, 10, 20 and 30 km on 20 April 1992 at 500 nm.

$$N_z = \frac{3 \sigma_R (1 + \cos^2 \theta) \phi \rho_z}{8 \pi \left(\frac{2\pi}{\lambda}\right)^{\nu-2} \eta \cdot \nu \Gamma_1 \nu \rho_0} \quad (4.14)$$

where  $\sigma_R$  is the Rayleigh scattering cross section at wavelength  $\lambda$ ,  $\theta$  is the scattering angle and  $\eta$  is the Mie angular function [Bullrich, 1964].  $\rho_0$  and  $\rho_z$  are the air densities at the ground level and at altitude  $z$ , respectively. Sensitivity of the assumed refractive index of aerosol (taken as  $1.43 - i1 \times 10^{-8}$  at 550 nm corresponding to 75%  $H_2SO_4$  droplets) and the lower limit of the particle size, taken as  $0.04 \mu\text{m}$  in the Mie scattering computations are found to introduce an error of about  $\pm 0.2$  in the derived  $\nu$  values and an uncertainty of about 20% to 35% in the derived aerosol number density.

Figures 4.14a and 4.14b show the derived aerosol number density profiles for the

October and April flights. A large increase in the aerosol number density is seen above the tropopause and up to about 30 km. In October 1991 the aerosol number density is found to decrease from about 500 particles per  $\text{cm}^3$  at 10 km to about 8 particles at 19 km. The aerosol layer peak occurs at 23 km with about 40 particles per  $\text{cm}^3$ . Using balloonborne optical particle counters *Deshler et al.* [1992] have reported that the particle concentration over Wyoming ( $41^\circ\text{N}$ ) which was less than 1 particle per  $\text{cm}^3$  before the volcanic impact in June 1991 had increased to few tens of particles by July 1991. By the end of August and mid-September a broad volcanic aerosol layer is seen above the local tropopause up to an altitude of about 30 km. A period of about 24 days is found typical [*McPeters, 1993*] for the chemical conversion of  $\text{SO}_2$  to  $\text{H}_2\text{SO}_4$  droplets. The observed increase in aerosol concentration is the result of the  $\text{H}_2\text{SO}_4$  vapour formed after the Pinatubo eruption. Hence, these results obtained about 4 months after the eruption represent the fully grown aerosol particles. Also, the higher aerosol concentration observed over Hyderabad compared to Wyoming results confirm the fact that the aerosols were confined over the equatorial region during the initial period after the eruption. In April 1992 the aerosol number densities (Figure 4.14b) have already shown a decline, with a peak aerosol number density of about 20 particles per  $\text{cm}^3$  at an altitude of about 20 km. The enhancement of particle number density below the tropopause is due to local effects [*Jayaraman and Subbaraya, 1993a*] where there is an accumulation of wind derived dust particles till summer, which however will get rainwashed after the Indian monsoon which is active during the June-September period.

Figures 4.15a and 4.15b show the altitude variation of the size parameter  $\nu$ , the slope of the power law curve for the aerosol size distribution for the October and April flights. The size distribution of the optically effective aerosol particles well above the submicron size range could be described by a simple power law, the steeping edge in the case of a lognormal curve, such that a low value of the slope, represented by a low  $\nu$  value, indicates a greater number of larger particles compared to a higher  $\nu$  value. A value of 3 is found typical for  $\nu$  which represents background aerosol particles. In October 1991 the region between 17 and 23 km shows a marked decrease in the  $\nu$  value which is around 1.8 compared to all other altitudes. This result, derived from the scattered radiation measurement complements the obtained extinction profiles (Figures 4.12a-d)

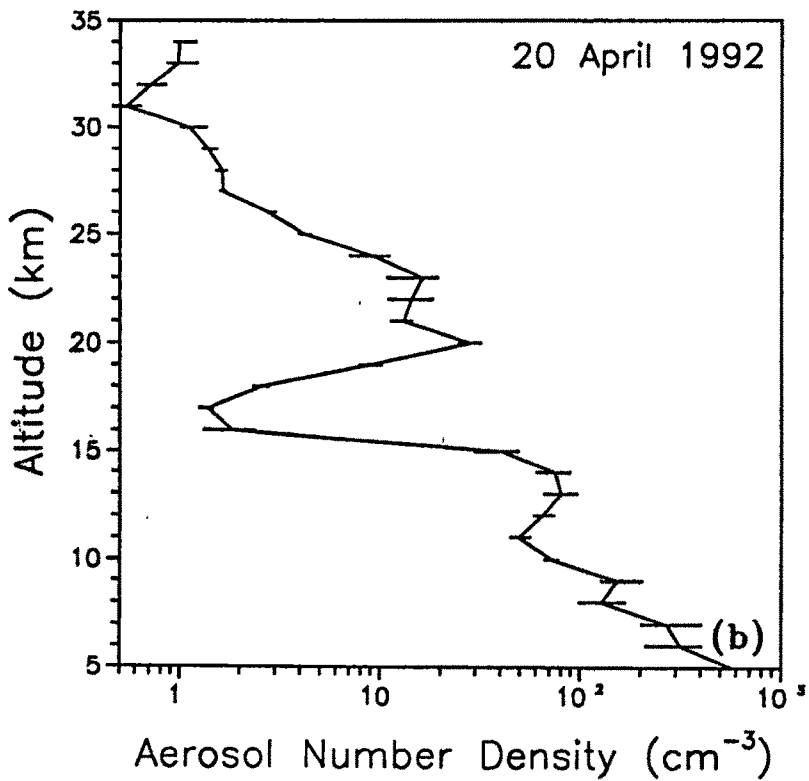
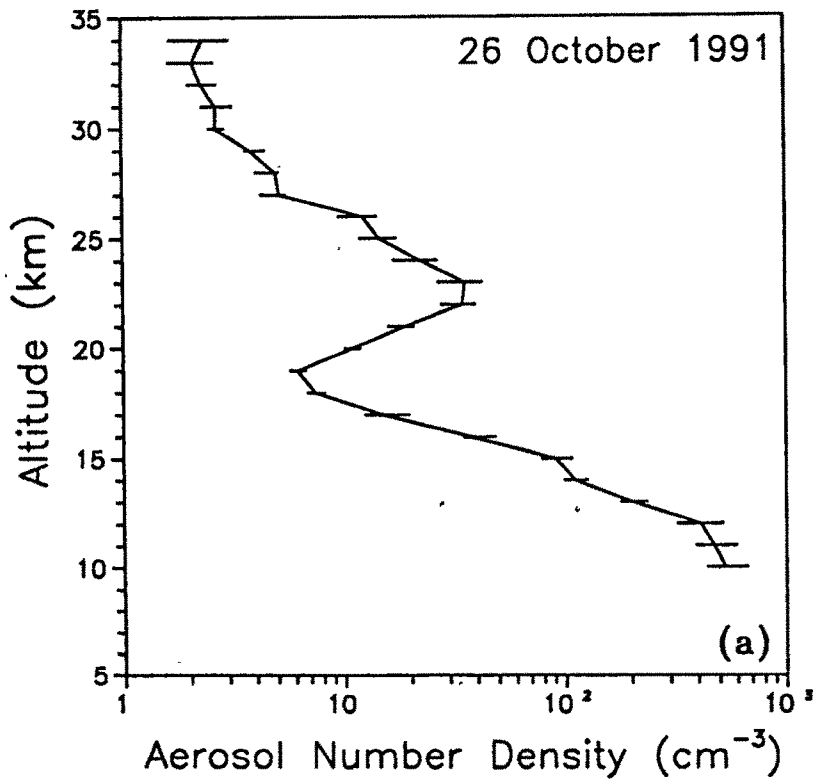


Figure 4.14: The aerosol number density profiles obtained from the scattered radiation intensity data with the lower limit of the particle size taken as  $0.04 \mu\text{m}$ .

derived independently from the direct solar radiation intensity measurements. Though the extinction profiles show a broad maximum above the tropopause which extends to about 30 km, only the lower part of the layer, between 17 and 23 km, contains the larger sized particles. However, the April results show two distinct layers above the tropopause with  $\nu$  less than 2. One layer lies between 16 and 22 km and the other between 25 and 30 km. However, the number density (Figure 4.14) in the 25 to 30 km altitude region shows no corresponding increase. On the contrary, a decrease in density of about 2 particles per  $\text{cm}^3$  is seen during April 1992 compared to about 6 particles in October 1991 in the 25 to 30 km region. This apparent decrease could have been caused both by meridional displacement to higher latitudes and by a coagulation of smaller particles into larger particles and subsequently a reduction in the total number of particles. Any loss of particles due to sedimentation would be insignificant at these altitudes, as a particle of size  $0.5 \mu\text{m}$  having a typical settling velocity of about  $0.015 \text{ cm s}^{-1}$  [Lamb, 1970] takes around 2 years time to be removed from the stratosphere. Deshler *et al.* [1992] using optical particle counters found that at 22-23 km the typical mode radius of aerosols was about  $0.35 \mu\text{m}$ , during July 1991. Since, the experiments were conducted within an year, sedimentation would not have affected significantly the number density of aerosols. The third layer seen in the  $\nu$  profile of April flight, with a corresponding increase in aerosol number density in the 10 to 13 km region, could be due to locally produced dust particles from the arid and semiarid regions of central India. This layer, typical of the Indian region, has been found to exhibit an annual cycle similar to the Indian monsoon [Jayaraman and Subbaraya, 1993a].

### 4.5.3 Ångström coefficient

With an attempt to get further insight into the problem of aerosol size variation with respect to altitude, the parameter  $\alpha$ , defined as

$$\tau = \beta\lambda^{-\alpha} \quad (4.15)$$

where  $\tau$ , the aerosol optical depth and  $\beta$  the so called Ångström coefficient, is derived from the aerosol extinction values, independent of the scattered sky radiation measurement used for deriving  $\nu$ . The obtained  $\alpha$  values are also plotted along with  $\nu$  in Figures 4.15a

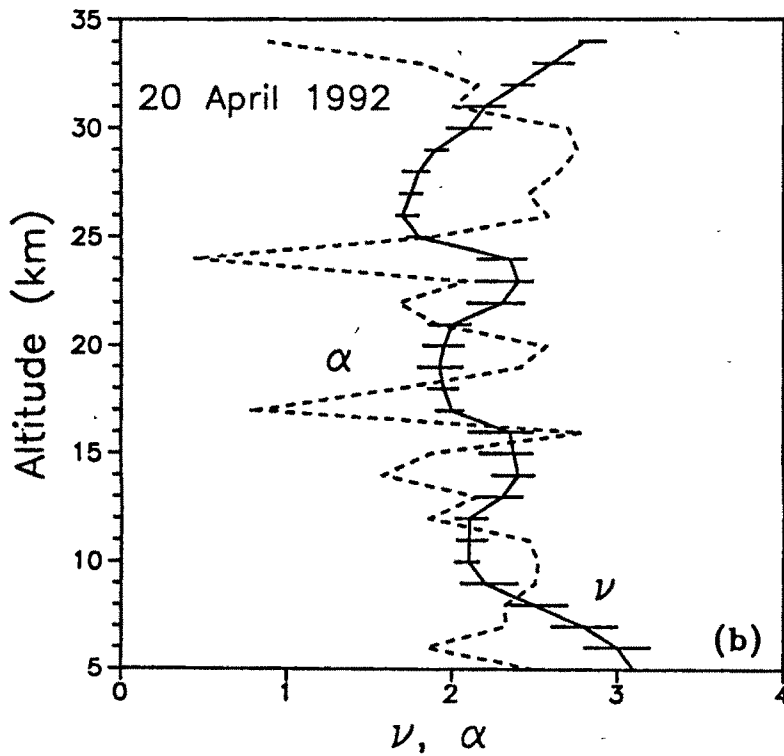
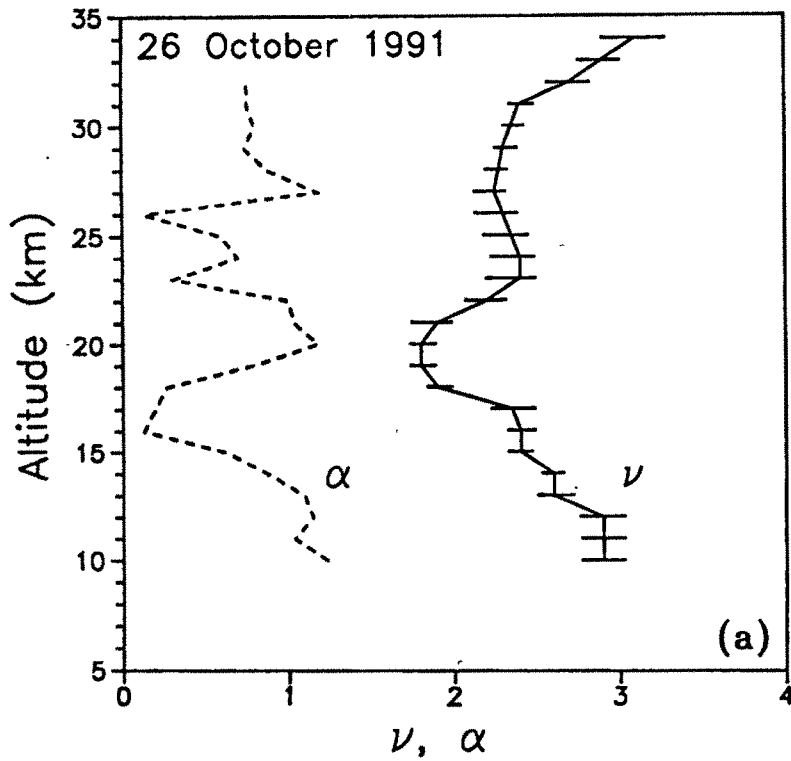


Figure 4.15: Profiles of the aerosol size parameter  $\nu$ , defined as the slope of the Junge power law curve and the wavelength exponent  $\alpha$ , of Eqn. 4.15.

and 4.15b. The  $\alpha$  values obtained during October 1991 are found to be less than or equal to 1 at most altitudes and satisfy the relation  $\alpha = \nu - 2$ , as proposed by *Bullrich* [1964]. In April 1992 however, such a relation is not found to be valid because of the increase in  $\alpha$  values by about 2 at all altitudes while there is no corresponding change in  $\nu$ . While fitting a curve through the extinction coefficients through a limited number of wavelength points, about five in this case, it is not clear why there should be a systematic increase in  $\alpha$  at all altitudes during April, while the error in fitting  $\alpha$  (the error in  $\alpha$  values in general, is in the range of 0.2-0.4), is same in both flights. Another interesting feature observed is the apparent anticorrelation which exists between the  $\alpha$  and  $\nu$  profiles in both flights. The  $\alpha$  and  $\nu$  profiles, in principle should correlate with each other, at least qualitatively, because as the relative size of the particle increases, the slope of the power law curve decreases, as well as does  $\alpha$ , indicating that the aerosol scattering is less dependent on  $\lambda$ . The absence of such a correlation on the experimentally observed data sets indicates that determining  $\alpha$  directly from the extinction coefficients and inferring about the size distribution could be erroneous as it has the inherent assumption that the aerosol absorption is absent and extinction is purely due to scattering. However, in the determination of  $\nu$ , only the measured scattered radiation intensities are used which are compared with the computed scattered radiation intensities.

#### 4.5.4 Mode radius

*Yue and Deepak* [1983, 1984] have proposed a method of retrieving aerosol mode radius from the aerosol extinction coefficients  $\beta$  at two wavelengths. Assuming that the stratospheric aerosol size distribution can be best fitted using a lognormal distribution (LND) function of the form

$$\frac{dn(r)}{dr} = \frac{A}{\sqrt{2\pi} \ln \sigma} \frac{1}{r} \exp \left[ -\frac{\ln^2 \left( \frac{r}{r_m} \right)}{2 (\ln \sigma)^2} \right] \quad (4.16)$$

where  $A$  is the total number concentration ( $\text{cm}^{-3}$ ),  $\sigma$  is the width of the lognormal curve and  $r_m$  is the mode radius, one can retrieve  $r_m$ . A value of 1.86 for  $\sigma$  is considered acceptable in literature [*Pinnick et al.*, 1976] for the stratospheric aerosol layer. On the other hand, if the measurements are made after a major volcanic eruption, such as Mt. Pinatubo, one may decide to choose zero order logarithmic distribution (ZOLD) [*Toon*

and Pollack, 1976] of the form

$$\frac{dn(r)}{dr} = A \exp \left[ -\frac{\ln^2 \left( \frac{r}{r_m} \right)}{2 (\ln \sigma)^2} \right] \quad (4.17)$$

where  $A$  is an arbitrary constant and  $\sigma = 1.8$ . The method involves computing  $\beta$  as a function of  $r_m$  for  $A = 1$  using Mie theory, given by the expression

$$\beta_\lambda = \int_{r_1}^{r_2} \frac{dn(r)}{dr} Q(m, \lambda, r) \pi r^2 dr \quad (4.18)$$

where  $dn(r)/dr$  is the number of particles per  $\text{cm}^3$  whose radii are between  $r$  and  $r+dr$ ,  $Q(m, \lambda, r)$  is the Mie extinction efficiency factor and  $m$  is the refractive index of the aerosol particle. Mie computations are made for the selected photometer wavelengths of 440 and 1050 nm taking the  $m$  values as  $1.432 - i1 \times 10^{-8}$  and  $1.423 - i1.5 \times 10^{-6}$  for the two wavelengths, respectively. The ratio of aerosol extinctions,  $R$  is defined as,

$$R = \frac{\beta_{440}}{\beta_{1050}} = \frac{\int_{r_1}^{r_2} \frac{dn(r)}{dr} Q(m, \lambda = 440, r) \pi r^2 dr}{\int_{r_1}^{r_2} \frac{dn(r)}{dr} Q(m, \lambda = 1050, r) \pi r^2 dr} \quad (4.19)$$

where  $r_1$  and  $r_2$  are the lower and upper radii limits of the integration and chosen such that the aerosol number density falls by  $1 \times 10^{-6}$  with respect to the maximum value in the size distribution.  $R$  values are plotted as function of  $r_m$  in Figure 4.16 for different  $\sigma$  values. It should be noted that the retrieved  $r_m$  is sensitive to the assumed  $\sigma$  value. For  $R$  greater than 2 an increase of 0.3 in  $\sigma$  will cause a decrease of about  $0.05 \mu\text{m}$  in  $r_m$  and the uncertainty in  $r_m$  due to variation in  $\sigma$  increases with decreasing  $R$ . In the present work  $r_m$  values are determined separately from both curves corresponding to lognormal distribution of  $\sigma = 1.86$  and ZOLD with  $\sigma = 1.8$ .

Figure 4.17 shows the measured aerosol extinction coefficients at 440 and 1050 nm at stratospheric altitudes and their ratio during October 1991. The aerosol extinctions are about  $10^{-2} \text{ km}^{-1}$  at these altitudes, which are about 2 orders of magnitude higher in comparison to the values obtained over Hyderabad in October 1985, a period considered to be volcanically quiescent [Jayaraman and Subbaraya, 1988]. Mode radii of the Pinatubo aerosols at these altitudes are determined from the aerosol extinction ratio as detailed above for the lognormal distribution and ZOLD (Figure 4.18). The mode radius of the aerosol layer is found to be around  $0.22 \mu\text{m}$  with a prominent peak at 23 km with a value

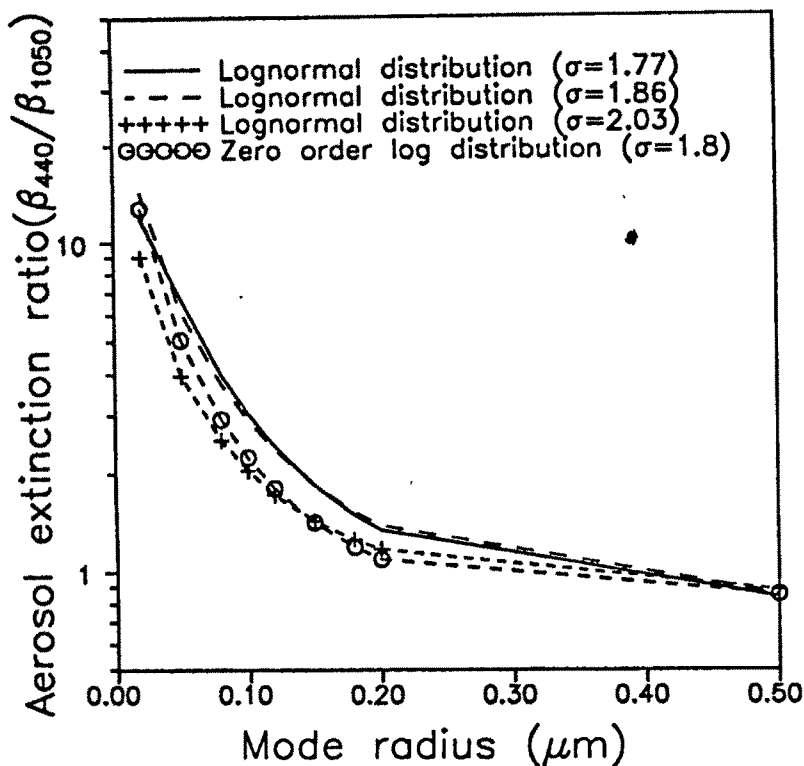


Figure 4.16: The aerosol extinction ratio as a function of the variable parameter  $r_m$  for lognormal ( $\sigma = 1.77, 1.86$  and  $2.03$ ) and zero order logarithmic ( $\sigma = 1.8$ ) distributions.

of  $0.31 \mu\text{m}$  in the case of lognormal distribution and around  $0.17 \mu\text{m}$  with a peak value of  $0.195 \mu\text{m}$  in the case of ZOLD within the layer [Ramachandran *et al.*, 1994c].

The effective radius,  $r_{\text{eff}}$  [Lenoble and Brogniez, 1984] described as

$$r_{\text{eff}} = \frac{\int_{r_1}^{r_2} r^3 \frac{dn(r)}{dr} dr}{\int_{r_1}^{r_2} r^2 \frac{dn(r)}{dr} dr} \quad (4.20)$$

is a more meaningful parameter for comparison, as it incorporates both  $r_m$  and  $\sigma$ . The corresponding  $r_{\text{eff}}$  computed using the above equation for LND and ZOLD are  $0.58 \mu\text{m}$  and  $0.57 \mu\text{m}$ , respectively. Using balloonborne optical particle counters at Laramie, Wyoming ( $41^\circ\text{N}$ ), during July 1991, Deshler *et al.* [1992] have found  $0.35 \mu\text{m}$  as a typical mode radius of the Pinatubo aerosols for a lognormal distribution of  $\sigma = 1.6$  around 23 km. This gives an  $r_{\text{eff}}$  of  $0.61 \mu\text{m}$  which is however slightly higher due to the fact that Deshler's measurements were made 3 months earlier to our measurements and about a month after

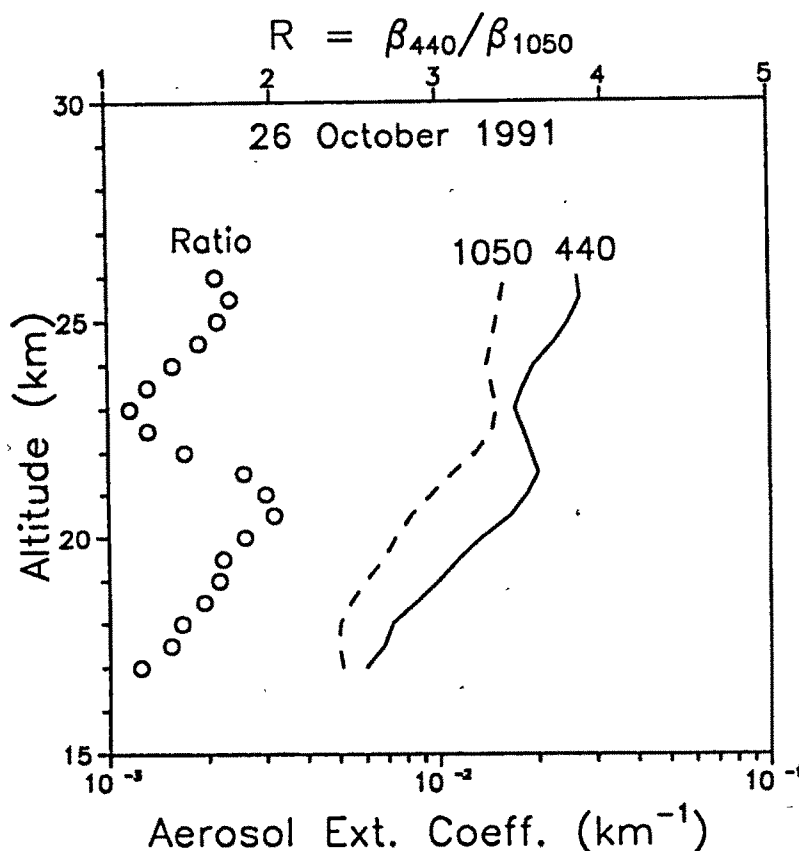


Figure 4.17: Aerosol extinction profiles at 440 (solid line) and 1050 (dashed line) nm and their ratios (circles) measured in October 1991, using balloon-borne Sun-tracking photometers over Hyderabad.

the eruption.

#### 4.5.5 Asymmetry factor

The asymmetry factor  $g$  is defined as the average of the cosine of the scattering angles for scattered radiation. Theoretically, the asymmetry factor can vary between  $-1$  and  $+1$ . For particles with isotropic scattering properties  $g = 0$ . The more the particles scatter in the forward direction, which is the case with larger particles the higher is the asymmetry factor. In the troposphere  $g$  is found to vary from 0.6 to 0.8 depending on the type of aerosols [d'Almeida *et al.*, 1991] for  $\lambda = 500$  nm, but the distribution of  $g$  at the stratospheric altitudes is not well known, though an attempt was made over

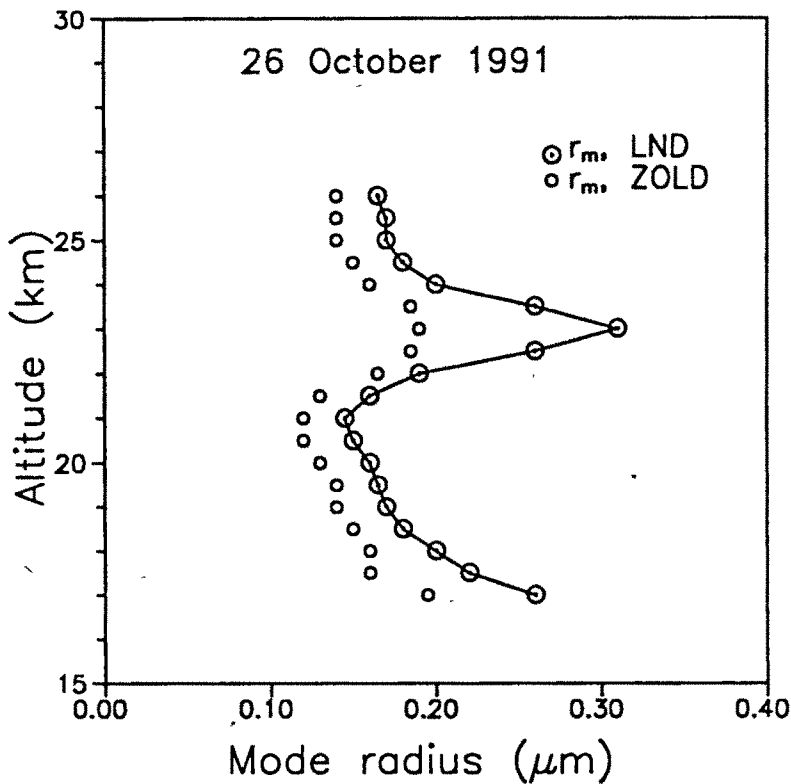


Figure 4.18: *The mode radius of the stratospheric aerosols obtained on 26 October 1991 using lognormal distribution (LND) and zero order logarithmic distribution (ZOLD).*

Alaska, using laser nephelometer measurements, in the altitude region of 11 to 13 km [Grams, 1981]. Here, an attempt has been made to obtain the vertical distribution of  $g$  at stratospheric altitudes, from the aerosol scattering phase function, derived from the scattered sky radiation measurements.

Though LND and ZOLD may describe better the stratospheric aerosol size distribution, for optically effective particles (in the size range of 0.05 to 10  $\mu\text{m}$ ) Junge power law can also be taken as a good representation [Volz and Sheehan, 1971] as the Mie scattering contribution of the smaller particles (less than about 0.05  $\mu\text{m}$ ) to the total integrated intensity is however marginal [Jayaraman, 1991]. The total extinction coefficient is found to increase only by 0.4% or less if the power law is truncated at  $r_{\text{min}} = 0.01 \mu\text{m}$  instead of 0.05  $\mu\text{m}$  [Ramachandran *et al.*, 1994c]. Further, the advantage of the Junge power law is that only one parameter,  $\nu$ , the slope of the power law curve best describes the size

distribution, compared to LND and ZOLD where two parameters,  $r_m$  and  $\sigma$  are required to define the shape of the size distribution. Mie scattering computations are made to obtain the aerosol scattering phase functions at 500, 750 and 850 nm, for various  $\nu$  values from 1 to 4, in steps of 0.2. The asymmetry factor  $g$  is determined from the aerosol phase functions  $P_a(\lambda, \theta)$  using the expression

$$g = \frac{\int_0^\pi \cos\theta P_a(\lambda, \theta) d(\cos\theta)}{\int_0^\pi P_a(\lambda, \theta) d(\cos\theta)} \quad (4.21)$$

The theoretically obtained phase functions are used to fit the experimentally obtained scattering phase functions computed from the measured angular distribution of the scattered radiation intensities from each altitude layer. The scattered radiation contribution from each layer is obtained by taking the difference between the values above and below. The obtained phase functions are also corrected for Rayleigh scattering. Attempt has been made to fit the data independently for the three photometer wavelengths and the mean values of the derived  $g$  and  $\nu$  profiles alongwith standard deviation ( $\pm 1\sigma$ ) are shown in Figures 4.19a and 4.19b. The uncertainty in determining asymmetry factor  $g$  is found to be about  $\pm 0.05$ .

As the particle size increases, the asymmetry factor  $g$  of the aerosol phase function increases and the slope  $\nu$  of the power law curve fitted for the size distribution decreases and hence  $\nu$  and  $g$  are anticorrelated, which is observed. In October 1991, it is interesting to note that while both  $\nu$  and  $g$  show a large layer like structure above the local tropopause height, from 16 km to about 23 km the derived  $r_m$  values (Figure 4.18) show the peak at 23 km. Both the results are complementary to each other in the sense that while  $\nu$  and  $g$  are representative of an ensemble of particles,  $r_m$  gives the mode radius at which the number of particles is maximum. Also, for the determination of  $r_m$  the width of the size distributions  $\sigma$ , for LND and ZOLD are assumed to be independent of altitude. In other words, while the bulk of the material produced after the eruption still remains at the 16 to 23 km region, the larger particles are formed at the expense of smaller particles. The aerosol extinction profiles also show that while the peak in the case of 440 nm occurs at the 21-22 km, in the 1050 nm extinction, which is sensitive to larger particles, the peak occurs at a slightly higher altitude of 23 km. In April 1992, two distinct layers are seen, consisting of larger particles, one with  $g$  values around 0.85, between 16 and 22 km

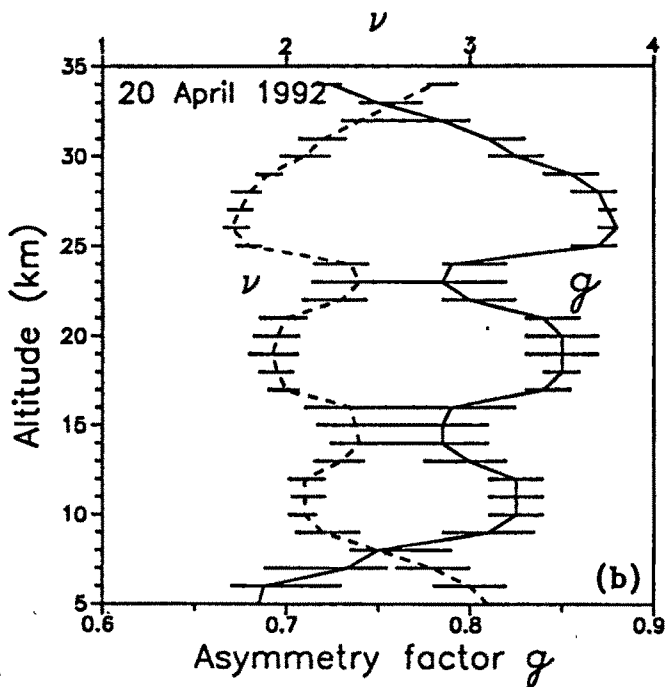
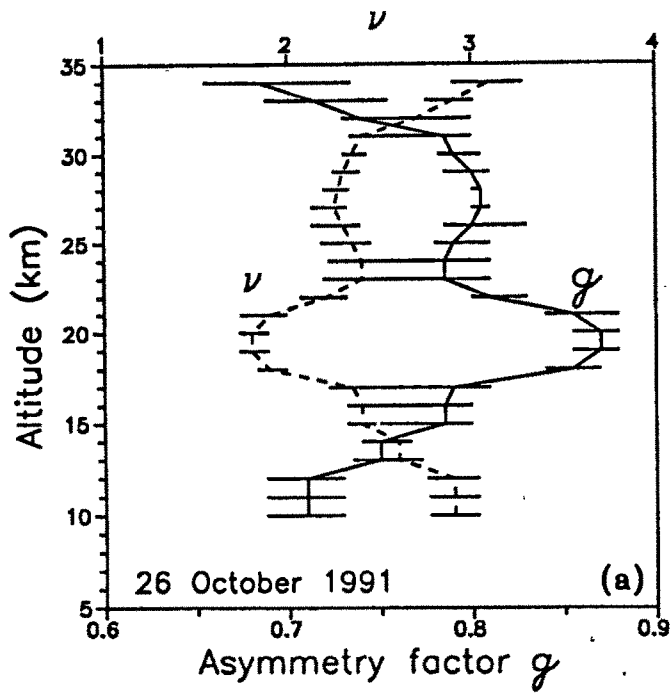


Figure 4.19: Vertical profiles of the asymmetry factor  $g$  and the aerosol size distribution parameter  $\nu$  obtained on 26 October 1991 and 20 April 1992 from the measured angular distribution of the scattered radiation intensities.

and other with  $g$  values around 0.88, between 25 and 30 km. However, in comparison in October 1985, a volcanically quiescent period,  $g$  values are less than 0.7 in these altitudes.

Also an attempt has been made to intercompare the two independent techniques, namely, the estimation of  $r_m$  from the  $\beta_{440}/\beta_{1050}$  ratio, obtained from the direct radiation measurements and the estimation of  $g$  and  $\nu$  profiles from the scattered radiation measurements, obtained during October 1991. Mie scattering computations are made using LND and ZOLD models with the  $r_m$  profiles of Figure 4.18 and  $g$  values are derived. It is found that though the exact shape (Figure 4.19a) could not be reproduced, the average  $g$  value for the Pinatubo layer obtained from both the techniques compare well with each other and is in the range of  $0.83 \pm 0.04$ . Similarly using the Junge power law with the  $\nu$  profile of Figure 4.19a,  $\beta_{440}/\beta_{1050}$  are computed and  $r_m$  values are derived using the calibration curve (Figure 4.16), for LND  $\sigma = 1.86$ . While the mean value of  $r_m$  derived from direct radiation measurements is  $0.22 \pm 0.05 \mu\text{m}$  for the layer, the mean  $r_m$  value derived from the Junge power law is found to be  $0.20 \pm 0.01 \mu\text{m}$ .

#### 4.5.6 Mass density of Pinatubo aerosols

An attempt has been made to estimate the mass density (grams per cubic metre) of Pinatubo aerosols from the aerosol extinction profile of 500 nm, obtained during October 1991. Following *Jäger et al.* [1988] the mass densities ( $M$ ) and extinction coefficients ( $\beta_{500}$ ) are obtained using derived  $r_m$  (LND) and taking a density of  $1.65 \text{ g cm}^{-3}$  for 75%  $\text{H}_2\text{SO}_4$  droplets. The obtained  $M/\beta_{500}$  ratios are multiplied with the measured  $\beta_{500}$  values to get the altitude variation of the mass density. The peak value at 23 km corresponding to peak  $r_m$  of  $0.31 \mu\text{m}$  is found to be  $22 \mu\text{gm}^{-3}$  which is slightly less than  $28 \mu\text{gm}^{-3}$  the value reported by *Deshler et al.* [1992] for a mode radius of  $0.35 \mu\text{m}$  for the late July 1991 period. The integrated value for the whole Pinatubo layer (17 to 26 km) is found to be about  $0.053 \text{ gm}^{-2}$  which is about 3.75 times higher than the value reported by *Jäger et al.* [1988] for El Chichon aerosol layer, obtained about 4 months after the eruption.

#### 4.5.7 Comparison of Pinatubo results with previous major eruptions

In Figures 4.20a and b the results of aerosol concentration and  $\nu$  are compared with the earlier results obtained over Hyderabad in October 1985 and over Thumba (8.5°N) in February 1980. These two cases are selected to show the effect of volcanic eruptions at stratospheric levels over the equatorial region. While the Thumba results are 3 months after the Sierra Negra volcanic eruption, the October 1985 result over Hyderabad is taken as typical of a volcanically quiet period. Though a volcanically produced aerosol layer is seen above about 15 km in the Thumba result [Subbaraya and Jayaraman, 1982], it is however much less significant compared to the recent Pinatubo results (Table 4.1). But the  $\nu$  profiles (Figure 4.20b) show a decrease at the stratospheric level both after the Sierra Negra and Pinatubo eruptions, compared to the 1985 result indicating the presence of a layer having relatively a larger number of larger particles.

In Figure 4.21a a comparison between the aerosol extinction profile for 500 nm in the October flight and the SAGE II 525 nm extinction profile for the same period except at a higher latitude of 39.7°N [Thomason and Osborn, 1992] is attempted. A very good agreement is seen between the data sets in the 15 to 23 km region. The higher extinction values above 23 km over Hyderabad is the indication of the initial confinement of the aerosol particles over the equatorial region, extending even above 30 km. In Figure 4.21b the 500 nm extinction values in the case of April flight are compared with the SAGE II results at 19°N during the same period and with the results of the Nd:YAG lidar experiment made at Ahmedabad (23°N), 2 weeks prior to the balloon experiment. The aerosol extinction values are obtained from the lidar backscattering coefficient by multiplying an altitude independent value of 50 which has the unit of steradian. Though an altitude dependent factor [Jäger *et al.*, 1988] can be more realistic, it can be shown that the error in the obtained extinction values are within 25%. A systematic increase in the extinction values is also seen above about 24 km with decreasing latitude indicating that the upper edge of the layer extends to higher altitudes in the equatorial region.

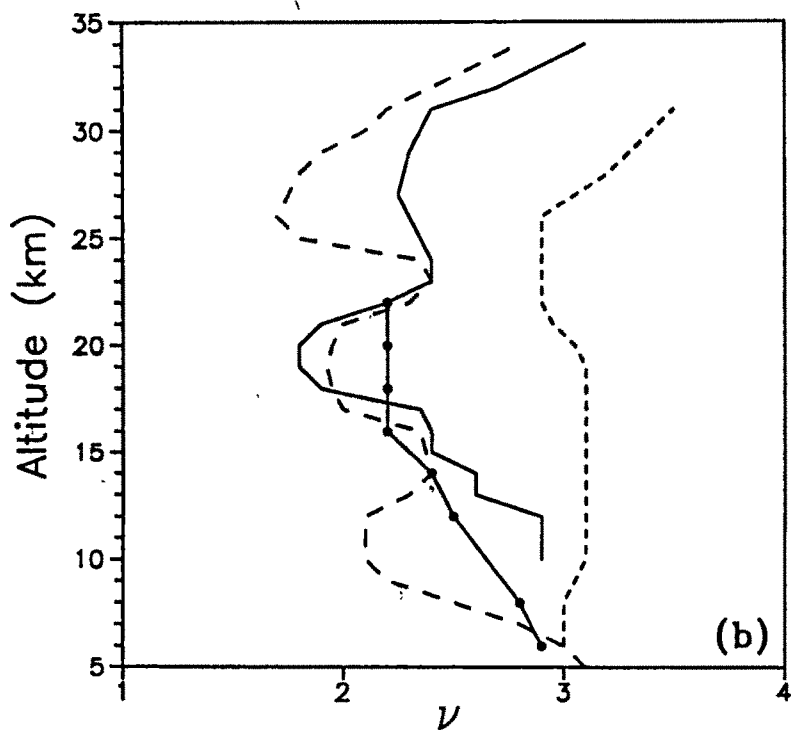
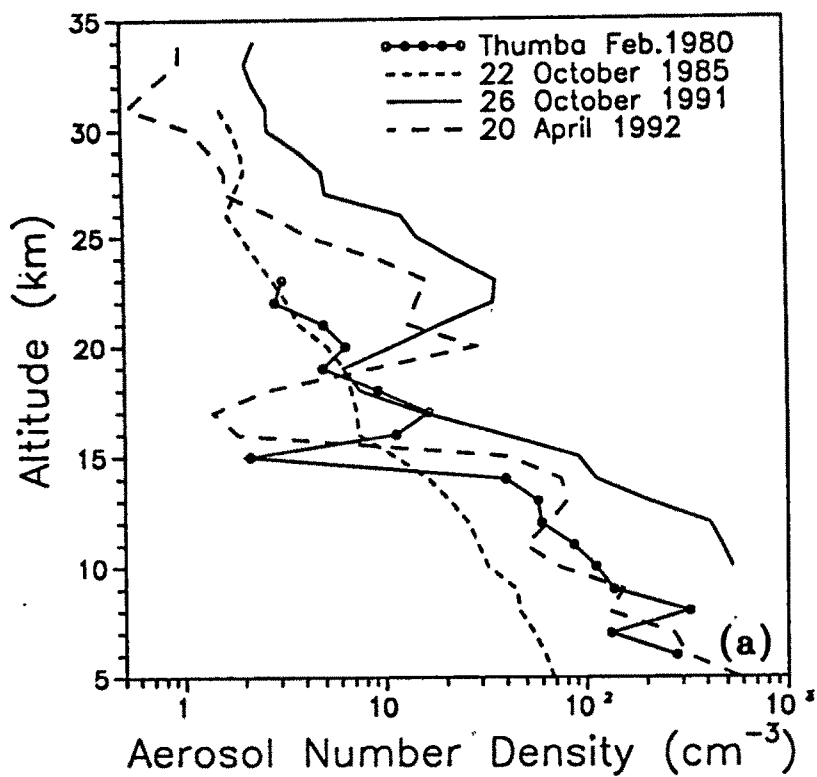


Figure 4.20: Comparison of the (a) aerosol number density and (b) aerosol size parameter data with the earlier results obtained during a volcanically perturbed period (Thumba, 1980) and a volcanically quiescent period (Hyderabad, 1985).

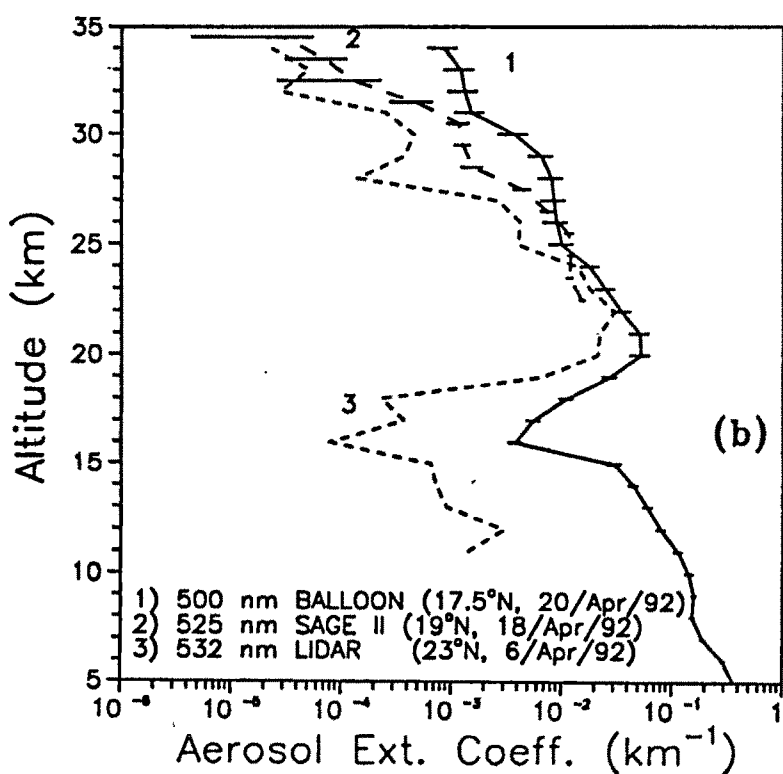
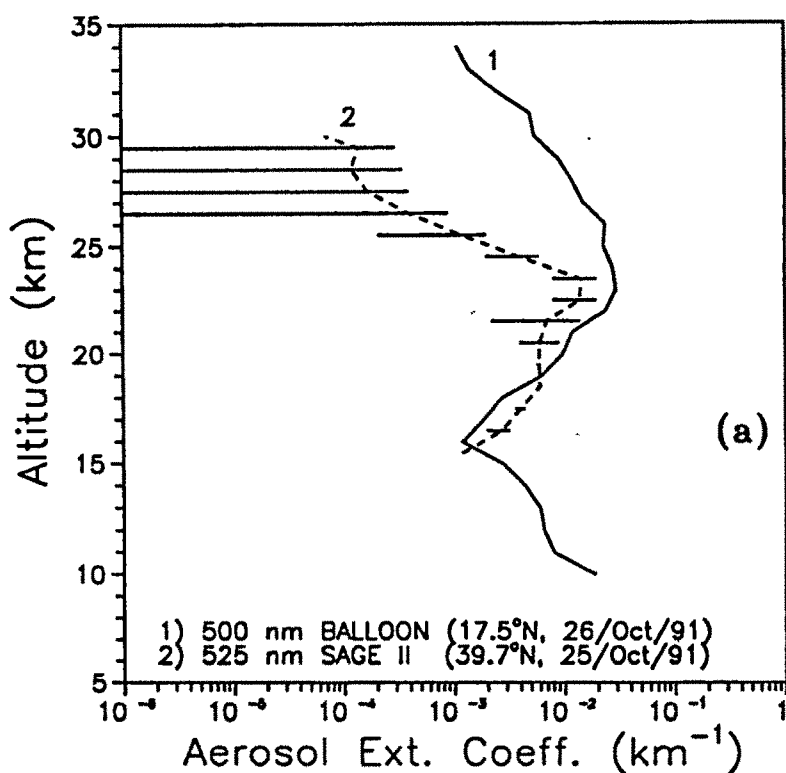


Figure 4.21: Comparison of the aerosol extinction at 500 nm with that of the SAGE II 525 nm results and with that of a Nd:YAG lidar experiment made in Ahmedabad (23°N) about 2 weeks prior to the balloon experiment in April 1992.

Table 4.1: Comparison of the aerosol size parameter ( $\nu$ ) and number densities obtained on 22 October 1985, 26 October 1991 and 20 April 1992 over Hyderabad.

Altitude (km)	Aerosol size parameter ( $\nu$ )			Aerosol number density ( $\text{cm}^{-3}$ )		
	22/10/85	26/10/91	20/04/92	22/10/85	26/10/91	20/04/92
5			3.10			572.80
6	3.00		3.00	62.01		316.71
7	3.00		2.80	54.59		270.48
8	3.00		2.50	46.19		127.83
9	3.05		2.20	44.55		153.43
10	3.10	2.90	2.10	32.18	531.26	72.53
11	3.10	2.90	2.10	28.82	472.61	49.15
12	3.10	2.90	2.10	25.76	411.25	64.58
13	3.10	2.60	2.30	20.86	202.87	79.90
14	3.10	2.60	2.40	16.27	111.45	74.68
15	3.10	2.40	2.38	11.13	91.10	40.49
16	3.10	2.40	2.35	7.31	38.12	1.84
17	3.10	2.35	2.00	7.20	15.22	1.38
18	3.10	1.90	1.95	6.73	7.46	2.54
19	3.10	1.80	1.93	6.26	6.17	8.75
20	3.05	1.80	1.95	5.13	10.90	28.19
21	2.95	1.90	2.00	3.73	18.90	13.06
22	2.90	2.20	2.30	3.27	34.65	14.32
23	2.90	2.40	2.40	2.75	35.66	16.27
24	2.90	2.40	2.35	2.31	22.31	9.30
25	2.90	2.35	1.80	1.96	14.54	4.23
26	2.90	2.30	1.70	1.66	12.23	2.77
27	3.05	2.25	1.75	1.80	5.15	1.63
28	3.20	2.28	1.80	2.03	4.96	1.62
29	3.30	2.30	1.90	1.96	3.81	1.28
30	3.40	2.35	2.10	1.78	2.67	1.11
31	3.50	2.40	2.20	1.53	2.66	0.54
32		2.70	2.40		2.29	0.71
33		2.90	2.60		2.09	0.98
34		3.10	2.80		2.32	0.99

### 4.5.8 Synthesis of results

With an attempt to study the physical properties of the Pinatubo aerosols, *Thomason* [1992] has used the SAGE II aerosol extinction measurements and studied their ratios. Figure 4.22 is adopted from *Thomason* [1992] but for the present results, where the aerosols are classified into three modes, aerosols with low extinction and high extinction ratio representing smaller size background type aerosols (I), aerosols with high extinction and high extinction ratio representing the larger number of smaller particles representing an early volcanic period (II) and aerosols with high extinction and low extinction ratio representing higher number of larger particles representing post-volcanic aerosols (III). While *Thomason* [1992] has shown that immediately (1 month) after the eruption the aerosols exhibited high extinction but a small inferred particle size, corresponding to mode II in Figure 4.22, a transitional phase between the very small aerosols created by gas-to-particle conversion mechanism and the large sized post-volcanic aerosols that exhibit high extinction and low extinction ratio values corresponding to mode III. The balloon observations made in October 1991, 4 months after the eruption show mode III type particles. For comparison, SAGE results corresponding to October 1991 are shown for two different latitudes, one at 17.9°N, close to the balloon observation site and the other at a latitude of 39.7°N. A good agreement is seen between the SAGE and balloon derived ratios, all exhibiting the post-volcanic type aerosols. For comparison the extinction ratios ( $\beta_{450}/\beta_{1000}$ ) obtained during 1985 over Hyderabad are shown which are found to represent mode I type particles corresponding to background aerosols.

It has been shown [*Turco et al.*, 1983] that condensation of sulphate aerosols would occur first on the large aerosols existing earlier and then on progressively smaller aerosols. *Deshler et al.* [1992] suggest that nucleation of new H<sub>2</sub>SO<sub>4</sub>/H<sub>2</sub>O aerosol occurred below 20 km during July and August 1991 over Laramie. Condensation on the already existing sulphate aerosol would increase the extinction and decrease the extinction ratio as the extinction becomes increasingly dominated by large aerosols whose scattering efficiency is almost the same at 500 nm and at 1050 nm. *Turco et al.* [1983] suggested in the case of Mt. St. Helens eruption, that if the concentration of sulphur dioxide is sufficiently large, conversion of H<sub>2</sub>SO<sub>4</sub> produces large numbers of new small H<sub>2</sub>SO<sub>4</sub>/H<sub>2</sub>O aerosol and coagulation proceeds at a higher rate. In the case of Pinatubo eruption, the same

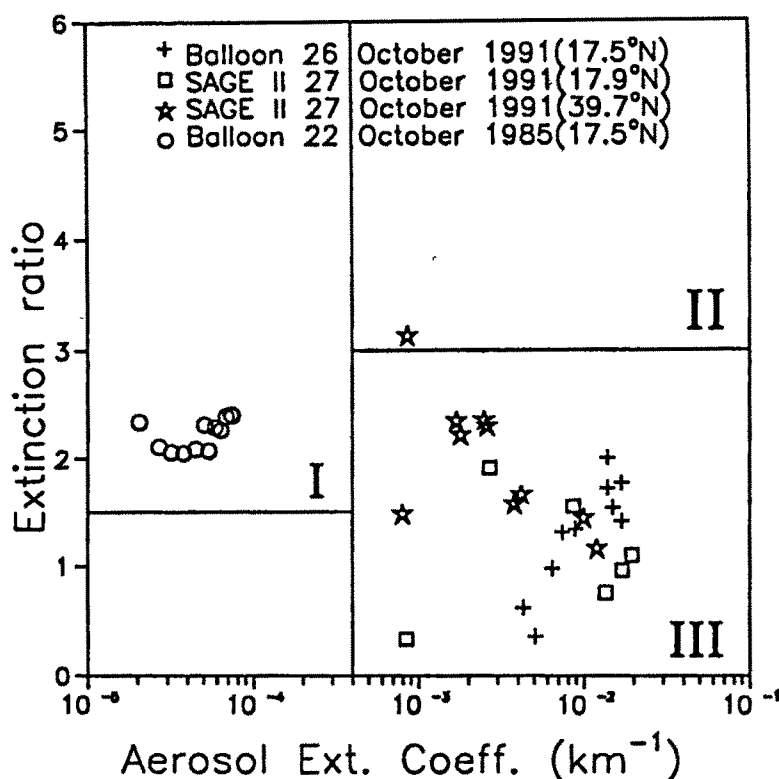


Figure 4.22: The scatter diagram, adopted from Thomason [1992], of the 525 to 1020 nm extinction ratio and 1020 nm extinction of SAGE II and the ratios of extinctions between 500 and 1050 nm and the extinction at 1050 nm of the balloon measurements made on 26 October 1991. The October 1985 balloon values over Hyderabad are also plotted for comparison. The scatter plot is divided into three regions (modes), the background type aerosols (mode I), the transition stage immediately after a major volcanic eruption (mode II) and the aged volcanic aerosols (mode III). See text for their characteristics.

phenomena would have occurred over the tropics between 20 and 25 km where the densest portions of the cloud were observed. Thus the condensation of  $\text{H}_2\text{SO}_4$  vapour on the already existing  $\text{H}_2\text{SO}_4/\text{H}_2\text{O}$  liquid droplets and subsequent coagulation is one of the major mechanisms, for the formation of larger aerosol particles at these altitudes. The high mode radius in the range of 0.2 to 0.3  $\mu\text{m}$  obtained in October 1991 over Hyderabad and by *Deshler et al.* [1992] during July 1991 over Laramie, which was about 0.35  $\mu\text{m}$  indicate the presence of aged volcanic aerosols, formed due to coagulation. In April 1992, a layer with  $\nu$  values less than 2 is seen between 25 and 30 km, indicating the formation of larger aerosols from smaller aerosols due to coagulation and this phenomenon has subsequently reduced the total aerosol number density at these altitudes.

## 4.6 Nd:YAG backscatter lidar measurements

### 4.6.1 Lidar system specifications and Data collection

Lidar, analogous to radar, has become one of the most widely used techniques for atmospheric aerosol research, with the advent of high-power pulsed lasers, technological advance in the field of low level light detection and fast data processing methods. A continuous monitoring of the Pinatubo volcanic aerosol layer is essential to study the physical and chemical processes involved in the formation and decay of the layer, which will help in the assessment of its overall impact on climate [*Hofmann, 1987; Kiehl and Brieglab, 1993*]. A laser radar (lidar) system is an apt tool to conduct such a study. The Pinatubo aerosol layer has been continuously monitored by the newly set up Nd:YAG lidar operating at 532 nm at the Physical Research Laboratory (PRL), Ahmedabad (23°N, 72.5°E) since April 1992 [*Jayaraman et al., 1995a*]. Results obtained on the vertical profiles of the scattering ratios, aerosol extinction coefficients and mass of the Pinatubo layer and its decay from April 1992 to May 1994 are reported here.

The specifications and the technical block diagram of the PRL lidar system used for the measurements are given in Table 4.2 and Figure 4.23, respectively. The system employs a transmitter consisting of a pulsed Nd:YAG laser, a 0.40 m diameter Cassegrain telescope which acts as the receiver, a thermoelectrically cooled photomultiplier tube operating in the photon counting mode, signal processing unit and data processor. The wavelength

Table 4.2: *Specifications of the PRL Lidar system.*

Item	Specifications
<b>LASER</b>	
(581C-10, Quantel, France)	
Material	Nd:YAG
Average output power	10 W
Output energy per pulse	440 mJ (532 nm)
Repetition rate	10 Hz
Pulse duration	7 ns
Beam diameter	9 mm
Beam divergence	0.3 mrad
<b>RECEIVING OPTICS</b>	
Telescope type	Cassegrain
Diameter	0.40 m
Field of view	6 mrad
Interference filter bandwidth	1 nm
Maximum $\lambda$	532 nm
Maximum transmission	48%
Photomultiplier	9813A (Thorn EMI, UK) (Photon counting mode)
<b>SIGNAL PROCESSOR</b>	
(SR430, Stanford Research Systems, USA)	
Bin width	640 ns (= 96 m alt. resolution) (with no interchannel dead time)
Integration	500 s (5000 records, typical)

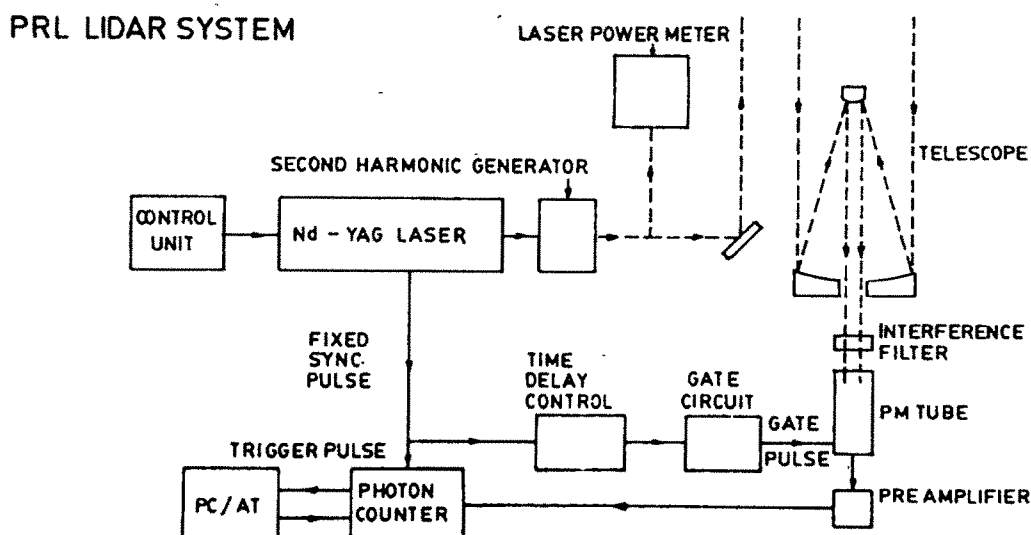


Figure 4.23: Block diagram of the Nd:YAG backscatter lidar system at PRL.

used for the measurement is 532 nm which is the second harmonic of Nd:YAG's fundamental wavelength of 1064 nm. The laser beam is transmitted vertically upwards with the help of a 45° incidence, 2-inch diameter ultrahard dielectric-coated high-energy laser mirror. The optical axis of the telescope is at a distance of 0.5 m from the transmitting optics. The field of view of the telescope is kept large in comparison to the laser beam divergence (Table 4.2) so as to accommodate the beam totally above a certain altitude, which is about 300 m in the present case. An interference filter having central wavelength at 532 nm with a bandwidth of 1 nm is used to reduce the background light noise in the collected backscattered signal. The backscattered photons are then detected by a gated photomultiplier which is cooled to below  $-25^{\circ}\text{C}$  using a thermoelectric cooler. By gating process, the PMT is electrically switched OFF (by applying a reverse bias between the photo cathode and the first dynode) for a selected time, to avoid intense backscattered signals from low altitudes, which could cause saturation of the detector and can give rise to signal induced noise [Shimizu *et al.*, 1985]. In the present setup, the photomultiplier is turned ON for a time interval of 0.5 ms. A programmable time delay pulse is used to

switch ON the PMT from a desired altitude level. For the results presented here, a time delay of 60  $\mu$ s is used corresponding to an altitude of 9 km which is the starting altitude of the measurement. The signal is range detected using a scalar averager operating at 200 MHz count rate and integrated for 5000 laser shots. The signals are corrected for the counting loss [Donovan *et al.*, 1993] typical of the counting procedure. Background noise is estimated individually for each measurement, which is the observed photon count rate from altitudes where it does not decrease with altitude but takes more or less a constant value and subtracted from the signal. In general, the signal is about 40 times higher than the noise at 35 km (signal-to-noise-ratio of 40) and the factor reduces to about 10 at 45 km.

#### 4.6.2 Data analysis

The range-corrected photon counts are normalised with model atmosphere [U. S. Standard Atmosphere, 1966] air density profiles in the altitude regions above 35 km, where the aerosol content is negligible. January 30°N air density profile is used for lidar observations taken during the 6 months from October to March and July 30°N profile is used for the months from April to September, taking into account the  $\pm 7\%$  change in the air density values, between these two profiles, in the altitude region around 35 km.

The total backscattering coefficient  $\beta_z$  is obtained using the top to bottom inversion algorithm proposed by Klett [1985]

$$\beta_z = \frac{\exp(S - S_m)}{\frac{1}{\beta_m} + 2 \int_z^{z_m} \frac{\exp(S - S_m)}{B_a} dz} \quad (4.22)$$

where  $S$  and  $S_m$  are the logarithm of the range-corrected photon counts at any altitude  $z$  and at the maximum altitude of the obtained profile  $z_m$ , respectively.  $\beta_m$  is the backscattering coefficient at altitude  $z_m$  which is the Rayleigh backscattering coefficient at these altitudes in the absence of aerosols.  $B_a$  ( $\text{sr}^{-1}$ ) is the ratio between aerosol backscattering and extinction coefficients. If  $B_a$  is taken as a constant and not dependent on altitude as it is done in the present work, then the above solution is similar to that obtained by Fernald [1984].

This top to bottom inversion procedure, proposed by Klett becomes an excellent choice for analysing the lidar data if backscattered signal can be measured well above the aerosol

layers (35 km and above). Above 35 km the contribution from aerosol scattering to the total backscattering is negligible and hence  $\beta_m$  becomes the Rayleigh backscattering coefficient at the maximum altitude which can be readily computed from air density values. For a given wavelength,  $B_a$  depends on the aerosol size distribution which can be different at different altitudes [Jayaraman and Subbaraya, 1988]. Using lidar and simultaneous balloonborne optical particle counter data Jäger and Hofmann [1991] have obtained values of  $B_a$  for 532 nm, for the El Chichon volcanic eruption. The values are found to be in the range between 0.016 and 0.03 with a mean value of about 0.02 in the lower stratosphere from 20 to 30 km. Recent results for Pinatubo by D'Altorio et al. [1993] using DIAL technique show that the ratio varies from 0.02 to 0.033 for 589 nm during the August 1991 to December 1992 period. In the present calculations, an altitude independent value of  $0.02 \text{ sr}^{-1}$  for  $B_a$  has been used for the retrieval of  $\beta_z$ .  $\beta_z$  values derived using three independent values for  $B_a$ , namely, 0.015, 0.02 and 0.025 show that the uncertainty in  $\beta_z$  increases from 1% at 30 km to about 25% at 20 km for a volcanically perturbed case such as after the Pinatubo eruption, while the uncertainty is well within 10% for background aerosol level for the same altitude region.

From the backscattering coefficient profiles the scattering ratio R is obtained as,

$$R = \frac{\beta_{\text{air}}(z) + \beta_{\text{aerosol}}(z)}{\beta_{\text{air}}(z)} \quad (4.23)$$

where  $\beta_{\text{air}}(z)$  and  $\beta_{\text{aerosol}}(z)$  are the air and aerosol backscattering coefficients at altitude  $z$ . Thus for an aerosol free Rayleigh atmosphere, R is unity and with increasing aerosol concentration R increases.

### 4.6.3 Lidar observations

The lidar observations are being made since April 1992, every fortnight, during clear nights, with breaks in the observations due to Indian monsoon which is active during June-September period over Ahmedabad. About 36 profiles have been chosen for the present study of the Pinatubo volcanic aerosol layer and its decay.

## 4.7 Results and Discussion

### 4.7.1 Scattering ratios

Figure 4.24 shows the variations in the obtained scattering ratio profiles with respect to time, starting from April 1992 until May 1994, a period corresponding to about 10 months after the Pinatubo eruption to about 3 years. The volcanic aerosol layer is seen very prominently as an increase in the scattering ratios from about 17 km (1 km above the local tropopause) to about 30 km. The layer peaks initially at 23 km and by May 1994, the peak has come down to 20 km. Also, the maximum scattering ratio is about 8 in April 1992, which increases to about 22 in May 1992 and decreases to about 3 in October 1992. During the rest of the observation period, though the Pinatubo layer is seen, the broad layer which was seen in the initial period reduces to an insignificant layer between 17 and 25 km, with a simultaneous decrease in peak scattering ratio to about 1.5 in May 1994. In the initial periods of the observations, two layers are seen, indicating inhomogeneities within the layer, which by the end of May 1992, merge to form one broad homogeneous layer. Similar observations of inhomogeneities within the layer which then disappeared by early 1992, have been reported by *Deshler et al.* [1993] using balloonborne optical particle counters over Laramie, Wyoming (41°N) and also by *Shibata et al.* [1994] using Nd:YAG-lidar at Wakkanai (45.4°N), Japan.

### 4.7.2 Aerosol extinction coefficients

Figure 4.25 shows the derived vertical profiles of aerosol extinction coefficients from lidar measurements made during April 1992. The Pinatubo layer is seen between 17 and 30 km, with aerosol extinction in the range of  $0.5 \times 10^{-5} \text{ km}^{-1}$  at 17 km which increases by more than 2 orders of magnitude to  $0.3 \times 10^{-2} \text{ km}^{-1}$ , between 20 and 25 km, where most of the aerosol cloud remained over the tropics. The assumption of a constant (altitude independent) extinction to backscatter ratio of  $0.02 \text{ sr}^{-1}$  used for the inversion of lidar data is found to introduce an error of about 1% in the derived extinction coefficient values at 30 km which increases to more than 25% at 20 km. The errors (horizontal bars) plotted in profile 1 of Figure 4.25 at every kilometre, however, do not look significant in the logarithmic scale. For comparison the Stratospheric Aerosol and Gas Experiment

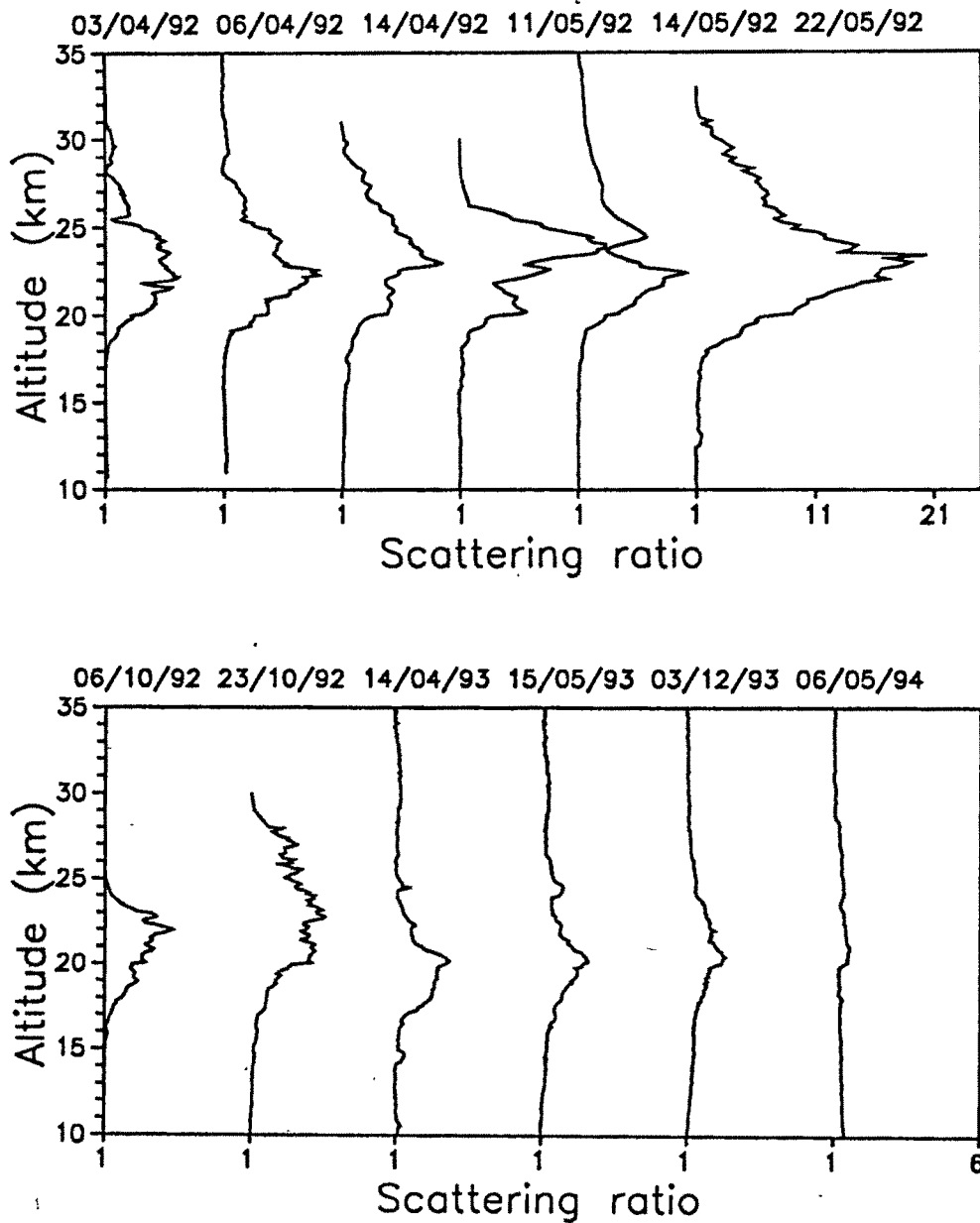


Figure 4.24: Sample profiles of the scattering ratio obtained during April 1992 to May 1994, showing the time evolution of the Pinatubo volcanic aerosol layer. The dates of measurements are given at the top as dd/mm/yy.

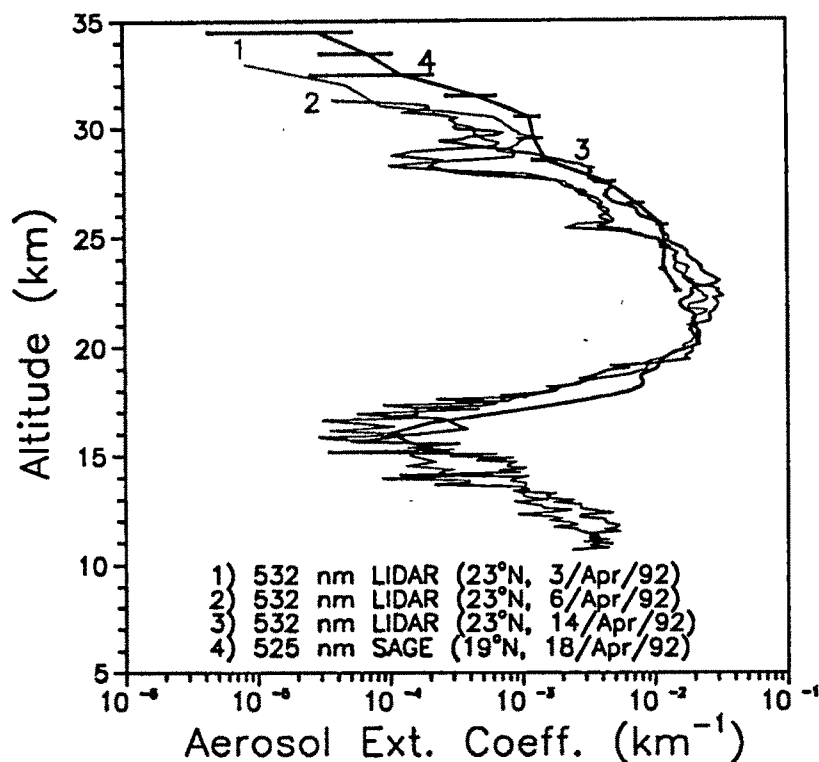


Figure 4.25: Profiles of aerosol extinction coefficients obtained over Ahmedabad (23°N, 72.5°E) during April 1992 using Nd:YAG lidar. SAGE II extinction profile for 19°N, 71.3°E is also plotted for comparison. The error in extinction coefficient values, which is of the order of 25% in the layer altitude and plotted in profile 1 at every km is, however, not quite visible.

(SAGE) II satellite extinction profile obtained on 18 April 1992 at 19°N, 71.3°E has also been plotted. The lidar data agrees well with SAGE II data, between 22 and 29 km and differing beyond 29 km, where the SAGE II values are higher, indicating that the altitude extent of the layer increases to higher altitudes, even above 30 km over lower latitude regions. This feature has already been observed from balloon-borne observations of aerosol extinctions, made using Sun-tracking photometers over Hyderabad (17.5°N, 78.6°E), during April 1992.

The aerosol backscattering coefficients obtained between 17 and 30 km, are integrated to study the decay of the Pinatubo layer and are plotted with respect to days after the

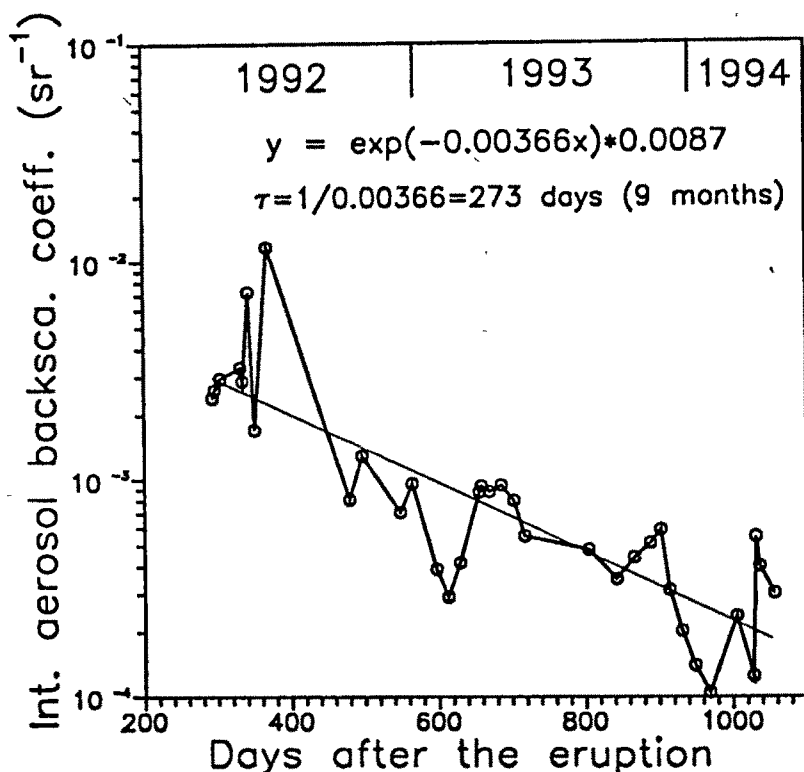


Figure 4.26: The integrated aerosol backscatter (17 to 30 km) decay with time from April 1992 to May 1994.

eruption in Figure 4.26. An exponential fit to the data gives a 1/e folding time of 9 months compared to a value of about 7 months reported by *Grant et al.* [1994] for the tropical aerosol loading in a 10° latitude band centered on the densest aerosol region in 1991. As the Mt. Pinatubo eruption occurred in June 1991, situated at a latitude of 15.14°N, the low latitude region became the source of aerosols to higher latitude regions. The poleward detrainment of particles was the dominant mechanism in distributing the particles at stratospheric altitudes, than the gravitational settling during the initial period after the eruption [*Trepte et al.*, 1993].

Earlier measurements made using balloon-borne Sun-tracking photometers after the El Chichon eruption in 1982, showed that the layer produced after the eruption decayed in about 3 years over the tropics [*Jayaraman*, 1991]. Since Mt. Pinatubo had put as much as 2 to 3 times more material into the stratosphere compared to El Chichon, it

was not clear whether the lifetime of these aerosols will also be longer because of the larger number density of aerosols or, perhaps, the physical processes such as growth, coagulation and sedimentation will take place at a much faster rate to give more or less the same decay time. It is shown through model calculations [*Pinto et al.*, 1989] that as the mass of injected sulphur dioxide increases beyond 10 Mt, the aerosol microphysical processes of condensation and coagulation produce larger particles as the SO<sub>2</sub> injection rate is increased rather than a larger number of particles of the same size, due to which the size of sulphate aerosols increases and the removal rate accelerates. Consequently, the residual sulphate masses could be quite similar after about 2 years for eruptions of widely different magnitudes. Interestingly, if the Pinatubo layer decays at the present rate, with a 1/e folding time of 9 months, then it could take about 4.5 years, to reach the background aerosol extinction coefficient value of about  $2 \times 10^{-5} \text{ km}^{-1}$ , a value representative of a volcanically quiescent period for the tropical stratosphere obtained from the balloon-borne measurements of stratospheric aerosols over Hyderabad [*Jayaraman*, 1991].

### 4.7.3 Decay of Pinatubo aerosol layer mass

The aerosol backscattering coefficient values are used to obtain the mass density ( $\text{gm}^{-3}$ ) of the aerosols following the procedure described by *Jäger and Hofmann* [1991]. The mass densities ( $M$ ) and backscattering coefficients ( $\beta_{532}$ ) are calculated for lognormal size distributions of aerosols with mode radii ( $r_m$ ) 0.1, 0.2 and 0.3  $\mu\text{m}$  having  $\sigma = 1.86$  (value accepted in the literature for stratospheric aerosols [*Pinnick et al.*, 1976]) and taking a density of  $1.65 \text{ g cm}^{-3}$  for 75% H<sub>2</sub>SO<sub>4</sub> droplets. *Deshler et al.* [1993] using balloonborne optical particle counters and fitting the obtained aerosol number density, with lognormal distributions have shown that the mode radius in the altitude region of 17 to 23 km is in the range of 0.1 to 0.5  $\mu\text{m}$ , between July 1991 and January 1993. Also, our results on the mode radius obtained using balloon-borne Sun-tracking photometers, during October 1991 [*Ramachandran et al.*, 1994c], show that it is in the range of 0.1 to 0.3  $\mu\text{m}$ , in the 17 to 26 km altitude region. *D'Altorio et al.* [1993] using DIAL technique at L'Aquila (42°N), Italy, have shown that the mode radius in the 15 to 25 km altitude region lies in the range of 0.1 and 0.25  $\mu\text{m}$ , during the August 1991 to December 1992 period. As in a monostatic lidar system like ours, it is not possible to retrieve  $r_m$ , calculations of aerosol

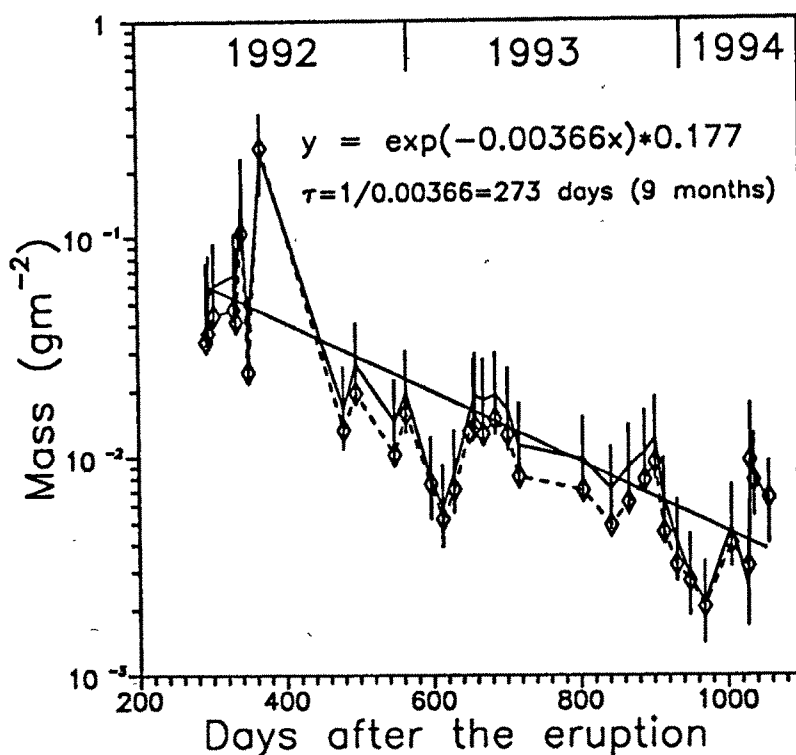


Figure 4.27: Time evolution of Pinatubo aerosol mass (integrated from 17 to 30 km) computed using the backscattering coefficient values. Vertical bars represent the variation in mass due to the  $r_m$  values taken as 0.1, 0.2 and 0.3  $\mu\text{m}$ . Dashed line represents the mass value estimated using the conversion factors given by Jäger and Hofmann [1991].

mass densities are repeated for  $r_m$  values of 0.1, 0.2 and 0.3  $\mu\text{m}$ .

The obtained  $M/\beta_{532}$  ratios for the mode radii, 0.1, 0.2 and 0.3  $\mu\text{m}$ , are then multiplied with the lidar measured  $\beta_{532}$  values to get the altitude variation of the mass and are integrated between 17 and 30 km (Pinatubo layer). The variation of integrated mass density of the Pinatubo layer for the three mode radii is plotted in Figure 4.27 as a function of days after the eruption. The vertical bars show the variation in the derived mass due to different  $r_m$  values assumed. The continuous line is drawn through values corresponding to  $r_m = 0.2 \mu\text{m}$  while the top and bottom values correspond to  $r_m = 0.3$  and 0.1  $\mu\text{m}$ , respectively.

Further, the obtained integrated aerosol backscattering coefficient for the layer is con-

verted into mass ( $\text{gm}^{-2}$ ) using the conversion table given by *Jäger and Hofmann* [1991]. The conversion model is based on a number of *in situ* aerosol measurements made during 1980 to 1987 which encompasses the El Chichon eruption. The conversion factors are taken from the table, taking into account the number of days elapsed after the eruption, in our case, the Mt. Pinatubo eruption. The results are shown as dashed line in Figure 4.27. A good agreement is seen with the result (continuous line) obtained from a more elaborate way of calculating the  $M/\beta_{532}$  ratio using Mie scattering theory and using the conversion values of Jäger and Hofmann (dashed line). The interesting feature is that the aerosol mass obtained using the conversion factor agrees better with the mass calculated using a mode radius value of  $0.1 \mu\text{m}$  and also no considerable change is seen in the aerosol size distribution during the decay phase of the aerosol layer. However, there are at least two instances when the values agree better for a mode radius of  $0.2 \mu\text{m}$ , one during May 1992 and the other in March-April 1994. On both the occasions, an increase in mass is also observed indicating a possibility of further input of particles of unknown origin into the stratosphere.

An increase in the aerosol backscatter and mass is seen at times during the decay phase which otherwise is quite smooth and uniform, with no considerable change in the aerosol size distribution. *Jäger et al.* [1995] and *Uchino et al.* [1995] from the results obtained while studying the evolution, spread and decay of Pinatubo aerosols in the northern hemisphere over a period of 3 years from 1991 to 1994 using lidars at Garmisch ( $47.5^\circ\text{N}$ ), Tsukuba ( $36.1^\circ\text{N}$ ) and Naha ( $26.2^\circ\text{N}$ ) have seen similar variations in the stratospheric aerosol optical depth, integrated aerosol backscatter and mass and attributed these seasonal changes to the tropopause height variations and due to the effective transport of aerosols from the equatorial reservoir to midlatitudes with planetary wave activity.

#### 4.7.4 Aerosol mass decay at three stratospheric altitude regions

Aerosol layer mass at three altitude regions, namely, 15 to 20 km, 20 to 25 km and 25 to 30 km, is obtained from the vertical profiles of the integrated aerosol backscattering coefficient values and multiplied with the conversion factors given by *Jäger and Hofmann* [1991]. The monthly mean values for the three layers are shown in Figure 4.28 for the

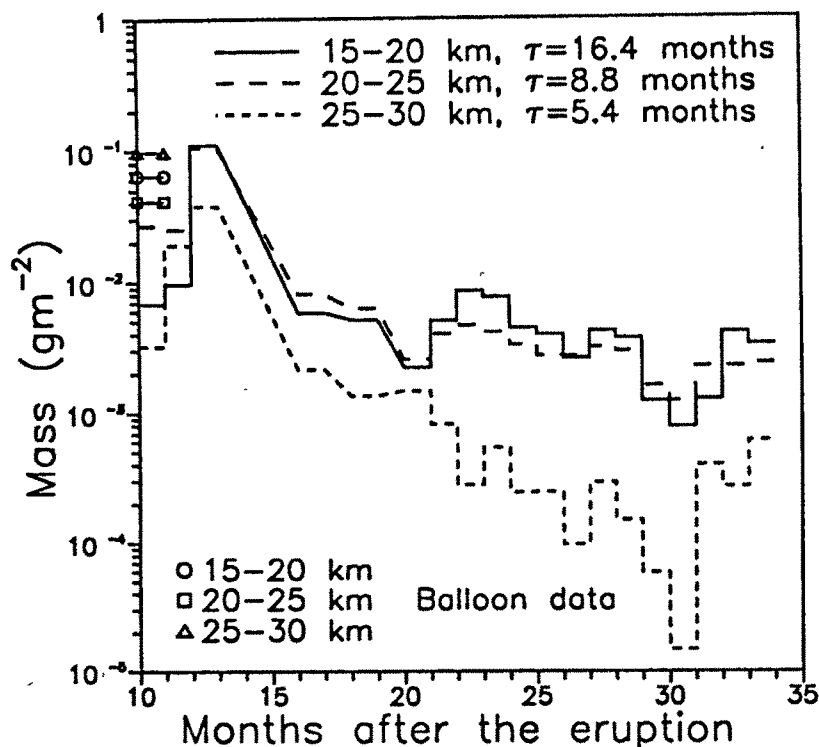


Figure 4.28: Mass of the Pinatubo volcanic aerosol layer estimated for three height regions 15-20 km, 20-25 km and 25-30 km, using the conversion factors given by Jäger and Hofmann [1991]. For comparison, masses estimated in the case of a balloon measurement made at Hyderabad ( $17.5^\circ\text{N}$ ) in April 1992 are also shown.

observation period. Exponential best fits are made for the three layers and  $1/e$  decay times are estimated as 16.4, 8.8 and 5.4 months, respectively.

As expected, the top layer shows a faster decay compared to the bottom layers because the settling velocity of aerosols in the micron and submicron size ranges increases with increasing altitudes [Lamb, 1970]. It should be noted that the decrease in aerosol mass at a particular altitude layer is both due to removal of particles downward due to gravitational settling and horizontal dispersal to other latitudes. While a detailed dynamical model is necessary to quantify the amount of material displaced by these two processes, qualitatively, the upper layer becomes the source of particles to the lower altitude regions. This further explains the faster decay pattern observed for the top layer, while the bottom

two layers not only lose particles due to gravitational settling but also gain particles from the top layer and hence exhibit a slower decay. From April 1992 to February 1993, the 20-25 km layer has the maximum mass of particles. However, after this period the layer has a reduced mass with a subsequent gain in the lower layer, between 15 to 20 km. An increase seen in the aerosol mass in all the three layers about 30 months after the eruption could be due to the influx of particles into the stratosphere from an unknown source. For comparison, the mass of the Pinatubo layer is computed for the balloon-borne optical measurements data obtained over Hyderabad (17.5°N) in April 1992 [*Ramachandran et al.*, 1994b] and are shown for the three layers. The higher mass value obtained over Hyderabad indicates that at lower latitudes the layer has been broader and extends to higher altitudes as discussed earlier and these particles become the source to the higher latitude regions with time.

#### 4.7.5 Peak scattering ratio

Figure 4.29 shows the variation in the peak scattering ratio, with values ranging from about 10 and above during April-May 1992 which declines to about 1.5 during May 1994. An exponential best fit gives a  $1/e$  folding time of about 12.5 months, which is higher than a value of 9 months obtained in the case of integrated particulate backscattering or the mass of the layer. Similar differences between the estimated decay times have been observed earlier, both after the Fuego eruption as well as in the case of El Chichon eruption. In the case of Fuego, the  $1/e$  folding times for the vertically integrated backscattering coefficient (IBC) and the peak scattering ratio have been 8 and 11 months, respectively [*Russell and Hake*, 1977]. In the case of El Chichon, the  $1/e$  folding time for IBC is reported as 11.5 months [*Jäger and Carnuth*, 1987]. A value of 15.65 months as  $1/e$  folding time was obtained for the peak scattering ratio of the El Chichon layer by plotting the scattering ratio values available in the literature [*Hofmann*, 1987] corresponding to a period from 200 to 1100 days after the eruption. Sedimentation removes the particles at low altitudes below the aerosol peak more effectively from the layer, while the major contribution to the vertically integrated particulate backscattering comes from these altitudes. Hence the total integrated aerosol backscattering or the mass of the whole layer shows a faster decay time than the decay time shown by the peak scattering ratio value alone.

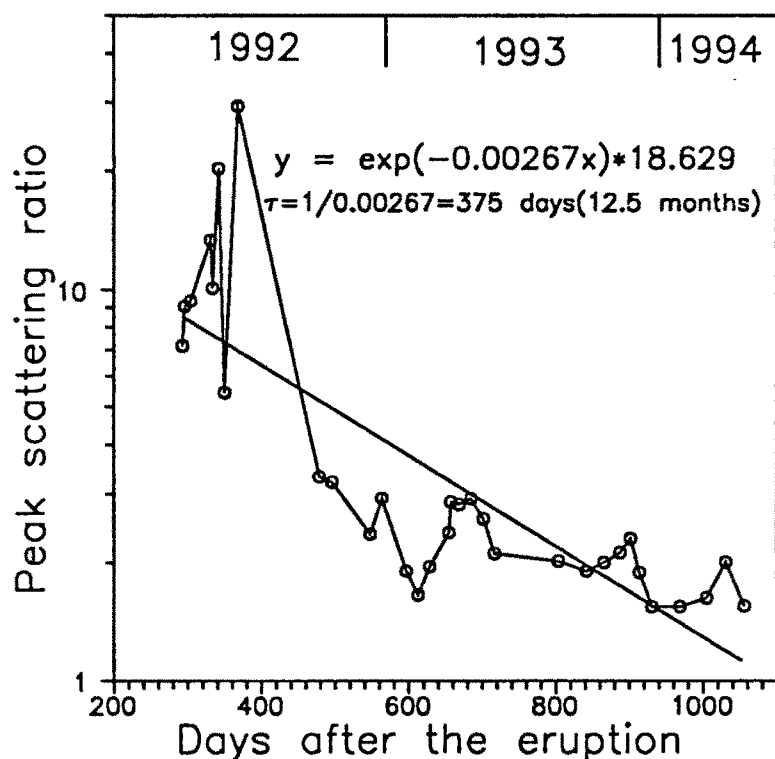


Figure 4.29: Time variation of the peak scattering ratio value from April 1992 to May 1994.

Similar argument has been given by *Russell and Hake* [1977] in explaining the observed difference in the two decay times, in the case of Fuego eruption. This has implications in the calculation of the radiative effects of the volcanic aerosols. While for estimating the impact of stratospheric volcanic aerosol on surface temperature, the integrated value of aerosol scattering for the layer is sufficient, for a detailed calculation of the impact at stratospheric altitudes, the altitude variations of the extinction coefficients within the layer should also be taken into account whose decay patterns can be different as shown above.

#### 4.7.6 Comparison of results with El Chichon data

Table 4.3 shows a comparison between the mass of the aerosol layer as well as the IBC values obtained by *Jäger and Hofmann* [1991] for the case of El Chichon at 694.3 nm

Table 4.3: Comparison of the mass of the volcanic aerosol layer and the integrated aerosol backscattering coefficient (IBC) at 532 nm in the case of El Chichon eruption as reported by Jäger and Hofmann [1991] and in the case of Pinatubo eruption, the results of the present study.

Time after eruption	El Chichon		Mt. Pinatubo	
	Mass ( $\text{gm}^{-2}$ )	IBC ( $\text{sr}^{-1}$ )	Mass ( $\text{gm}^{-2}$ )	IBC ( $\text{sr}^{-1}$ )
1 year	$3.75 \times 10^{-2}$	$2.25 \times 10^{-3}$	$2.39 \times 10^{-1}$	$1.17 \times 10^{-2}$
2 years	$1.25 \times 10^{-2}$	$6.88 \times 10^{-4}$	$1.12 \times 10^{-2}$	$5.50 \times 10^{-4}$
1056 days	$6.00 \times 10^{-3}$	$3.13 \times 10^{-4}$	$6.11 \times 10^{-3}$	$3.00 \times 10^{-4}$

but corrected for 532 nm wavelength [Jäger, 1992] and the values obtained in the case of Mt. Pinatubo eruption. In both cases the results are integrated from tropopause +1 km to 30 km. In spite of the large latitudinal difference between the two measurement sites, Garmisch-Partenkirchen (47.5°N) and Ahmedabad (23°N) and a large difference in the quantity of mass injected by the two eruptions, the mass of the aerosol layer and the integrated backscattering coefficients become comparable, about 2 years after the eruption, as also shown by the model studies of Pinto *et al.* [1989].

## 4.8 Modeling studies of aerosol characteristics

### 4.8.1 A brief survey of existing aerosol models

Modeling of aerosols can be broadly classified on the basis of aerosol properties which they address to, namely optical and physical. The particle size distribution, shape and composition form usually the core of all serious optical models. These models find their application in the interpretation of data from both satellite and ground based remote optical sensors that monitor aerosols. The aerosol microphysical processes responsible for the formation, evolution, transport and removal of aerosols are the focal point of physical models, which are most often associated with chemical-radiative-dynamical effects. While there have been several attempts on both the fronts, with an emphasis on the global distribution, a recall of some important efforts would be in order, with a note that the

focus of majority of these efforts has been on stratospheric aerosols.

*Rosen et al.* [1978] developed a one-dimensional steady-state i.e. during quiet periods stratospheric aerosol model which included the effects of sedimentation, diffusion, particle growth and coagulation. The results obtained indicated that the model was capable of describing many aspects of the stratospheric aerosol layer, such as the size distribution and the vertical profiles for particles  $> 0.3 \mu\text{m}$  diameter. However the model could not incorporate the necessary input parameters to explain for example, the observed condensation nuclei profiles.

*Turco et al.* [1979a] developed a time-dependent one-dimensional model, incorporating a wide range of basic physical and chemical processes to describe the stratospheric aerosols. The model could explain most of the observed experimental features regarding stratospheric aerosols such as sulphate mass, large particle ( $r > 0.15 \mu\text{m}$ ) mixing ratio, ratio of particles  $> 0.15 \mu\text{m}$  radius to those  $\geq 0.25 \mu\text{m}$  radius etc. [*Toon et al.*, 1979] and in detail the sensitivity of the various processes were also discussed. The sensitivity tests and comparisons with observations suggested that coagulation controls the large particle mixing ratio. Some of the unresolved aerosol related problems in this model, included the role of volcanoes and other sulphur sources in maintaining the sulphate aerosol layer.

*Capone et al.* [1983] developed a two-dimensional model of sulphate photochemistry, transport and aerosol microphysics to study the evolution of El Chichon volcanic aerosols, for a period of 2 years. It was found that the residence time of the aerosol cloud in the stratosphere exceeded 2 years and also the model could reproduce the observed optical depth, lidar backscatter and infrared extinction coefficients if about 10 Mt of  $\text{SO}_2$  was injected.

*Hofmann and Rosen* [1984] studied the stratospheric aerosol size and mass during the first 1.5 years after El Chichon eruption over Laramie and southern Texas ( $27\text{-}29^\circ\text{N}$ ) using balloonborne particle counters and compared the observations with the theory of particle growth in the stratosphere to characterise the sulphuric acid vapour temporal variations suggested by the data.

More recently, *Tie et al.* [1994] developed a two-dimensional model taking into account the coupling between dynamical, chemical, microphysical processes to simulate the observed results on El Chichon volcanic aerosols. The model could simulate most of the

observations like aerosol size distributions, surface area, aerosol mass etc., quantitatively. It was also pointed out that the model substantially underestimated the aerosol load, if only gas phase  $\text{SO}_2$  is considered to be ejected out of the eruption and so it was estimated that the direct ejection of sulphate particles is a very important process. The model calculations suggested that approximately 20% of the sulphate aerosols could have been provided by direct injection of aerosols during the eruption while the remaining 80% have been produced by the conversion of gas phase  $\text{SO}_2$ . Also using the model developed they have studied the Pinatubo aerosols and their effect on the stratospheric ozone [Tie *et al.*, 1994]. The results showed that the highest surface area was found in the tropical region consistent with the observations. One year after the eruption the volcanic aerosols have been dispersed by transport processes. In October 1991 (4 months after the eruption), the largest amount of aerosol is located in the tropics and midlatitudes between 20 and 30 km. The calculated evolution and distribution of the aerosol surface areas were found to be in reasonable agreement with the observations.

*Bekki and Pyle* [1994] developed a global two-dimensional chemical-radiative-dynamical model, which contains a detailed treatment of sulphate aerosol microphysics and simulated the formation and temporal evolution of the sulphate aerosol cloud generated by Mt. Pinatubo, in June 1991. Though the model could simulate the observed  $\text{SO}_2$ , due to the absence of homogeneous nucleation of aerosols in the model, there were discrepancies in the timing of the peak in aerosol loading and the magnitude of the surface area density, which made them to suggest that homogeneous nucleation plays an important role in the early stages of volcanic eruption in determining the average size of the volcanic sulphate particles and their residence times in the atmosphere. Also, the modeled aerosol layer had still not recovered to its background level 2 years after the eruption.

*Pudykiewicz and Dastoor* [1995] numerically simulated the global distribution of sulphate aerosol produced after a major volcanic eruption using a dynamic model and applied those results to Pinatubo eruption. Verification of results showed that the numerical model reproduced accurately the global distribution of sulphates and the aerosol optical depths derived for an eruption of magnitude Mt. Pinatubo matched well with experimentally observed results.

Recently *Zhao et al.* [1995] simulated the evolution of Pinatubo volcanic aerosols in

the stratosphere and used the model to study the chemical, microphysical and radiative properties of volcanic aerosols. The model reproduced reasonably well the basic aerosol properties such as size distribution, total mass and concentration, temporal and altitude variation and radiative properties.

On the optical side, emphasis was given to the development of models based on a size distribution which will comply with direct measurements. *Pinnick et al.* [1976] proposed a simple exponential and lognormal size distribution function based on a large data base of directly measured submicrometer size aerosol. The model was utilised to compare particle concentration measurements observed with lidar backscattering. It was also used to estimate the dependence of aerosol extinction and backscatter on wavelength and to calculate the planetary albedo of stratospheric aerosols.

*Toon and Pollack* [1976] proposed a global stratospheric aerosol model based on a zero order logarithmic distribution (ZOLD) function, which is equivalent to a lognormal distribution, index of refraction and total optical depth consistent with several observations available then. The model was used in radiative transfer calculations to study long term climatic effects. Also for the first time, an attempt was made to model a volcanically perturbed stratosphere due to Agung eruption, with the data available at 20 km of *Mosson* [1964] and it was suggested that even under highly perturbed conditions the stratospheric sulphate aerosol size distribution may be similar to the ZOLD function proposed in the model. As tropospheric aerosols are composed of many diverse substances and as their sources and sinks are distributed nonuniformly in space and time, the tropospheric aerosol component is quite variable in addition to being complex. As only a few useful measurements of total aerosol optical depth were available then, it became a difficult task to model the tropospheric aerosols, even at one location, let alone globally, as the greatest restriction placed on the available data was temporal and geographical averaging and with all the variations observed in tropospheric aerosols, this assumption of averaging becomes meaningless, though an attempt was made by *Toon and Pollack* [1976].

There was an effort by *Russell et al.* [1981] to utilise all the existing aerosol size distributions in one unified approach. The optical model demonstrated the ability of deriving profiles of aerosol number density, extinction and backscatter obtained from satellites, lidars and dustsondes, during two extensive field measurements [*Russell et al.*,

1981, 1984].

*Rosen and Hofmann* [1986] developed a stratospheric optical model for direct measurements from dustsondes for the altitude range above the tropopause to 30 km, for an observation period covering both background and volcanically perturbed situations, for the midlatitudes. The proposed model could explain most of the experimental features on the aerosol number density, lidar backscatter and optical depth.

*Jäger and Hofmann* [1991] proposed an optical model for midlatitudes based on balloonborne particle counter data from Laramie, Wyoming (41°N) and lidar backscatter data from Garmisch-Partenkirchen (47.5°N) obtained during the 1980-1987 period. The model essentially gave factors for conversion from aerosol backscatter to mass, area and extinction for the altitude range of 15 to 30 km, for three wavelengths 532, 694 and 1064 nm and two refractive indices 1.44/1.45. These conversion factors when applied to the lidar data of Garmisch gave very good results on optical depth, mass and area.

A global climatology of stratospheric aerosols was created by using SAM, SAGE I and SAGE II observations for about a decade by *Hitchman et al.* [1994] for the first time providing a global view of the long term average aerosol distributions on decadal, quasi-biennial and seasonal timescales. The role of quasi-biennial oscillation on the stratospheric aerosols was discussed in detail and the dynamical effects of the aerosol distributions were attempted.

*d'Almeida et al.* [1991] from the data available on tropospheric aerosols constructed a global optical aerosol climatology model for a wide variety of aerosols ranging from Saharan dust to Antarctic. A wide variety of aerosol optical parameters including extinction, scattering, absorption, phase function, asymmetry factor and single scattering albedo for a large wavelength range from 0.3 to 40  $\mu\text{m}$  and the variation of these parameters with relative humidity and their implications were discussed in detail.

#### 4.8.2 Aerosol microphysical processes responsible for the formation and decay of stratospheric aerosol layer

The aerosol continuity equation can be written as

$$\frac{\partial n}{\partial t} = \left( \frac{\partial n}{\partial t} \right)_{\text{nuc}} + \left( \frac{\partial n}{\partial t} \right)_{\text{growth, evap.}} + \left( \frac{\partial n}{\partial t} \right)_{\text{coa.}} + \left( \frac{\partial n}{\partial t} \right)_{\text{sed.}} + \left( \frac{\partial n}{\partial t} \right)_{\text{diff.}} + \left( \frac{\partial n}{\partial t} \right)_{\text{washout}} \quad (4.24)$$

where the various terms refer to the rate of change of aerosol concentration due to processes such as nucleation, growth or evaporation, coagulation, sedimentation, diffusion and washout.

Nucleation refers to the formation of a new stable solid or liquid particle from a gas phase consisting of either gaseous species only (*homogeneous, homomolecular nucleation*) or involving two or more gaseous species, one of which most commonly is water (*homogeneous, heteromolecular nucleation*) or when two or more gaseous species condense onto preexisting particles (*heterogeneous, heteromolecular nucleation*) [Hamill *et al.*, 1977a]. The nucleation lifetime is of the order of a few days [Turco *et al.*, 1979a]. Immediately after the El Chichon as well as Mt. Pinatubo eruptions, high concentrations of aerosol droplets were observed suggesting that homogeneous nucleation is the most likely production mechanism of aerosols at the stratospheric altitudes [Hofmann and Rosen, 1983; Deshler *et al.*, 1992].

After nucleation the sulphuric acid-water solution droplets can grow by heteromolecular condensation of  $\text{H}_2\text{SO}_4$  and  $\text{H}_2\text{O}$  vapours. At a given temperature, the water vapour equilibrium uniquely determines the weight percentage of  $\text{H}_2\text{SO}_4$  in the solution and consequently the  $\text{H}_2\text{SO}_4$  vapour pressure over the droplet. Accordingly, on the basis of  $\text{H}_2\text{SO}_4$  vapour pressure, some of the sulphuric acid molecules incident on the droplet are absorbed or could be evaporated from the existing droplet [Turco *et al.*, 1979a].

Under stratospheric conditions, Brownian coagulation, which occurs when particles impinge during random thermal motions is important [Turco *et al.*, 1982]. The rate of change of concentration of particles of radius  $r$  due to coagulation can be expressed as the difference between two integrals over the particle size distribution: one integral represents the production rate of particles of size  $r$  by the coagulation of two smaller particles and the second integral represents the loss rate of particles of size  $r$  by coagulation with all other particles. The coagulation integrals are calculated from Turco *et al.* [1979b]. The coagulation kernels for each pair of particles, is calculated based on Fuchs [1964] and Hamill *et al.* [1977b]. In our model, we have adopted a discrete formulation of the particle size distribution. In this formulation, coagulation is considered as an interaction process between pairs of particles whose sizes are limited to a finite set of discrete values. Turco *et al.* [1979b] state that even the continuous particle size distribution yields the

same results for the average rates of particle coagulation, but the discrete formulation is much simpler to use.

The dynamical or transport (removal) mechanisms are diffusion (horizontal dilution i.e. spreading of aerosols to other latitudes and vertical diffusion) and gravitational sedimentation. When the aerosols grow to a few micron size, gravitational sedimentation, in which particles fall with respect to the air surrounding them and are returned to the troposphere, becomes important. The equation for settling velocity is given as

$$v_s = \frac{2\rho r^2 g}{9\eta} [1 + (\lambda/r)(A + B \exp\{-Cr/\lambda\})] \quad (4.25)$$

where  $\rho$  is the mass density of aerosols ( $1.65 \text{ g cm}^{-3}$  for 75%  $\text{H}_2\text{SO}_4$  droplets),  $g$  is the gravitational acceleration,  $\lambda$  is the mean free path and  $A$ ,  $B$  and  $C$  are constants whose values are 1.249, 0.42 and 0.87, respectively [Kasten, 1968]. Using the above equation it is estimated that a particle of radius  $1 \mu\text{m}$  will fall from 20 to 10 km in less than a year but a  $0.1 \mu\text{m}$  particle will take about 10 years to fall the same distance. Therefore gravitational sedimentation is a significant removal mechanism for particles with radius  $\geq 1 \mu\text{m}$  and this accounts for the fact that the fraction of particles  $\geq 1 \mu\text{m}$  is smaller in the stratosphere than in the troposphere. Gravitational sedimentation is not a significant removal process for particles in the size range  $\leq 0.1 \mu\text{m}$  [Hamill *et al.*, 1977b].

## 4.9 A time dependent stratospheric aerosol layer model: Present work

In order to understand better the relative roles of the aerosol microphysical processes in influencing the stratospheric aerosol layer formation and decay, a simple model has been developed, taking into account the aerosol microphysical processes such as growth, coagulation and sedimentation, to explain the time evolution of the Pinatubo layer (17 to 30 km) and the results obtained have been compared with that of balloon and lidar measurements, as well as with the data for El Chichon available in literature.

### 4.9.1 Model specifications

As homogeneous-heteromolecular nucleation and heterogeneous-heteromolecular nucleation are the most important production mechanisms of aerosols only in the initial stages of volcanic eruption and also as the nucleation life time is of the order of a day (the process is almost instantaneous), the process of nucleation is not included in the model. *Hamill et al.* [1977a] showed through model calculations that the heterogeneous-heteromolecular nucleation rate is generally many orders of magnitude higher than the nucleation rate for any competing process. An analysis of the volcanic particles suggested that large numbers of sulphate particles have been formed by homogeneous nucleation in the early stages of Pinatubo volcanic eruption [*Sheridan et al.*, 1992; *Deshler et al.*, 1992]. Recent model studies of Pinatubo aerosol layer evolution by *Zhao et al.* [1995] showed that the new particle formation by homogeneous nucleation almost ceases in about a month after eruption. The enormous amount of  $\text{SO}_2$  injected gets rapidly converted into  $\text{H}_2\text{SO}_4$  in about 30 days, which is the chemical conversion time and the  $\text{H}_2\text{SO}_4$  vapour thus formed build up very quickly to levels sufficient for homogeneous nucleation to occur. This chemical oxidation of  $\text{SO}_2$  into  $\text{H}_2\text{SO}_4$  is crucial for aerosol formation and evolution and the conversion rate is controlled by OH concentration. The  $\text{H}_2\text{SO}_4$  vapour thus formed results in the nucleation of new particles followed by co-condensation with water to form the observed aerosol. *Winker and Osborn* [1992] estimate that one month after the eruption of Mount Pinatubo, about half the  $\text{SO}_2$  had been converted into sulphate aerosols. Both experimental (TOMS [*Bluth et al.*, 1992] and MLS [*Read et al.*, 1993]) observations and model calculations [*Bekki and Pyle*, 1994] show that more than 90% of the conversion of  $\text{SO}_2$  to sulphate aerosols was complete within 3 months after the Pinatubo eruption. In the case of El Chichon, the characteristic aerosol growth time was about 45 days [*Hofmann*, 1987].

Hence, in these calculations an aerosol size distribution is chosen which starts from  $t + 45$  days and not at  $t = 0$ . Also, the process of aerosol evaporation due to the negative growth rate is not included. Average growth rates of aerosols for the altitude region of 20-30 km are taken from *Hofmann and Rosen* [1984] for a sulphuric acid concentration of  $10^7 \text{ cm}^{-3}$  (estimated after 40 days of El Chichon eruption) and a water vapour mixing ratio of 3 ppmv.

In general, the sedimentation flux is calculated as

$$\left(\frac{\partial n}{\partial t}\right)_{\text{sed.}} = -\frac{\partial}{\partial z}(-v_s n) \quad (4.26)$$

where  $v_s$  is the settling velocity ( $\text{cm s}^{-1}$ ) and  $n$  is the aerosol number density ( $\text{cm}^{-3}$ ).

In the case of a layer (17-30 km), the total number of particles,  $n$  can be assumed to be distributed throughout the 13 (30-17) km regime of the stratosphere and hence the sedimentation flux becomes

$$\left(\frac{\partial n}{\partial t}\right)_{\text{sed.}} = \frac{(-v_s n)}{13} \quad (4.27)$$

A bimodal lognormal aerosol size distribution signifying an eruption of magnitude of El Chichon or Pinatubo with  $r_1 = 0.02 \mu\text{m}$ ,  $\sigma_1 = 2.2$ ,  $N_1 = 5000 \text{ cm}^{-3}$  and  $r_2 = 0.7 \mu\text{m}$ ,  $\sigma_2 = 1.6$ ,  $N_2 = 50 \text{ cm}^{-3}$ , after 45 days of eruption, is taken as the initial boundary case (Model 2). Model 1 has a higher aerosol concentration by a factor of 10 when compared to Model 2 and Model 3 is lower by a factor of 10, while the mode radii and sigma are unchanged. This size distribution is taken, based on the optical particle counter data of stratospheric aerosols following El Chichon volcanic eruption by *Hofmann* [1988] and Mt. Pinatubo eruption by *Deshler et al.* [1993]. 15 size bins which cover the aerosols in the radius range of  $0.01 \mu\text{m}$  to  $15 \mu\text{m}$  are considered. The initial size distribution ( $t + 45$  days) is made to undergo the physical processes of growth, coagulation and sedimentation and the evolution of the final size distribution after  $t + 2$  months,  $t + 3$  months,  $t + 6$  months,  $t + 1$  year,  $t + 1.5$  years,  $t + 1.8$  years,  $t + 2$  years and  $t + 3$  years is considered for the present study. In the current model no inflow of aerosols from the lower and upper altitudes i.e. from below 17 km and above 30 km is considered and hence an average aerosol size distribution representing the volcanically perturbed case in the stratosphere is taken. The initial size distribution ( $t + 45$  days) has apart from the volcanically produced bimodal size distribution, embedded in it the background aerosol size distribution. The aerosol continuity equation in addition to the terms for growth, coagulation and sedimentation, has a contribution of aerosols from the background conditions, which is referred to as C here. Hence the equation becomes

$$\frac{\partial n}{\partial t} = \left(\frac{\partial n}{\partial t}\right)_{\text{growth}} + \left(\frac{\partial n}{\partial t}\right)_{\text{coa.}} + \left(\frac{\partial n}{\partial t}\right)_{\text{sed.}} + C \quad (4.28)$$

If the number density  $n$  becomes equal to the background aerosol size distribution which is in an equilibrium condition i.e.  $n = n_{eq}$  then

$$\frac{\partial n}{\partial t} = \frac{\partial n_{eq}}{\partial t} \quad (4.29)$$

Therefore the contribution from the background, equilibrium condition  $C$  becomes

$$C = \left( \frac{\partial n_{eq}}{\partial t} - \frac{\partial n}{\partial t} \right)_{\text{growth}} - \left( \frac{\partial n}{\partial t} \right)_{\text{coa.}} - \left( \frac{\partial n}{\partial t} \right)_{\text{sed.}} \quad (4.30)$$

This contribution  $C$  is subtracted from the volcanic aerosol size distribution at each time step and hence, the volcanic stratospheric aerosol size distribution is corrected for the background, equilibrium aerosol size distribution, in this manner.

The horizontal and vertical diffusion of aerosols have not been considered due to the following reasons: lack of data on wind speed and movement of aerosols to other latitudes and as altitudinal dispersion of aerosols is not considered. Only gravitational settling of aerosols out of one vertical bin (17-30 km), which becomes the important and dominant removal mechanism for large aerosols, is considered here.

Since, washout is effective only below tropopause, it is not included in the model.

Figure 4.30 shows the evolution of volcanic aerosol size distribution after background corrections. Results corresponding to Model 2 aerosol size distribution are shown as an example. About 2 months after the eruption, the primary mode in the bimodal lognormal distribution grows to an average size of  $0.08 \mu\text{m}$  and also the secondary mode is not prominent. About 3 months after the eruption the total number of particles starts to decay as a result of growth, coagulation and sedimentation. Aerosols in the size range  $0.2-1 \mu\text{m}$  continue to grow through coagulation process, even for about an year or so, making the secondary mode to shift to a higher radius of about  $1-2 \mu\text{m}$ , with a subsequent reduction in the total number density. It is clearly seen, that as gravitational sedimentation is a very effective removal mechanism for larger aerosols in the range of a few microns, their removal rate is faster and in about 2-3 years, the size distribution returns to the background aerosol size distribution. Similar features of the evolved size distribution have been observed by *Tie et al.* [1994] while studying the El Chichon eruption over the equator as well as at midlatitudes.

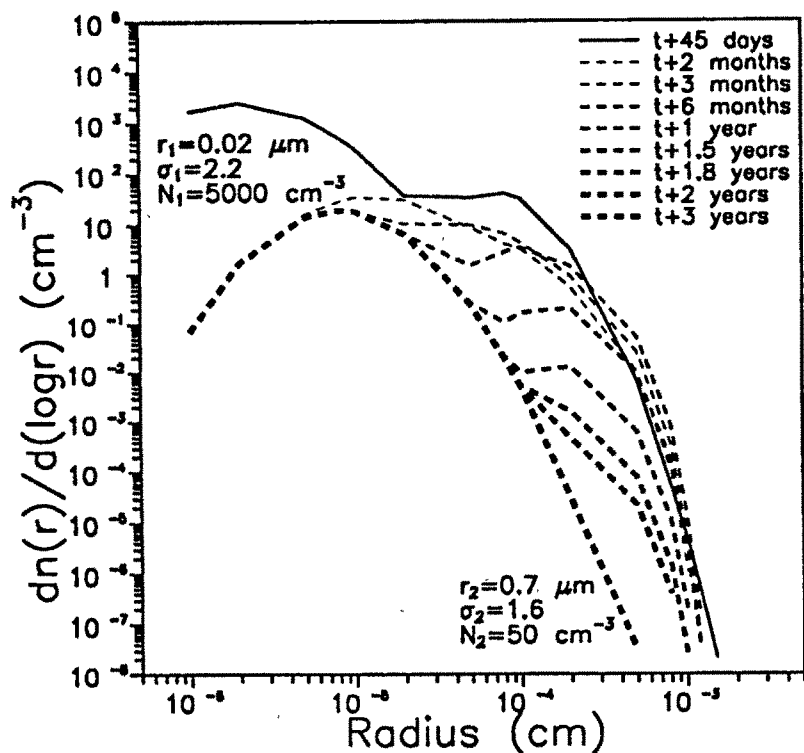


Figure 4.30: The final evolved size distributions after they have undergone the aerosol microphysical processes of growth, coagulation and sedimentation and after applying background corrections. Model 2 size distribution is shown here as an example.

#### 4.9.2 Results and Discussion

The evolved size distributions are used to calculate the aerosol extinction coefficient at 500 nm (75%  $\text{H}_2\text{SO}_4$  droplets,  $m = 1.431 - i1 \times 10^{-8}$ ) and then integrated for the whole layer, to study the time evolution of the optical depth of the Pinatubo layer.

The percentage contribution of the different physical processes considered in the model namely growth, coagulation and sedimentation to the evolution of the aerosol size distribution show that coagulation dominates immediately after the eruption to about 150 days, whereafter growth and sedimentation become dominant (Figure 4.31). While condensational growth aids in producing larger particles, gravitational sedimentation becomes an effective removal mechanism for larger particles. Though the results shown are representative of Model 2 size distribution, they are found to be more or less similar for other size

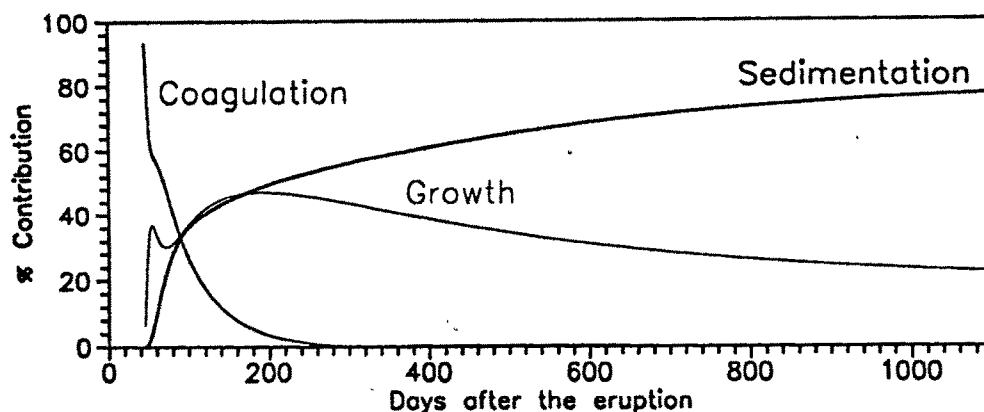


Figure 4.31: *Percentage contribution of the different physical processes to the evolution of aerosol size distribution at different times after a volcanic eruption.*

distributions also.

Sensitivity studies conducted by changing the growth rates and coagulation kernels by  $\pm 10\%$  indicate that the percentage change in the calculated aerosol optical depth steadily increases from about  $\pm 2\%$  to about  $\pm 20\%$  in the case of growth rate, while due to coagulation, the change increases from about  $\pm 0.5\%$  to about  $\pm 8\%$ , for a period corresponding from  $t + 2$  months to  $t + 14$  months (Figure 4.32). Afterwards, the percentage change in optical depth decreases and becomes less than  $\pm 1\%$  in about 2 years, indicating that the processes of growth and coagulation are important, in the first year of the eruption in maintaining the aerosol layer, whereafter when the particles grow sufficiently larger, of the order of a few microns, sedimentation becomes important. These results obtained with a change in the growth rates and coagulation kernels are in gross agreement with the results obtained from the percentage contribution calculations.

Figure 4.33a shows the aerosol optical depth obtained for the three model size distributions. The values decrease by about 5 to 9%, when calculated for 532 nm. Though in the initial stages of the eruption, eruptions of widely varying magnitudes, corresponding to the three model size distributions, used here, exhibit large differences in the optical

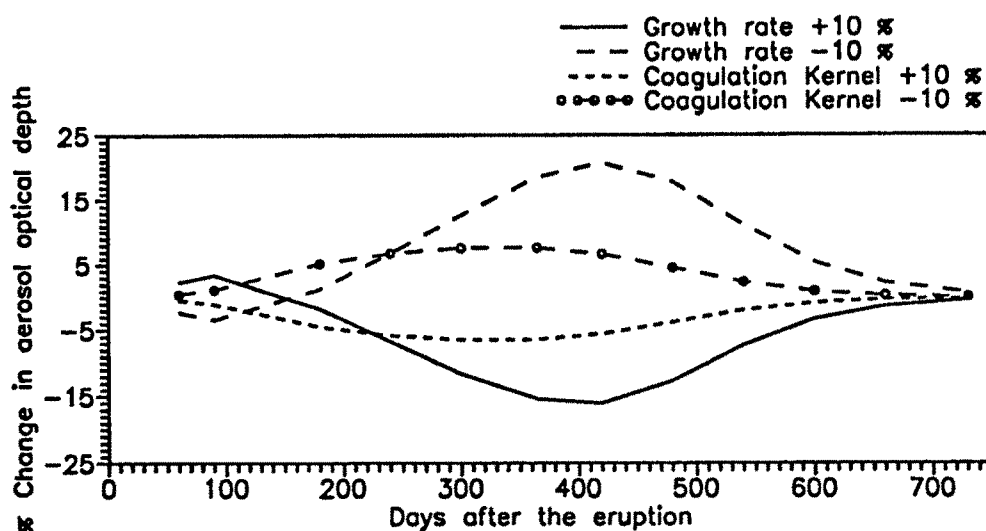


Figure 4.32: Results of sensitivity studies conducted by changing the growth rate, and coagulation kernels by  $\pm 10\%$ .

depths, but after about 2 years, they are almost the same. The comparison of the model results with the experimental observations are done in 4.33b for both Pinatubo and El Chichon volcanic eruptions. The fact that nucleation and diffusion of aerosols have not been included in the model should be borne in mind while interpreting the results obtained. The October 1991 balloon data, measured 4 months after the Pinatubo eruption, lies very close to the third model and the April 1992 balloon data, measured 10 months after the eruption, lies close to the first model, indicating that the particles were still growing and coagulating to produce larger particles. The size parameter  $\nu$  obtained during April 1992, indicates formation of larger particles at higher altitudes (25-30 km) by coagulation with a subsequent reduction in the total number density [Ramachandran *et al.*, 1994b]. The lidar optical depth values derived by multiplying the aerosol backscattering coefficient with an altitude independent value of 50 sr and then integrated for the layer (17-30 km) also exhibit a close correlation with all the models, in various stages.

The stratospheric aerosol optical depths obtained in the case of El Chichon by Jäger *et al.* [1988] and Robinson and DeFoor [1988] using lidars are included here to test the applicability of the model, in explaining the evolution of the aerosol layer formed after a

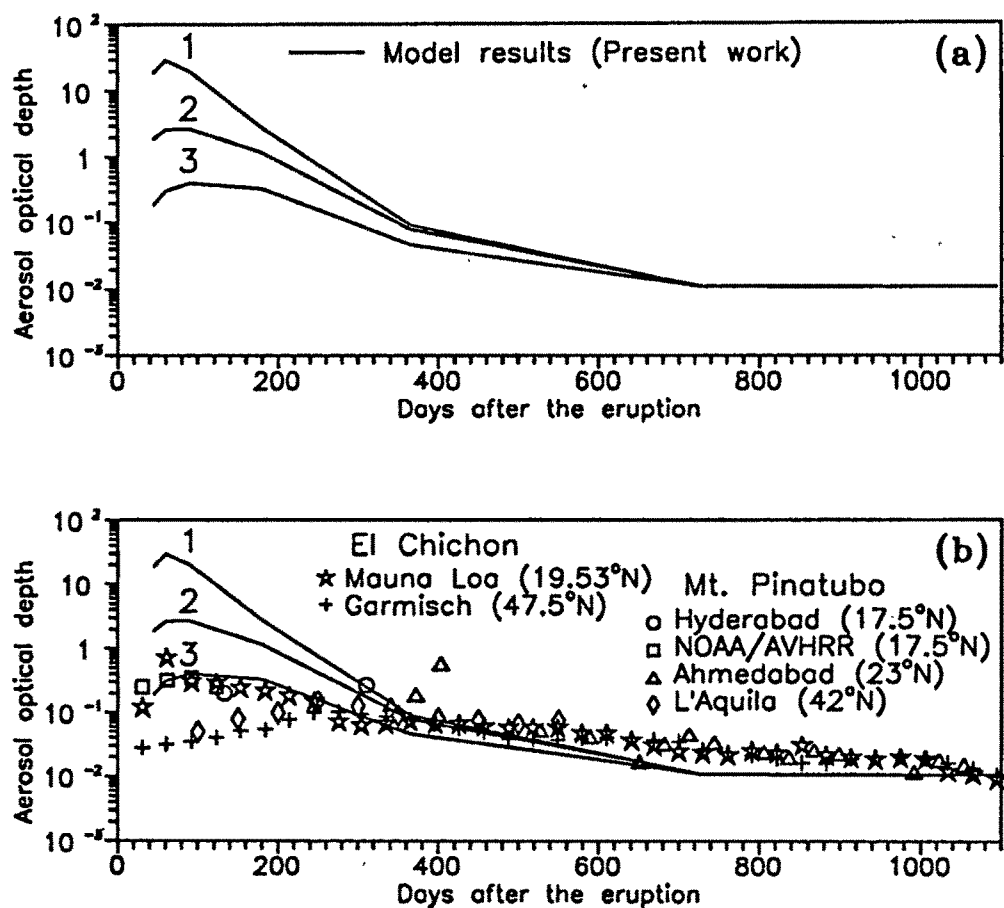


Figure 4.33: (a) The aerosol optical depths calculated for 500 nm for the three model aerosol size distributions used. (b) The aerosol optical depths obtained in the case of Pinatubo and El Chichon volcanic eruptions, using balloons, lidars and satellite are compared with the model results. See text for more details.

major volcanic eruption. It is seen that the model reproduces the data obtained in both the cases. Though the model does not take into account the latitudinal dependence, as only conditions over tropics are considered, the data obtained by *Jäger et al.* [1988] in Garmisch-Partenkirchen at 47.5°N clearly shows that in the initial stages of the El Chichon aerosol layer, about an year or so, the optical depth obtained for the layer is much less when compared to the Mauna Loa (19.53°N) data of *Robinson and DeFoor* [1988]. In both the cases, the data obtained at 694 nm is wavelength corrected, for 532 nm using the values given by *Jäger* [1992]. In case of Mauna Loa data, the NonRayleigh BackScatter obtained for the stratospheric aerosol layer is multiplied by 50, to get the optical depth and then wavelength corrected. It is interesting to note that the same feature of latitudinal dependence is repeated in the case of Pinatubo eruption. The stratospheric aerosol optical depth (15-30 km) at L'Aquila (42°N), Italy obtained by *D'Altorio et al.* [1993] using DIAL measurements at 589 nm reproduces the same feature of the latitudinal dependence in the initial stages of the eruption. This feature was observed by using balloon-borne Sun-tracking photometers over Hyderabad during October 1991 and April 1992, about 4 and 10 months after Pinatubo eruption, where a systematic increase in the aerosol extinction coefficients was seen above 24 km with decreasing latitude, indicating that the upper edge of the layer extends to higher altitudes in the equatorial region [*Ramachandran et al.*, 1994b]. This feature is expected, as both El Chichon and Pinatubo, are in tropical latitudes and also for the first few months after the eruption, bulk of the aerosol cloud lay in the tropics [*Hofmann*, 1987; *Trepte et al.*, 1993] which were then carried to the higher latitudes. The aerosol optical depths obtained at 500 nm for Pinatubo layer using NOAA/AVHRR satellite data [*Minnis et al.*, 1993] at 17.5°N match very closely with Model 3. The NOAA/AVHRR data could be obtained only for the first 4 months after the Pinatubo eruption. In all the above results, only the monthly mean values are plotted. *Bekki and Pyle* [1994] using a global two-dimensional chemical-radiative-dynamical model, simulated the formation and temporal evolution of Pinatubo layer. Due to the absence of homogeneous nucleation of aerosols in the model, there were discrepancies in the timing of the peak in aerosol loading and the magnitude of surface area density, which made them to suggest that homogeneous nucleation plays an important role in the early stages of the volcanic eruption in determining the average size of the volcanic sulphate particles

and their residence times in the atmosphere.

The decay of both the El Chichon and Pinatubo aerosol layers in about 3 years to values very close to background level, shows that though the mass injected by Pinatubo was more than 2 times as compared to El Chichon, faster growth rate and coagulation resulted in larger particles and due to faster removal rate, by sedimentation, the residual aerosol masses and hence the aerosol optical depths and the decay rates can remain the same (Table 4.3). This feature was also seen by *Pinto et al.* [1989] who through model calculations showed that when the mass of SO<sub>2</sub> injected increases beyond 10 Mt, the aerosol microphysical processes of condensation and coagulation produce larger particles, as the SO<sub>2</sub> injection rate is increased rather than a larger number of particles of the same size, due to which the size of sulphate aerosol increases and the removal rate accelerates. Consequently, the residual sulphate masses could be quite similar after about 2 years for eruptions of wide range of magnitudes, suggesting that volcanic effects may be self-limiting. Recently *Rosen et al.* [1994] from conjugate *in situ* observations of the stratospheric aerosol following Pinatubo eruption over Laramie, Wyoming (41°N) and Lauder (45°S), New Zealand, using balloonborne backscattersondes, showed that similar aerosol loading and decay rates occurred over both midlatitude stations. A comparison of the results obtained on El Chichon over Laramie indicated higher mixing ratios in the case of Pinatubo but very similar decay rates for both the eruptions.

When the models used were fitted with an exponential curve to study the 1/e folding times, they were found to be 4.1 months (Model 1), 5.6 months (Model 2) and 9 months (Model 3), showing that eruption of higher magnitude produces larger particles to give a faster decay time. This was experimentally verified by fitting an exponential fit to the Mauna Loa data, which gave a 1/e folding time of 11 months, for the El Chichon aerosol layer. For Pinatubo, an eruption which ejected 2 to 3 times more material into the stratosphere compared to El Chichon, a faster 1/e folding time of about 9 months, was found.

Some differences between the model and experimental results, could have been due to the assumption of average conditions, inside the layer, whereas it has been found using lidar data that the decay pattern can be different in different altitude regions [*Jayaraman et al.*, 1995b] as has been shown earlier. The integrated aerosol extinction coefficient

obtained from lidar for three altitude regimes, namely, 15-20 km, 20-25 km and 25-30 km give  $1/e$  folding times of 16.4, 8.8 and 5.4 months, respectively. It should be noted that the decrease in aerosol extinction coefficient at a particular altitude layer is both due to removal of particles downward due to gravitational settling and horizontal dispersion to other latitudes. Also, the lower layers have a slower decay pattern compared to the top layer, because they not only lose particles due to gravitational settling but also gain particles from above. Recent model studies of *Zhao et al.* [1995] indicate that the aerosol optical depth at 500 nm at different altitudes in the stratosphere can be different and hence an average picture for the stratosphere is not sufficient to explain the evolution.